University of Southampton Research Repository ePrints Soton

UNIVERSITY OF SOUTHAMPTON

Faculty of Engineering, Science and Mathematics

School of Mathematics

Towards a three-dimensional model for the separated flow of an inviscid fluid around an impermeable membrane.

by

John F. Martin

Thesis for the degree of Master of Philosophy

UNIVERSITY OF SOUTHAMPTON

<u>ABSTRACT</u>

Faculty of Engineering, Science and Mathematics
School of Mathematics

<u>Master of Philosophy</u>

Towards a three-dimensional model for the separated flow of an inviscid fluid around an impermeable membrane.

by John F. Martin

In this thesis, we take the first steps towards developing a fully three-dimensional model for the separated flow of an inviscid fluid around an impermeable membrane. We begin by justifying the need for such a model by examining the difficulties encountered in understanding and modelling insect flight, and thus go on to justify the use of a boundary integral method, employing the theory of vortex dynamics, for developing this model. A review of the theoretical work done by other authors in the area of vortex dynamics leads us to identify the difficulties encountered in extending that work to three dimensions. This review prompts us to prioritise the rigorous analytical treatment of the governing no-penetration boundary condition, and the remainder of the work seeks to set a precedent for the level of rigorousness required. This is done by considering the problem of an axisymmetric disc travelling perpendicular to itself. This formulation contains some but not all of the features of a fully three-dimensional problem, and we avoid exploiting its axisymmetric nature to an extent that does not have a natural extension into the fully three-dimensional case. Two methods of parameterising and solving the governing no-penetration boundary condition are offered; both methods involve the derivation and inversion of a Fredholm integral equation of the first kind to give a Fredholm integral equation of the second kind, which is solved by finding the eigenfunctions of the integral operator in terms of the Chebyshev polynomials. The first method is complete but offers an unsatisfying level of accuracy, and the second shows great promise for the development of a highly accurate numerical method but, regrettably, remains incomplete, and the suspected reasons for this are discussed. Both methods are formulated and tested by solving the attached flow problem but have simple, natural extensions to the separated problem. A discussion of the work required to extend this formulation to a fully three-dimensional and separated flow model is offered.

Contents

List of Tables

List of Figures

DECLARATION OF AUTHORSHIP

I, John F. Martin, declare that the thesis entitled "Towards a three-dimensional model for the separated flow of an inviscid fluid around an impermeable membrane." and the work presented in the thesis are both my own, and have been generated by me as the result of my own original research. I confirm that:

- this work was done wholly or mainly while in candidature for a research degree at this University;

- where I have consulted or quoted from the work of others, this is always clearly attributed. With the exception of such quotations, this thesis is entirely my own work;

- I have acknowledged all main sources of help;

- where the thesis is based on work done by myself jointly with others, I have made clear exactly what was done by others and what I have contributed myself.

Signed:

Date: 5th June 2011

List of Publications

The author has no publications to date.

Acknowledgements

I must start by thanking my wife Katy, whose support for me stretched beyond that of any other. Without the sacrifices you made for me none of this thesis would ever have happened, so I dedicate this work to you.

Huge thanks are also due to Dr. Marvin Jones. Without the belief you had in me and the efforts you were willing to go to for me I would never have even applied for postgraduate study. I thank you for your support and guidance.

I thank Prof. Colin Please for his moral and academic support, especially in the final months.

Finally, I thank all my friends in the department, especially the guys from the office, Keith, Chris and Jamie, whose constant distraction through academic and, shall we say, non-academic discussion was a godsend, and all my other friends in the department, especially Tom and Rich. You guys made the whole experience not just bearable but truly enjoyable.

Chapter 1

Introduction

It is widely recognised amongst biomechanists that the steady state aerodynamics used to explain and model fixed and rotary-wing aircraft flight can not be used to account for the forces created in flapping flight. Insects and birds have evolved novel methods of manipulating the fluid that surrounds them for the purpose of flight and propulsion. The muscle and bone structure of birds' wings makes them heavy and less efficient than insects[1], for which they compensate by spending more of their flight time gliding; the bigger the bird, the more it tends to glide. Insects, on the other hand, rely almost entirely on flapping flight. The mechanisms at work in their technique have intrigued and often confused scientists for generations; so much so that Magnan (1934) 'declared' that insect flight was impossible: *'Tout d'abord poussé par ce qui [se] fait en aviation, j'ai appliqué aux insectes les lois de la resistance de l'air, et je suis arrivé avec M. Sainte-Lague à cette conclusion: que leur vol est impossible.'*[2] To understand insect flight one must first understand the vortices that form in unsteady solid-fluid interactions, as well as their interactions with one another and the body creating them. Such an understanding is of considerable practical and fundamental interest.

1.1 Understanding insect flight

There are a number of physical situations where organisms and human inventions exploit the properties of vortices. We could study the propulsion of fish, the wind-flow around

---

[1]This is with the exception of hummingbirds, which can be treated as notional insects.

[2]*'Primarily driven by what is done in aviation, I applied to insects the laws of air resistance, and I arrived with Mr. Saint-Lague (his student) at this conclusion: that their flight is impossible.'*

a yacht sail or the fluid-flow around a ship, but it is the complex movement and precise design of insect wings that make them such a difficult phenomenon to understand and model.

Early studies into insect flight were primarily concerned with understanding the wing kinematics. It is not the purpose of this work to look at the wings' motion in any detail; the interested reader is referred to Dickinson, et al. (1999). Instead, we will describe some of the fluid dynamic mechanisms at work. Whilst the study of wing kinematics became increasingly easy, with the advent of improved image capture technology, biofluiddynamicists were often hampered by the shortage of non-intrusive flow measuring devices to examine the fluid flow around the wing. Early experiments did, however, give rise to a flurry of theories. Weis-Fogh (1973) analysed the aerodynamics of the tiny parasitic wasp *Encarsia formosa* and explained that the insect generated a greater amount of lift than that predicted by steady-state aerodynamic theory since it employed an unsteady 'clap-and-fling' mechanism at the end of every wing-beat. He observed that by clapping together and then separating their wings in a particular way, the wasp could cause the surrounding air to rush into the gap between its two wings in such a way that the wing experienced the resulting lift more quickly. It has since been confirmed that this mechanism is used by other insects (see e.g. Cooter & Baker (1977)) and it is now widely recognised as a fundamental feature of insect flight.

Work by Maxwothy (1979) used a simplified mechanical model of an insect to test the 'clap-and-fling' mechanism, and espoused the idea that the large leading edge vortex (LEV) that forms on an insect wing's downstroke could account for the high lift required. He conjectured that the LEV generates a spanwise (along the length of the wing) flow, which advects vorticity away from the LEV into a tip vortex. Maxworthy said that this mechanism, similar to that used by delta wing aircraft, allowed for the formation of a large LEV with high lift whilst maintaining its quasi-steady nature. The idea did not catch on. A two-dimensional model by Dickinson & Gotz (1993) found that while the LEV did seem to generate a great deal more lift, it was unstable and was shed from the wing after 3 or 4 chord lengths of travel; much less than the observed length of an insect wing's downstroke. Later work by Grodnitsky & Morozov (1993) measured the flow over a number of insects and stopped just short of ruling the theory out entirely, claiming that *'it seems likely that the flow moves smoothly about the leading edges during the entire stroke cycle, with neither separation nor stalling.'*

Other studies such as that by Brodsky (1991), who performed tests on the flight of

a tethered butterfly in a smoke tunnel, predicted that insect flight was made possible by discrete pairs of vortex rings in the wake of the butterfly, a theory which was also ruled out by Grodnitsky & Morozov, and still others placed the emphasis on the wing capturing the energy in its own wake (Dickinson 1994) or the creation of starting vortices when the wing reverses at the end of a half-stroke (Dickinson 1996). However, no combination of these mechanisms could quite account for the lift required to sustain flight.

The breakthrough came via Ellington, et al. (1996) who observed a large LEV on their mechanical model of a hawkmoth (*Manduca sexta*) which released smoke from its leading edge while it flapped. This LEV generated the strong spanwise flow predicted by Maxworthy. Further experimental confirmation came through Willmott, et al. (1997) who observed the spanwise flow structure within the LEV from a hawkmoth flying in a wind tunnel with a smoke rake. Later on, Birch, et al. (2004) used Digital Particle Image Velocimetry (DPIV) to measure the flow field induced by a model fruit fly wing. This modern measurement technique allowed them to produce very accurate digital images of the flow field, and has allowed more recent authors (Poelma, et al. 2006, Lu & Shen 2008) to produce three-dimensional images of vorticity shedding from model wings. All three of these authors confirmed the existence of LEV-induced spanwise flow.

Despite these advances in qualitative understanding of insect flight, Zbikowksi (2002) points out that our understanding is *'incomplete even on the phenomenological level.'* and that *'not only is the qualitative picture unfinished, but also the quantitative analysis is wanting.'* As is so often the case, mathematical modelling of such processes lags well behind conceptual understanding. We will now go on to outline some of the difficulties involved in this modelling and some of the methods that can be used.

1.2   Mathematical modelling of the mechanisms at work in insect flight

The main reason that a quantitative understanding of insect flight is so elusive is the fact that the flow around an insect wing involves solid-fluid interactions that are *fully unsteady* and *fully three-dimensional*. Whenever a solid moves through a fluid it acquires a boundary layer of fluid in its immediate vicinity. This boundary layer is the transition region between the no-slip boundary condition on the solid surface and the 'outer' flow. Its thickness is inversely proportional to the (square root of the) Reynolds number (*Re*), so fluids of a very low viscosity, and therefore high Reynolds number, develop very thin boundary layers.

This means there are large velocity gradients within the boundary layer, giving rise to non-negligible viscous forces and rotational flow. As the flow in the boundary layer approaches a stagnation point or a sharp edge it can *separate* from the surface. This can create sheets of highly rotational fluid, creating shear layers in the flow; that is, regions where the flow experiences a large change in direction over a very short distance. Since the boundary layer thickness is inversely proportional to the Reynolds number, it is a reasonable assumption that so is the thickness of these shear layers. They are eventually dissipated by viscosity. Despite occurring in a very low viscosity environment, insect flight is entirely dependent on the viscous forces that cause this boundary layer separation (which we look at later in the discussion of the Kutta condition), giving rise to a flow field dominated by separated shear layers and their associated turbulent flow structures.

Furthermore, most insects operate in the $10^2 < Re < 10^6$ domain, a regime where slight changes in the flow are not rapidly dissipated by viscosity and can therefore build up to have a leading order effect on the flow. Both these previous points imply that an appropriate modelling method needs to be able to handle the large scale structure of the wing and the forces acting upon it, as well as the small scale structure of its wake. We now go on to look at a number of attempts to model fluid flow around a thin, impermeable membrane such as an insect wing.

1.2.1   Computational fluid dynamics

Advances in computational power have prompted a number of researchers to explore numerical methods of solving the governing Navier-Stokes equations; such methods are generically referred to as computational fluid dynamics (CFD). Inspired by the work of Ellington et al. (1996), studies by Liu, et al. (1998) and Liu & Kawachi (1998) used a Reynolds-average Navier-Stokes (RANS) solver to model the flow around a *Manduca sexta* wing in hover and confirmed their results against the empirical data of van den Berg & Ellington (1997). Despite the fact that this was one of the first studies to correctly predict the LEV-induced spanwise flow along the wing, their numerical approach had a number of limitations. These are discussed in some detail in Mittal (2004), but perhaps the most significant is the difficulty that RANS has in predicting separation and modelling separated flows, which becomes a serious drawback given the flow regime we are considering. A similar method has been employed by other authors such as Sun & Tang (2002) with relative success, but more recent authors have sought more appropriate numerical solvers.

Ramamurti & Sandberg (2002) used a finite element solver to model flow around a *Drosophilia* wing. Whilst their results showed good agreement with those of Dickinson et al. (1999), their method, like most other CFD methods, did not attempt to directly model the fluid dynamic structures at work; merely to model the flow and observe those structures as they duly appeared. In this way, CFD methods seem to try to 'force' a solver designed for flow solutions that are absent of large velocity gradients to model structures that give rise to exactly that by introducing increasingly complex features. As Mittal (2004) points out, this makes it difficult to *'delineate flow features/mechanisms that are universal from those that are specific to a particular configuration'*, thus making it difficult to use such solvers to find optimal solutions for applications such as micro air vehicle design. Further to this, extending CFD studies whilst maintaining realism and improving accuracy requires a great deal more time and resources.

1.2.2   Vortex dynamics: an introduction

After a short review of empirically based research and CFD models, Ho, et al. (2003) remarked that *'The periodicity of the wing motion and the resultant vortices leads to the conclusion that any quantitative model must be based on unsteady aerodynamics and vortex dynamics.'* The aim of aerodynamic modelling is to provide a mathematical method, derived from physical principles, that describes the important aerodynamic mechanisms at work and that allows the user to quantitatively analyse the effects of these mechanism whilst, as Zbikowksi (2002) puts it, avoiding the *'extremes of mathematical oversimplication and intractable complexity.'* The field of vortex dynamics provides one such method.

Before attempting to describe some of the finer aspects of vortex dynamics, we must define a number of essential terms. In general, we follow the convention used by Saffman & Baker (1979) and Saffman (1992). *Vorticity* is a measure of the local rotation of a fluid flow, and a *vortex line* is a theoretical material curve whose tangent at every point is the instantaneous axis of rotation at that point. We make a distinction between the *vorticity* on a vortex line and its *strength*. Technically, a finite region of vorticity has been compressed onto an infinitely small one, so the vorticity can be thought of as a delta function that is 'weighted' by the strength. A *vortex sheet* is a surface across which the pressure and normal components of velocity are continuous, but the tangential components of fluid velocity are discontinuous, that is a shear layer. The *vortex sheet strength* is a measure of the jump in the tangential component of the fluid velocity across the vortex sheet, and is a vector in the plane of the sheet. For the purpose of this work, we define a *vortex filament* as a vortex

line of constant strength. A vortex sheet can be thought of as a continuous distribution of vortex filaments.

The relevant length, time and viscosity scales associated with flow regimes such as those induced by insect flight give rise to a high Reynolds number and allow us to assume ideal fluid conditions; that is, conditions that are *inviscid* and *incompressible*. The velocity vector field, henceforth denoted $\boldsymbol{u}$, associated with an ideal fluid flow obeys the partial differential equations

$$\boldsymbol{\nabla} \cdot \boldsymbol{u} = 0, \tag{1.1}$$

$$\boldsymbol{\nabla} \times \boldsymbol{u} = 0, \tag{1.2}$$

and can therefore be defined in terms of a velocity potential

$$\boldsymbol{u} = \boldsymbol{\nabla}\phi, \tag{1.3}$$

where ϕ satisfies Laplace's equation and the appropriate Neumann boundary conditions on solid bodies.

As mentioned earlier, a (inviscid) fluid which comes into contact with a solid body enters a thin boundary layer within which the no-slip boundary condition is satisfied. These boundary layers can separate at stagnation points or sharp edges on the surface of the body giving, rise to shear layers in the flow within which the flow is rotational i.e. vorticity is present. The presence of rotational fluid within these shear layers would seem to contradict the irrotational nature of an ideal fluid in the second of the conditions of ideal fluid flow from above. Nevertheless, such a set of circumstances is permissible provided one makes a distinction between the *irrotational* flow in the bulk of the fluid, and the *rotational* flow which is wholly confined to the (attached and separated) boundary layers.

In any physical flow, the presence of viscosity acts to dissipate vorticity. However, in problems such as insect flight the time scale over which vorticity is dissipated is much larger than the periodicity of the wing. This means that the shear layers remain incredibly thin until they are far away enough from the insect to have only a negligible effect on the insect's flight. For that reason, we assume that the shear layers remain infinitely thin for all time, and thus work in the limit of vanishing viscosity, implying infinite Reynolds number, and we model the shear layers as surfaces of discontinuity, or vortex sheets.

Since the flows we are interested in concern the motion of a thin, impermeable mem-

brane, representing the wing, moving through an ideal fluid, the properties of that membrane are the same as those of a vortex sheet; it is very thin and the normal components of velocity are continuous and the tangential components are discontinuous across its surface. We assume the no-slip boundary condition is satisfied in the boundary layer and do not apply that condition to the outer flow solution. We can therefore replace the membrane altogether by modelling it as a vortex sheet of a prescribed shape. In doing so, we are effectively modelling the boundary layer on the membrane as an *attached* (or *bound*) vortex sheet, and we maintain a distinction between it and the *separated* vortex sheet away from the membrane; the two are continuously connected at the point of separation.[3] With this in mind, we can say that the attached vortex sheet separates from the surface to become the separated vortex sheet. The rate at which it does so is considered later in the discussion of the Kutta condition.

The underlying principle of mathematical simplification in vortex dynamics is to model the flow field in terms of the evolution of the vortex sheets rather than that of the velocity field. We think of the flow as 'induced' by the vortex sheets (rather than thinking of the flow regime creating vortex sheets). The way they do so is analogous to the way an electric current induces a magnetic field, and if the properties of a vortex sheet (i.e. its strength and position) are known at a given time, it is possible to compute the flow field that is induced at any point in the flow $\boldsymbol{r}$ through the Biot-Savart law

$$\boldsymbol{u}(t, \boldsymbol{r}) = \frac{1}{4\pi} \int_{S(t)} \frac{dS\left((\boldsymbol{\lambda} - \boldsymbol{r}) \times \boldsymbol{\gamma}(t, \boldsymbol{\lambda})\right)}{|\boldsymbol{\lambda} - \boldsymbol{r}|^3}, \tag{1.4}$$

where $\boldsymbol{\lambda}$ is a point (a dummy variable) on the vortex sheet $S(t)$, which has strength $\boldsymbol{\gamma}(t, \boldsymbol{\lambda})$ (see e. g. Saffman (1992)). Figure 1.1 might help the reader to picture the variables used. As we mentioned earlier, this 'strength' is a measure of the jump in the tangential component of the velocity field that is supported across the vortex sheet, and can be expressed in terms of the fluid velocity at a specific point $\boldsymbol{\zeta}$ on the vortex sheet[4] as approached from above or below through the formula $\boldsymbol{\gamma}(t, \boldsymbol{\zeta}) = \hat{\boldsymbol{n}}(\boldsymbol{\zeta}) \times [\boldsymbol{u}^{\pm}(t, \boldsymbol{\zeta})]_{-}^{+}$, where $\hat{\boldsymbol{n}}(\boldsymbol{\zeta})$ is the unit normal to the vortex sheet at $\boldsymbol{\zeta}$, the square brackets are used to define the difference in

---

[3]Throughout this work we maintain a distinction between a 'free' and a 'separated' vortex sheet. It is assumed that a 'separated' vortex sheet is one that has been created by the motion of a solid through a fluid, whereas a 'free' vortex sheet is one that exists as an object in its own right; it has not necessarily been 'created' by any physical mechanism and has therefore not necessarily undergone 'separation'. Both types are advected with the fluid.

[4]Note that we will generally use $\boldsymbol{\zeta}$ to refer to a point on a vortex sheet, and $\boldsymbol{\lambda}$ to refer to a dummy variable on a vortex sheet.

the sense that $[\chi^{\pm}]_{-}^{+} = \chi^{+} - \chi^{-}$, and $\boldsymbol{u}^{\pm}(t, \boldsymbol{\zeta}) = \lim_{\boldsymbol{r} \to \boldsymbol{\zeta}^{\pm}} \boldsymbol{u}(t, \boldsymbol{r})$ (an expression for which is derived later on). Since the normal component of velocity is necessarily continuous across the sheet, $[\boldsymbol{u}^{\pm}(t, \boldsymbol{\zeta})]_{-}^{+}$ will have no component in the $\hat{\boldsymbol{n}}(\boldsymbol{\zeta})$ direction, and $\boldsymbol{\gamma}(t, \boldsymbol{\zeta})$ is therefore a vector quantity in the plane of the sheet.
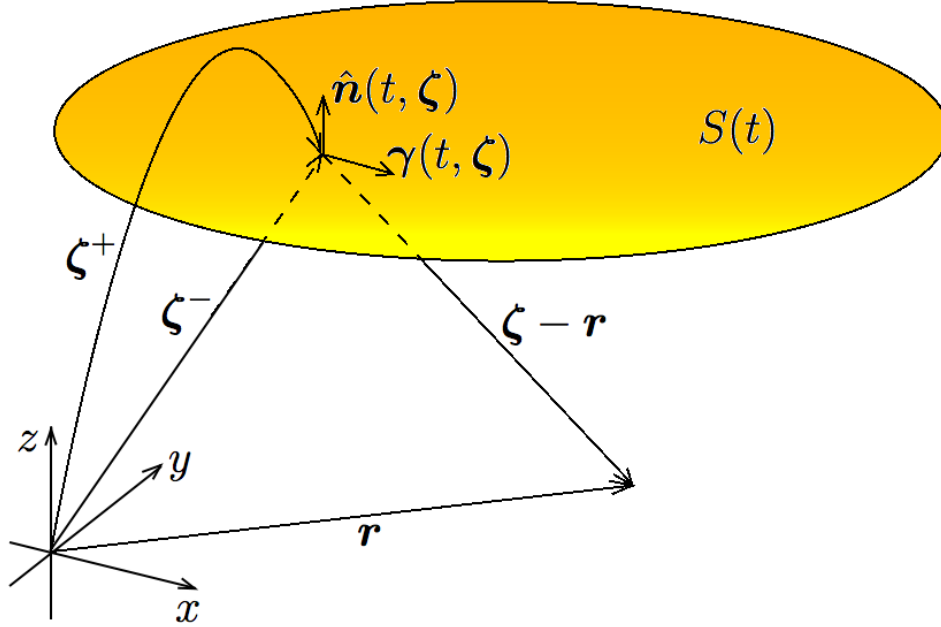
Figure 1.1: Diagram of a flat, disc-shaped vortex sheet $S(t)$ to show the variables used. It is necessary to distinguish between $\boldsymbol{\zeta}^{+}$ and $\boldsymbol{\zeta}^{-}$ because of the jump in tangential velocity across a vortex sheet. Both points lie *on* the vortex sheet but just above or below it.

The formulation in equation (1.4) not only automatically ensures the fluid velocity vanishes at infinity, but also satisfies the equations of an ideal fluid (proof of which is given in the opening pages of Saffman (1992)), with the exception of $\boldsymbol{\nabla} \times \boldsymbol{u}(t, \boldsymbol{r}) = \boldsymbol{\gamma}(t, \boldsymbol{\zeta})\delta(\boldsymbol{r} - \boldsymbol{\zeta})$ where δ is the delta function, and is zero everywhere except on $\boldsymbol{r} = \boldsymbol{\zeta}$ where it is infinite; this is the aforementioned 'weighting' of the infinite vorticity on the vortex sheet. This equation in turn implies $\boldsymbol{\nabla} \cdot \boldsymbol{\gamma} = 0$. Quantitatively therefore, the problem of modelling the flow reduces to that of determining the properties of the attached and separated vortex sheets for all time.

Another useful quantity to consider is the circulation. It is defined, mathematically, as the line integral of the fluid velocity around a simple closed contour, namely

$$\Gamma = \oint_{C} \boldsymbol{u} \cdot d\boldsymbol{l}.$$

Kelvin's circulation theorem states that for an inviscid, barotropic flow (one where pressure and density are functions only of one another) such as those encountered in incompressible fluids, the circulation around a closed contour that moves with the fluid remains constant for all time. This implies that a fluid flow that has been started from rest (whereby the circulation is zero everywhere) will remain free of circulation for all time.

The introduction of a vortex sheet of non-zero strength introduces vorticity and therefore rotational fluid into the flow and seems to contradict Kelvin's theorem. However, our methodology *is* consistent with the theorem provided the *total* circulation within a control volume enclosing the system remains constant for all time. We can define the (non-zero) circulation on a vortex sheet (of non-zero strength) as the circulation around a simple closed contour that pierces the sheet exactly once at $\boldsymbol{\zeta}$, namely

$$\Gamma(t, \boldsymbol{\zeta}) = \oint_{C(t, \boldsymbol{\zeta})} \boldsymbol{u}(t, \boldsymbol{\eta}) \cdot d\boldsymbol{l},$$

where $C(t, \boldsymbol{\zeta})$ is the aforementioned contour and $\boldsymbol{u}(t, \boldsymbol{\eta})$ is the velocity at the point $\boldsymbol{\eta}$ along C. Plugging in the velocity potential definition of $\boldsymbol{u}$ in equation (1.3) and making use of the fundamental theorem of calculus we have that

$$\Gamma(t, \boldsymbol{\zeta}) = \oint_{C(t, \boldsymbol{\zeta})} \boldsymbol{\nabla}\phi(t, \boldsymbol{\eta}) \cdot d\boldsymbol{l} = \left[\phi^{\pm}(t, \boldsymbol{\zeta})\right]_{+}^{-}, \tag{1.5}$$

where the superscript $\pm$ refers to the velocity potential just above and below the sheet at $\boldsymbol{\zeta}$. Note that since there is a jump in the velocity across the sheet, there will be a corresponding jump in the velocity potential. Equation (1.5) tells us that the circulation at a point on a vortex sheet is a measure of the jump in the velocity potential across the sheet. We subtract the value of the velocity potential on the top from that on the bottom of the sheet because of the convention that the contour C goes from top to bottom. The circulation forms a continuous function across a smooth vortex sheet with a continuous strength distribution (such as those encountered in physical problems). Lines of constant circulation can therefore be used to define material curves (and thus a Lagrangian coordinate system) on a vortex sheet.

In their review article, Saffman & Baker (1979) split the problems of vortex sheet motion into two classes. In the first class the properties of a (separated) vortex sheet are given at an initial time, and the problem lies in determining its self-induced evolution in the absence of solid bodies. The second class is concerned with vortex sheets created by the motion of a body and their subsequent interaction with that body. Whilst we are

primarily interested in the second class of problems, a description of the evolution of the separated vortex sheet has been an important development in the field of vortex dynamics and would be essential to a fully three-dimensional description of insect flight. For that reason, it is worth looking at it a little closer.

1.2.3   Motion of a free vortex sheet

The first attempt to model the motion of a free vortex sheet was by Rosenhead (1931). (For a distinction between free and separated vortex sheets see footnote 3 in chapter 1.2.2.) He attempted to model an initially perturbed two-dimensional vortex sheet by replacing it with a finite number of vortex lines and joining up these lines at every time step to represent the evolution of the position of the vortex sheet.

In two dimensions, a vortex sheet is assumed to be made up of a continuous distribution of vortex filaments whose direction is always perpendicular to the plane, thus extending to infinity in both directions. The vortex sheet strength can then be thought of as a scalar quantity. A vortex *line* (of constant strength) which extends to infinity perpendicular to the plane is referred to as a point vortex, because of its appearance in the two-dimensional plane. The strength of a point vortex is the circulation around a curve which bounds a surface pierced by the vortex line exactly once. In the normal convention this is referred to as Γ, and is also a scalar quantity. The velocity a point vortex induces at a distance r from itself is $\Gamma/2\pi r$ and always acts in the azimuthal direction to the vortex line it represents by the right-hand rule. Since vortex lines, and by extension point vortices, are advected with the flow, this poses a problem when evaluating the fluid velocity *at* the point vortex, since it is infinite. However, it can be shown that the velocity at a point vortex is the same as if the point vortex where not even there; that is, it is a linear combination of all other driving mechanisms in the flow, such as background flow and other point vortices/vortex sheets (see e. g. Batchelor (1967))

Chorin & Bernard (1973) pointed out that *'Rosenhead's approximation is only accurate if the rate of change of vorticity along the sheet is small compared with the spacing between the discrete vortices'* (Clements & Maull 1975) and Moore (1971) demonstrated that increasing the number of point vortices in the discretisation could actually make matters worse. A number of studies have sought ways of compensating for these errors and introducing factors such as vorticity dissipation, but with limited success (Chorin 1973, Benson, et al. 1989, Barber & Fonty 2003), and as Saffman & Baker (1979) point out, *'It appears that there may be a fundamental difference between vortex sheets and an assembly of point*

vortices.'

Birkhoff (1962) and Rott (1956) also considered the motion of two-dimensional vortex sheet. By using the circulation as a Lagrangian coordinate system on the surface of the sheet they were able to show that the sheet was advected with the fluid at a velocity equal to the average of the velocities on either side of it. The motion of the sheet was governed by the so-called 'evolution equation'. Birkhoff also conjectured that two dimensional initial value problems of vortex sheet motion with analytic initial data were well-posed for finite time; a theory which was later proven and extended to three dimensions by Sulem, et al. (1981). In doing so they also extended Birkhoff's evolution equation to three dimensions, and Kaneda (1990) went on to simplify their formulation.

However, the 'finite time' clause of this theory proved rather restrictive for advocates of the use of vortex sheets. Kelvin-Helmholtz instability (see e.g. Batchelor (1967)) predicts that a small amplitude perturbation on an otherwise flat interface between two regions of fluid with different velocities (such as a vortex sheet) grows exponentially. This growth is proportional to the size of the discontinuity (the vortex sheet strength) and inversely proportional to the wavelength of the perturbation. Moore (1979) performed an asymptotic analysis of Birkhoff's evolution equation and confirmed that it is ill-posed; it develops a singularity in its curvature in finite time (called the 'formation time'). Despite Moore's own admission that the asymptotic expansion becomes invalid in the neighbourhood of the singularity, his result is supported by a number of computational studies (Baker, et al. 1982, Krasny 1986a, Shelley 1992) and his analysis has since been rigorously validated by Caflisch & Orellana (1986) and extended to a three-dimensional vortex sheet by Ishihara & Kaneda (1995).

This feature of vortex sheets made the initial value problem of determining the evolution of a vortex sheet for times past the formation time rather difficult. One numerical method, which uses a 'smoothing parameter' to desingularise the Biot-Savart kernel in the two-dimensional evolution equation, was proposed by Chorin & Bernard (1973) and refined by Krasny (1986b). Both Krasny (1987) and Krasny (1991) present very convincing numerical evidence suggesting that this method, which has come to be known as the 'vortex-blob method', converges past the formation time as the smoothing parameter tends to zero. Lindsay & Krasny (2001) used this method to develop a particle method for tracking vortex sheet evolution in three dimensions, and also offered an adaptive treecode to counteract the additional CPU time that arises from three-dimensional computations; an example of their results is shown in figure 1.2. Brady, et al. (1998) also used the vortex-blob method

to model three-dimensional vortex sheet evolution by representing the sheet surface as a triangular mesh.

Figure 1.2: Cross section of the computation of the three-dimensional evolution of a vortex sheet in the shape of an initially perturbed disc using the vortex blob method, from Lindsay & Krasny (2001).

For the remainder of this work, it is assumed that we are able to compute the evolution of a free vortex sheet with known initial shape and strength, and we now consider how to determine these properties for a vortex sheet that is created by the motion of a solid object.

1.2.4 Flow around an impermeable membrane

When considering the flow around an impermeable membrane, we must consider both the bound and the separated vortex sheets. In lieu of the assumption at the end of the previous section, the main problem of the separated vortex sheet is to determine the line along which it separates and its strength at separation. The shape and position of the bound vortex sheet are constrained to those of the membrane which it represents, and we must choose its strength as to satisfy the no-penetration boundary condition on the membrane.

Boundary layer separation

In the case of *steady* flow around a membrane, the separation line is uniquely determined by the Kutta condition. Usually applied to the steady flow over an airfoil with a sharp trailing edge, the Kutta condition states that *'the circulation in the case of a properly designed airfoil always adjusts itself so that [the trailing edge] is a stagnation point and the velocity at the trailing edge is finite'* (Milne-Thompson 1949). Let us consider how such a phenomenon comes about. In any physical fluid flow past a body which has a sharp edge of *finite* curvature, stagnation points need not necessarily form initially at the edge, and the fluid may have to flow *around* the edge, introducing a large change in the direction of

the fluid velocity over a short distance. This creates a velocity gradient that is inversely proportional to the radius of curvature and gives rise to non-negligible viscous forces acting on the fluid in that local region, which in turn prevent the fluid from flowing around the edge, creating a vortex in the flow. When the circulation in that vortex is at a unique value the stagnation point is held at the edge.

However, such a steady-state analysis is not appropriate for the unsteady cases we are interested in. In the theoretical problems that we model the surface is considered infinitely thin, and the edges therefore have zero radius of curvature, implying that the fluid which flows around the edge would have to do so at infinite speed. The *unsteady* Kutta condition states that circulation is shed into the fluid at such a rate that this singularity is cancelled out. This equates to vortex sheet separation occurring exactly at the sharp edges and uniquely determines the strength of the newly shed portion of vortex sheet.

Quantitatively, the unsteady Kutta condition determines the exact strength of the separated vortex sheet at the nascent portion, which remains constant in the Lagrangian sense. Imposing it mathematically, however, has given rise to a number of methods, some more realistic than others. It can be written that the correct imposition of the Kutta condition will ensure that the velocity at the edge is finite and moving away from the edge thus;

$$|\boldsymbol{u}(t, \boldsymbol{e})| < \infty, \qquad \boldsymbol{u}(t, \boldsymbol{e}) \cdot \hat{\boldsymbol{s}} \geq 0,$$

where $\boldsymbol{e}$ is a point on the edge of the bound vortex sheet (the membrane) and $\hat{\boldsymbol{s}}$ is a unit binormal vector to the membrane defined by $\hat{\boldsymbol{s}} = \hat{\boldsymbol{n}} \times \hat{\boldsymbol{t}}$ where the unit tangent to the edge, $\hat{\boldsymbol{t}}$, is defined in such a way that $\hat{\boldsymbol{s}}$ points away from the membrane. When the Kutta condition is not imposed mathematically the flow induced by the bound vortex sheet usually gives rise to singularities in the flow at its edges.

One method of implementing this condition in two-dimensions is through a point-vortex model. Rather than modelling the wake as a vortex sheet, some authors introduce vorticity into the fluid through a single point vortex. Originating near the point of separation (the sharp edge), the strength of this vortex is chosen so as to exactly cancel the singularity at the edge. As it is advected with the fluid, so its strength is adjusted to continue to keep the velocity field finite at the edge. Such a method has been successfully employed by such authors as Cortelezzi, et al. (1997) who used it to model flow past a flat plate, and Michelin & Smith (2009) who modelled flow past a two-dimensional flapping flag. Despite giving realistic results, this method introduces a certain amount of ambiguity owing to the

arbitrary choice of initial position of a newly shed point vortex, and the point vortex model itself is uninspiring as it does not truly reflect the flow physics.

Some authors model the wake as a vortex sheet and discretise it as a set of vortex 'elements' (sections of vortex sheet, often individually represented by point vortices or equivalents thereof), but many of these methods also introduce ambiguity in the initial placement of newly shed vortex elements. For example, when considering the flow past a flat disc, de Bernardinis, et al. (1981) placed the new vortex 'ring' at the midpoint of the newly shed element. In their quasi-three-dimensional model of an insect wing Ansari, et al. (2006a) and Ansari, et al. (2006b) placed new point vortices one third of the way between the edge and the previously shed element. In the work of Krasny (1991) and Nitsche & Krasny (1994), who respectively modelled two-dimensional flow past a flat plate and flow out of a piston tube, the creation of the separated vortex sheet is modelled by releasing a new vortex element *exactly* at the edge at every timestep, and the circulation in that element is determined by the expression given by Prandtl & Tietjens (1934, p. 218) for the rate of circulation shedding. However, there is still a certain amount of ambiguity in their numerical method for the shedding procedure, such as their decision to exclude a small part of the bound vortex sheet in computing the average fluid velocity at the edge of the vortex sheet and their decision to ignore edge velocities above and below the edge of the bound vortex sheet if they are negative (which would imply attaching flow rather than separating).

Jones (2003) sought to circumvent these issues. When considering the two-dimensional flow of an inviscid fluid around a flat plate under translation and rotation he used Kelvin's circulation theorem to derive a constraint on the circulation of the separated vortex sheet *at the points of separation* in terms of the bound vortex sheet strength along a line joining the two edges. The same constraint can be derived in full generality by considering the contour in figure 1.3. This contour technically never pierces the sheet, so assuming that the vortex sheet in question originated from a flow that was initially at rest it is a consequence of Kelvin's circulation theorem that the circulation around it will necessarily remain at zero.

Splitting the contour up into its constituent parts allows us to state this more formally. We have

$$\oint_C dC \, \hat{\boldsymbol{t}}(\eta) \cdot \boldsymbol{u}(\eta) = \left(\int_{C_1} dC_1 + \int_{C_2} dC_2 + \int_{L^+} dL^+ + \int_{L^-} dL^- \right) (\hat{\boldsymbol{t}}(\eta) \cdot \boldsymbol{u}(\eta)) = 0.$$
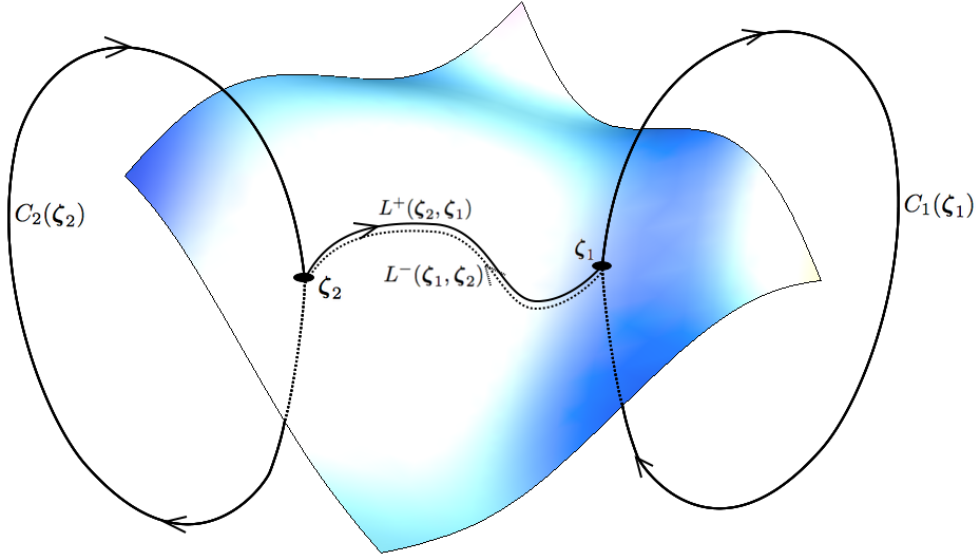
Figure 1.3: A simple, closed contour around a theoretical vortex sheet. The constituent parts $C_1(\boldsymbol{\zeta}_1)$ and $C_2(\boldsymbol{\zeta}_2)$ go to/from $\boldsymbol{\zeta}_1$ and $\boldsymbol{\zeta}_2$ respectively, but *do not* pierce the sheet. The lines L^+ and L^- lie just above and below the sheet respectively, but are, in effect, the same contour. Because this contour technically never pierces the sheet, the circulation around it will be zero.

The notation used here implies that we evaluate the integral around the entire contour, C, by evaluating the integral around each of its constituent parts separately, where $\hat{\boldsymbol{t}}(\eta)$ is the tangent to the contour at distance η along it. A number of deductions can be made in this equation. First, the integrals along the parts $C_1(\boldsymbol{\zeta}_1)$ and $C_2(\boldsymbol{\zeta}_2)$ alone give the circulation at $\boldsymbol{\zeta}_1$ and minus the circulation at $\boldsymbol{\zeta}_2$ respectively (because the definition of the circulation requires the contour to go from top to bottom of the sheet). Second, since the parts of the contour made up of $L^\pm$ lie on the sheet, their respective integrands will be $\hat{\boldsymbol{t}}(\eta) \cdot \boldsymbol{u}^\pm(\eta)$ (where the superscript $\pm$ refers to the fluid velocity just above and below the sheet). Finally, we have that $dL^+ \hat{\boldsymbol{t}}(\eta) = -dL^- \hat{\boldsymbol{t}}(\eta)$, and hence we can write

$$\Gamma(\boldsymbol{\zeta}_1) - \Gamma(\boldsymbol{\zeta}_2) = -\int_{L(\boldsymbol{\zeta}_2,\boldsymbol{\zeta}_1)} dL\, \hat{\boldsymbol{t}}(\eta) \cdot [\boldsymbol{u}^\pm(\eta)]_-^+,$$

where $L(\boldsymbol{\zeta}_2, \boldsymbol{\zeta}_1)$ defines the line between L^+ and L^-. Now recall that this work is being done to derive a constraint on the separated vortex sheet's circulation strength *at the edges of* the bound vortex sheet, in terms of the bound vortex sheet strength, so consider the case where $\boldsymbol{\zeta}_1 = \boldsymbol{e}_+$ and $\boldsymbol{\zeta}_2 = \boldsymbol{e}_-$, where $\boldsymbol{e}_\pm$ are points on the edge of the bound vortex sheet.

Then, expressing[5] $[\boldsymbol{u}^{\pm}(\eta)]_{-}^{+} = -\hat{\boldsymbol{n}}(\eta) \times \boldsymbol{\gamma}(\eta)$, and rearranging the order of the resulting scalar triple product we have

$$[\Gamma(\boldsymbol{e}_{\pm})]_{-}^{+} = \int_{L(\boldsymbol{e}_{+},\boldsymbol{e}_{-})} dL\big((\hat{\boldsymbol{t}}(\eta) \times \hat{\boldsymbol{n}}(\eta)) \cdot \boldsymbol{\gamma}(\eta)\big), \tag{1.6}$$

where $L(\boldsymbol{e}_{+}, \boldsymbol{e}_{-})$ is any line that lies on the bound vortex sheet joining $\boldsymbol{e}_{+}$ and $\boldsymbol{e}_{-}$ and has tangent vector $\hat{\boldsymbol{t}}(\eta)$.

Jones (2003) imposed the Kutta condition analytically by using this constraint as a condition on the behaviour of the bound vortex sheet strength near the limits of integration when tackling the ambiguity in the choice of inversion formula for the solution of the bound vortex sheet strength. In that way his model gave an expression for the bound vortex sheet strength that was *implicitly dependent* on the shed circulation in a way that *guaranteed* that the Kutta condition would be satisfied. This avoided the method of first computing the bound vortex sheet strength that satisfied the no penetration boundary condition but introduced singularities in the fluid velocity at the edges, then calculating the separated vortex sheet strength to cancel those singularities and allowed the process of vortex sheet separation could to be modelled in a 'natural' way.

His model did have some drawbacks, the main one being the apparent inability of his numerical method to deal with situations where the flow tried to attach rather than separate (as mentioned above in relation to the work of Nitsche & Krasny (1994)). This caused problems when the plate was made to interact with its own wake or travel at very low angle of attack, but he nonetheless produced impressive results which displayed good comparison with the empirical work of Keulegan & Carpenter (1958). Furthermore, his method has been used by later authors with equally impressive results. Jones & Shelley (2005) considered the problem of a flat card released from rest at some initial height and angle and modelled its path and shed wake as it fell under the action of gravity. Shukla & Eldredge (2007) adapted the method to model the flow past a deforming plate. Both experiments were able to model the process of boundary layer separation successfully.

No penetration boundary condition

We now consider the no penetration boundary condition on the bound vortex sheet and how to impose it (note that no penetration on the *separated* vortex sheet is guaranteed

---

[5]This can be shown by taking the cross product of $\hat{\boldsymbol{n}}$ and both sides of $\boldsymbol{\gamma} = \hat{\boldsymbol{n}} \times [\boldsymbol{u}^{\pm}]_{-}^{+}$ and using $\boldsymbol{x} \times (\boldsymbol{x} \times \boldsymbol{y}) = \boldsymbol{x}(\boldsymbol{x} \cdot \boldsymbol{y}) - |\boldsymbol{x}|^2 \boldsymbol{y}$ for any non-zero vectors $\boldsymbol{x}$ and $\boldsymbol{y}$, and noting that $\hat{\boldsymbol{n}} \cdot [\boldsymbol{u}^{\pm}]_{-}^{+} = 0$ (since normal velocity is continuous across a vortex sheet) and $|\hat{\boldsymbol{n}}|^2 = 1$ (since $\hat{\boldsymbol{n}}$ is a unit normal).

because it is advected with the flow). To derive the no penetration boundary condition, we first show that the fluid velocity induced *by* the sheet at a point $\boldsymbol{\zeta}$ *on* the sheet is given by

$$\boldsymbol{u}_b^\pm(t,\boldsymbol{\zeta}) = \mp\frac{1}{2}\hat{\boldsymbol{n}}(t,\boldsymbol{\zeta}) \times \boldsymbol{\gamma}(t,\boldsymbol{\zeta}) + \frac{1}{4\pi}\!\!\int_B dB\left(\frac{\boldsymbol{\lambda}-\boldsymbol{\zeta}}{|\boldsymbol{\lambda}-\boldsymbol{\zeta}|^3} \times \boldsymbol{\gamma}(t,\boldsymbol{\lambda})\right).$$

To derive this expression we must evaluate the limit $\boldsymbol{u}_b^\pm(t,\boldsymbol{\zeta}) = \lim_{\boldsymbol{r}\to\boldsymbol{\zeta}^\pm} \boldsymbol{u}_b(t,\boldsymbol{r})$ in equation (1.4) for $\boldsymbol{\zeta}^\pm$ a point on $B(t)$ as approached from above and below. We now go on to show how that limit is evaluated.

The integrand in equation (1.4) is singular at $\boldsymbol{\lambda} = \boldsymbol{r}$ if $\boldsymbol{r} = \boldsymbol{\zeta} \in B(t)$, so in order to evaluate the above limit, we use the linearity of the flow solution to split up the contribution from the bound vortex sheet into two constituent parts. We write $B = B' + C_\epsilon$, where C_ϵ is a disc of radius ϵ centered at $\boldsymbol{\zeta}$, and B' is the rest of the sheet excluding that disc. We then consider the limit $\boldsymbol{r} \to \boldsymbol{\zeta}^\pm$ *followed by* the limit $\epsilon \to 0$ (small enough values of ϵ ensure that we can always define C_ϵ as a disc for sufficiently smooth $B(t)$). The point $\boldsymbol{\zeta}$ now lies strictly away from B' so the velocity induced by B' at that point can be evaluated trivially through equation (1.4) and is single valued as approached from above or below. In the limit $\epsilon \to 0$ the contribution from this part is defined as the Cauchy principal value of equation (1.4), giving us

$$\lim_{\boldsymbol{r}\to\boldsymbol{\zeta}} \boldsymbol{u}_b(\boldsymbol{r}) = \frac{1}{4\pi}\!\!\int_B dB\frac{\boldsymbol{\lambda}-\boldsymbol{\zeta}}{|\boldsymbol{\lambda}-\boldsymbol{\zeta}|^3} \times \boldsymbol{\gamma}(\boldsymbol{\lambda}) + \lim_{\epsilon\to 0}\lim_{\boldsymbol{r}\to\boldsymbol{\zeta}^\pm}\frac{1}{4\pi}\underbrace{\int_{C_\epsilon} dC_\epsilon\frac{\boldsymbol{\lambda}-\boldsymbol{r}}{|\boldsymbol{\lambda}-\boldsymbol{r}|^3} \times \boldsymbol{\gamma}(\boldsymbol{\lambda})}_{I}. \qquad (1.7)$$

Note that we have dropped time from the notation for brevity WLOG. Now consider the integral I in equation (1.7). Assuming that $\boldsymbol{\gamma}(\boldsymbol{\lambda})$ has a Taylor expansion at $\boldsymbol{\zeta}$ we can subtract the first term in that expansion and write

$$I = \left(\int_{C_\epsilon} dC_\epsilon\frac{\boldsymbol{\lambda}-\boldsymbol{r}}{|\boldsymbol{\lambda}-\boldsymbol{r}|^3}\right) \times \boldsymbol{\gamma}(\boldsymbol{\zeta}) + \int_{C_\epsilon} dC_\epsilon\left(\frac{\boldsymbol{\lambda}-\boldsymbol{r}}{|\boldsymbol{\lambda}-\boldsymbol{r}|^3} \times \big(\boldsymbol{\gamma}(\boldsymbol{\lambda}) - \boldsymbol{\gamma}(\boldsymbol{\zeta})\big)\right). \qquad (1.8)$$

For simplicity, we now work in a coordinate frame where C_ϵ is centred at the origin and lies in the x-y plane. Indeed, this is possible for all $\boldsymbol{\zeta} \in B$ WLOG. This implies $\boldsymbol{\zeta} = \boldsymbol{0}$ and $\hat{\boldsymbol{n}}(\boldsymbol{\zeta}) = \boldsymbol{k}$. We then work in cylindrical polar coordinates with $\boldsymbol{\lambda} = \rho\hat{\boldsymbol{\rho}}(\phi)$ for $\rho \in [0,\epsilon]$ and $\phi \in [0,2\pi)$, where $\hat{\boldsymbol{\rho}}(\phi) = \cos\phi\boldsymbol{i} + \sin\phi\boldsymbol{j}$ is a radial unit vector in C_ϵ. We also write

$r = \pm\delta\boldsymbol{k}$, allowing us to simultaneously evaluate the limits $\boldsymbol{r} \to \boldsymbol{\zeta}^+$ and $\boldsymbol{r} \to \boldsymbol{\zeta}^-$ by $\delta \to 0$. Given that $\boldsymbol{\gamma}(\boldsymbol{\zeta})$ has no $\boldsymbol{\lambda}$ dependence, we parameterise the first integral in equation (1.8) and evaluate it trivially thus;

$$\lim_{\epsilon\to 0}\lim_{\delta\to 0}\left(\int_0^\epsilon \rho\,d\rho\int_0^{2\pi}d\phi\frac{\rho\hat{\boldsymbol{\rho}}(\phi)\mp\delta\boldsymbol{k}}{(\rho^2+\delta^2)^{\frac{3}{2}}}\right)\times\boldsymbol{\gamma}(\boldsymbol{0}) = \mp 2\pi\boldsymbol{k}\times\boldsymbol{\gamma}(\boldsymbol{0}) \equiv \mp 2\pi\hat{\boldsymbol{n}}(\boldsymbol{\zeta})\times\boldsymbol{\gamma}(\boldsymbol{\zeta}).\quad (1.9)$$

Now for the second integral in equation (1.8) we begin by expressing the difference in bound vortex sheet strengths at $\boldsymbol{\lambda}$ and $\boldsymbol{\zeta}$ as

$$\boldsymbol{\gamma}(\boldsymbol{\lambda}) - \boldsymbol{\gamma}(\boldsymbol{\zeta}) \sim (\boldsymbol{\lambda}\cdot\boldsymbol{\nabla})\boldsymbol{\gamma}(\boldsymbol{\lambda})\big|_{\boldsymbol{\lambda}=\boldsymbol{\zeta}} + O(\boldsymbol{\lambda}^2).$$

Note that $\boldsymbol{\lambda} = O(\epsilon)$ on C_ϵ so by rescaling the parameterising variable by $\rho = \epsilon\rho^*$, we have that $\boldsymbol{\lambda}\cdot\boldsymbol{\nabla} = \rho\dfrac{\partial}{\partial\rho} = \rho^*\dfrac{\partial}{\partial\rho^*}$. The integral then becomes

$$\int_{C_\epsilon}dC_\epsilon\left(\frac{\boldsymbol{\lambda}-\boldsymbol{r}}{|\boldsymbol{\lambda}-\boldsymbol{r}|^3}\times\big(\boldsymbol{\gamma}(\boldsymbol{\lambda})-\boldsymbol{\gamma}(\boldsymbol{\zeta})\big)\right)$$
$$= \int_0^1 \epsilon\rho^*\epsilon\,d\rho^*\int_0^{2\pi}d\phi\left(\frac{\epsilon\rho^*\hat{\boldsymbol{\rho}}(\phi)\mp\delta\boldsymbol{k}}{(\epsilon^2(\rho^*)^2+\delta^2)^{\frac{3}{2}}}\times\rho^*\frac{\partial}{\partial\rho^*}\boldsymbol{\gamma}(\epsilon\rho^*\hat{\boldsymbol{\rho}}(\phi))\Big|_{\rho^*=0}\right) + O\left(\epsilon^2\right).$$

Applying the chain rule to the derivative of $\boldsymbol{\gamma}$ and making use of the expansion

$$\left(1+\frac{\delta^2}{\epsilon^2(\rho^*)^2}\right)^{-\frac{3}{2}} \sim 1 - \frac{3}{2}\frac{\delta^2}{\epsilon^2(\rho^*)^2} + O(\delta^4),$$

near $\delta = 0$ it is possible to show that this term, and all subsequent terms in the Taylor expansion of $\boldsymbol{\gamma}$, disappear in the limit $\delta \to 0$ and $\epsilon \to 0$. This result, with equations (1.9) and (1.7), gives us the expression for the velocity induced *by* the vortex sheet *on* the vortex sheet

$$\boldsymbol{u}_b^\pm(\boldsymbol{\zeta}) = \mp\frac{1}{2}\hat{\boldsymbol{n}}(\boldsymbol{\zeta})\times\boldsymbol{\gamma}(\boldsymbol{\zeta}) + \frac{1}{4\pi}\int_B dB\left(\frac{\boldsymbol{\lambda}-\boldsymbol{\zeta}}{|\boldsymbol{\lambda}-\boldsymbol{\zeta}|^3}\times\boldsymbol{\gamma}(\boldsymbol{\lambda})\right).$$

As expected, there is a discontinuity in the tangential component of fluid velocity which is proportional to the bound vortex sheet strength. There will also be an additional part of the fluid velocity at $\boldsymbol{\zeta}$ that is induced by the separated vortex sheet, which we shall call $S(t)$. Since we have been defining $S(t)$ in terms of circulation rather than vortex sheet

strength, we continue to do so and include its contribution through the velocity *potential* it induces

$$\psi(\boldsymbol{r}) = \frac{1}{4\pi} \int_S \frac{dS(\hat{\boldsymbol{n}}(\boldsymbol{\sigma}) \cdot (\boldsymbol{\sigma} - \boldsymbol{r}))\Gamma(\boldsymbol{\sigma})}{|\boldsymbol{\sigma} - \boldsymbol{r}|^3}, \tag{1.10}$$

where $\hat{\boldsymbol{n}}(\boldsymbol{\sigma})$ is the unit normal at the point $\boldsymbol{\sigma}$ on S, and $\Gamma(\boldsymbol{\sigma})$ is the circulation there. It is possible to use the same method just outlined for deriving the velocity on the sheet to show that equation (1.10) is a suitable definition for the velocity potential (in that it satisfies equation (1.5)). The velocity induced on the *bound* vortex sheet by both the bound *and* separated vortex sheets therefore takes the form

$$\boldsymbol{u}^{\pm}(\boldsymbol{\zeta}) = \boldsymbol{\nabla}\psi(\boldsymbol{\zeta}) \mp \frac{1}{2}\hat{\boldsymbol{n}}(\boldsymbol{\zeta}) \times \boldsymbol{\gamma}(\boldsymbol{\zeta}) + \frac{1}{4\pi}\!\int_B dB\left(\frac{\boldsymbol{\lambda} - \boldsymbol{\zeta}}{|\boldsymbol{\lambda} - \boldsymbol{\zeta}|^3} \times \boldsymbol{\gamma}(\boldsymbol{\lambda})\right). \tag{1.11}$$

Taking the normal component of both sides of equation (1.11) and changing the order of the triple scalar product that arises in the integrand (as well as returning time to the notation for full generality) gives us the no penetration boundary condition on the bound vortex sheet strength

$$\frac{1}{4\pi}\!\int_{B(t)} \frac{dB(\hat{\boldsymbol{n}}(t, \boldsymbol{\zeta}) \times (\boldsymbol{\lambda} - \boldsymbol{\zeta})) \cdot \boldsymbol{\gamma}(t, \boldsymbol{\lambda})}{|\boldsymbol{\lambda} - \boldsymbol{\zeta}|^3} = \nu(t, \boldsymbol{\zeta}) - \boldsymbol{\nabla}\psi(t, \boldsymbol{\zeta}) \cdot \hat{\boldsymbol{n}}(t, \boldsymbol{\zeta}). \tag{1.12}$$

where $\nu(t, \boldsymbol{\zeta})$ is the normal component of the membrane's velocity (with which $B(t)$ is assumed incident) given by $\nu(t, \boldsymbol{\zeta}) = \boldsymbol{u}^{+}(t, \boldsymbol{\zeta}) \cdot \hat{\boldsymbol{n}}(\boldsymbol{\zeta}) = \boldsymbol{u}^{-}(t, \boldsymbol{\zeta}) \cdot \hat{\boldsymbol{n}}(\boldsymbol{\zeta})$. Equation (1.12) tells us that the velocity induced *by* the bound vortex sheet *on* the bound vortex sheet must be the same as the normal component of the bound vortex sheet's velocity (which is prescribed) minus the velocity *on* the bound vortex sheet as induced by the separated vortex sheet. Since the only unknown in this equation is the bound vortex sheet strength $\boldsymbol{\gamma}(t, \boldsymbol{\lambda})$, this equation, once parameterised by a given geometry, can be used to determine $\boldsymbol{\gamma}(t, \boldsymbol{\lambda})$ that will ensure no fluid flows through the bound vortex sheet, thus guaranteeing that the membrane which it represents is impermeable.

The remainder of this work is concerned with the solution of equation (1.12). It is not a new equation, and there do already exist numerical methods for solving it. Parameterisation of the equation for a given geometry usually gives rise to a Fredholm integral equation of the first kind with a Cauchy type kernel. When solving for the two-dimensional flow past a flat plate, Krasny (1991) discretised the bound vortex sheet by point vortices. Equa-

tion (1.12) was thus written as a system of linear equations which was solved by Gaussian elimination to ensure that (1.12) was satisfied at the midpoints of the point vortices. A similar method was employed by de Bernardinis et al. (1981), Nitsche & Krasny (1994) and Hou, et al. (2006).

However, numerical methods attempting to solve Fredholm equations of the first kind are prone to instability owing to the ill-posedness of equations of this type. This ill-posedness is well documented, and is due to, in part, to two main factors. First, the solution obtained may not be unique, and second, an $O(\epsilon)$ perturbation in the RHS can give rise to an order $O(1)$ perturbation in the solution; a property that we would expect to see replicated in a consistent numerical scheme. A more in depth discussion of this ill-posedness, with a number of further references, can be found in Anderssen, et al. (1980).

The work of Jones (2003) and Jones & Shelley (2005) eliminated these concerns by inverting the integral equation exactly by the formula in Muskhelishvili (1946, p. 249) and, as mentioned earlier, used the condition in equation (1.6) to satisfy the non-uniqueness of the solution. In the problems we will consider, an exact inversion is not possible. Instead, we will follow the method of Shukla & Eldredge (2007) and Alben (2009) to convert the Fredholm equation of the first kind into one of the second kind. Shukla & Eldredge (2007) used a similar parameterisation as Jones (2003) but considered the flow past a *deforming* body rather than a strictly flat one. They showed that in the limit of zero deformity (i.e. a flat plate) their equations reduced to the same as those of Jones (2003).

The aim of this work is to be a first stepping stone towards a *fully* three-dimensional theory of boundary layer separation. Such a theory would require massively increased computational time and resources than those involved in comparable calculations of a two-dimensional nature, and that increase would be even greater for flow solutions involving mathematically complicated geometries such as those encountered in insect flight. Indeed, it is precisely problems like that of insect flight that display fully three-dimensional flow and that are the inspiration for this work. For that reason, this work considers a three-dimensional, axi-symmetric flow problem which has, in essence, already been solved by de Bernardinis et al. (1981), but approaches it from a perspective that always 'keeps an eye' on the consequences of our decisions on an extension of the method to a fully three-dimensional calculation. In that respect, we pursue the rigorous analytical treatment of anything that might have a detrimental effect on the accuracy of a numerical procedure to solve equation (1.12); in particular, the explicit identification and exact integration of singularities in the governing equations. We are also careful to avoid exploiting the quasi-

two-dimensional nature of the problem that arises from the axi-symmetry of the geometry in a way that would not be transferable into a fully three-dimensional problem. It is hoped that by applying these guidelines to ourselves, a similar method to that developed in this work could be applied to the efficient and accurate solution of a fully-three-dimensional problem.

Certain three-dimensional flow problems of this nature have been considered in the past. The work of Nitsche & Krasny (1994) was also axi-symmetric, but their use of a stream-function exploited the quasi-two-dimensional nature of the problem to an extent that can never be transferred to three-dimensions. de Bernardinis et al. (1981) considered flow past a flat disc (the same problem that we will consider) but, restricted by the computational power available at the time, their treatment of the no-penetration boundary condition, boundary layer separation and evolution of the separated vortex sheet shows little promise for efficient conversion into problems of a three-dimensional nature. Ansari et al. (2006a) and Ansari et al. (2006b) split up the motion of a three-dimensional wing into a series of two-dimensional strips and summed the force and lift from each of them to give a quasi-three-dimensional model. They cited the work of Birch & Dickinson (2001) and Sane & Dickinson (2001), both of whom observed a strong LEV on an insect wing but *did not* observe that LEV inducing spanwise flow, as justification for not including any interaction between adjacent strips. For that reason, their model does not have a natural extension in three-dimensions. Furthermore, they exploited conformal mapping methods to map the bound vortex sheet onto a circle and solved the no penetration boundary condition there. Despite this method being used by a number of other authors (Cortelezzi et al. 1997, Yu, et al. 2003, Kelly & Xiong 2010) it is not used in our formulation because it *'could not be generalised in order to tackle three-dimensional problems'* (Jones 2003).

As mentioned earlier, this work is to be a first stepping stone. We are not concerned with solving a problem to the point of comparison with physical experimentation. We treat the problem of modelling the evolution of a three-dimensional separated vortex sheet as having already been solved, and we work under the pretence that imposing the Kutta condition is a natural extension to solving the no penetration boundary condition. We believe that it is the rigorous mathematical analysis of the no penetration boundary condition that will allow the development of a fully three-dimensional theory of boundary layer separation, and we aim to set a precedent for the depth of that analysis through this work.

The rest of the work proceeds as follows. In chapter 2 we directly parameterise equation (1.12) and develop an efficient numerical method for it before applying that numerical

method to the attached flow problem. Then in chapter 3 we show that taking a less naïve approach to the same problem can lead to an exact solution for the attached flow problem, and an extremely efficient numerical method for the full separated problem. Both chapters concern themselves solely with solving equation (1.12) in the absence of a wake (although the equations are developed in full generality) and therefore without the satisfaction of the Kutta condition. Laminar flow is assumed throughout. Then follow the appendices and references.

Chapter 2

The axisymmetric disc

We begin by considering the motion of a flat, axisymmetric disc travelling perpendicular to itself. We centre the disc at the origin in the (x, y) plane, and work in cylindrical polar coordinates, parameterising equation (1.12) by

$$
\begin{aligned}
\boldsymbol{\lambda} &= \rho\hat{\boldsymbol{\rho}}(\phi) + \zeta\boldsymbol{k} &, &\quad \text{a vector in the disc (dummy variable)}, \\
\boldsymbol{\zeta} &= r\hat{\boldsymbol{\rho}}(\theta) + \zeta\boldsymbol{k} &, &\quad \text{another vector in the disc}, \\
\hat{\boldsymbol{n}}(t, \boldsymbol{\zeta}) &= \boldsymbol{k} &, &\quad \text{normal to the disc at } \boldsymbol{\zeta}, \\
\nu(t, \boldsymbol{\zeta}) &= \nu &, &\quad \text{normal component of disc velocity at } \boldsymbol{\zeta},
\end{aligned}
\tag{2.1}
$$

where $\hat{\boldsymbol{\rho}}(\phi) = \cos\phi\,\boldsymbol{i} + \sin\phi\,\boldsymbol{j}$ is the unit radial vector. Notice that we maintain a distinction between the dummy variable $\boldsymbol{\lambda}$ parameterised in terms of ρ and ϕ (which become the new variables of integration) and the coordinate point $\boldsymbol{\zeta}$ parameterised in terms of r and θ. Either way, we have $\rho, r \in [0, 1]$, $\phi, \theta \in [0, 2\pi)$ and $\zeta \in (-\infty, \infty)$. The variable of integration dB becomes $\rho\,d\rho\,d\phi$ and we have dropped time from the notation for brevity.

The axisymmetric nature of this problem allows us to make some important simplifications regarding the unknown bound vortex-sheet strength $\boldsymbol{\gamma}(\boldsymbol{\lambda})$. First, its magnitude will only depend on its distance from the origin. Then, the vortex filaments that make up $B(t)$ will have no component in the radial direction. This comes from the axiom that all vortex filaments must be closed (or end on a solid surface), and allows us to write $\boldsymbol{\gamma}(\boldsymbol{\lambda}) = \gamma(\rho)\hat{\boldsymbol{\phi}}(\phi)$, where $\hat{\boldsymbol{\phi}}(\phi) = -\sin\phi\,\boldsymbol{i} + \cos\phi\,\boldsymbol{j}$ and $\gamma(\rho)$ is the magnitude, and is the only unknown.

2.1   Parameterisation and simplification of the no penetration boundary condition

In this section we begin by parameterising and simplifying the no penetration boundary condition equation (1.12) through the variables given in (2.1). Since the problem is axisymmetric, we then integrate over ϕ to derive a Fredholm singular integral equation of the first kind, and apply the method of removing the Cauchy type singularity used by Shukla & Eldredge (2007) to convert this into a Fredholm integral equation of the second kind. We extend this method by subtracting further logarithmic singularities and applying contour integral methods to integrate them analytically, circumventing the need to represent singular functions in the numerical method outlined in the next section.

Plugging in the variables in equation (2.1) into the no penetration boundary condition and writing in terms of $\alpha = \dfrac{2\rho r}{(r^2 + \rho^2)}$ and $u = \theta - \phi$ we have

$$\frac{1}{4\pi}\oint_B dB \frac{(\hat{\boldsymbol{n}}(\boldsymbol{\zeta}) \times (\boldsymbol{\lambda} - \boldsymbol{\zeta})) \cdot \boldsymbol{\gamma}(\boldsymbol{\lambda})}{|\boldsymbol{\lambda} - \boldsymbol{\zeta}|^3} = \frac{1}{2\pi}\int_0^1 d\rho \frac{\rho\gamma(\rho)}{(r^2 + \rho^2)^{\frac{3}{2}}} \int_0^\pi du \frac{\rho - r\cos u}{(1 - \alpha\cos u)^{\frac{3}{2}}}. \tag{2.2}$$

Notice, we would have expected the integrand in equation (1.12) to be singular at $\boldsymbol{\lambda} = \boldsymbol{\zeta}$, which in equation (2.2) is at $\rho = r$ and $\theta = \phi$, or $\alpha = 1$ and $u = 0$. We now go on to examine this behaviour more carefully. It is possible to integrate over ϕ (or the new variable u) by the integral identities in equations (B.7) and (B.8) in appendix B. Ultimately, equation (1.12) becomes a Fredholm singular integral equation of the first kind

$$\frac{1}{\pi}\int_0^1 d\rho\, \kappa(\rho, r)\gamma(\rho) = 2\nu - 2\boldsymbol{\nabla}\psi(r, \zeta) \cdot \boldsymbol{k}, \tag{2.3}$$

where the kernel κ is

$$\kappa(\rho, r) = \frac{1}{\rho + r}K\left(\frac{4\rho r}{(\rho + r)^2}\right) + \frac{1}{\rho - r}E\left(\frac{4\rho r}{(\rho + r)^2}\right), \tag{2.4}$$

in terms of the complete elliptic integrals of the first (K) and second (E) kind. Note that the argument of the elliptic integrals at $\rho = r$ is 1, and that $E(1) = 1$ and $K(m) \sim -\log(1-m)$ as $m \to 1$. Therefore, while both the terms in equation (2.4) are singular at $\rho = r$, the second term is more strongly so than the first.

For reasons set out in the previous chapter, it would be unwise to attempt a numerical method to solve equation (2.3) directly. Instead, we want to start by converting equation

(2.3) into a Fredholm integral equation of the *second* kind. To do this, we look more closely at the singular nature of $\kappa(\rho, r)$.

2.1.1 Desingularising the kernel and inverting the Fredholm equation of the first kind

Expanding the Cauchy type term in (2.4) close to $\rho = r$ gives

$$\frac{1}{\rho - r} E\left(\frac{4\rho r}{(\rho + r)^2}\right) \sim \frac{1}{\rho - r}\left(1 + O\big((\rho - r)^2 \log|\rho - r|\big)\right).$$

We see that the leading order singularity in $\kappa(\rho, r)$ is Cauchy type and we wish to remove this singularity analytically so that we do not have to try to approximate it numerically. We do this by rewriting equation (2.3) as

$$\frac{1}{\pi}\int_0^1 \frac{d\rho}{\rho - r}\gamma(\rho) = 2\nu - 2\boldsymbol{\nabla}\psi(r, \zeta) \cdot \boldsymbol{k} - \frac{1}{\pi}\int_0^1 d\rho M(\rho, r)\gamma(\rho), \tag{2.5}$$

where the new kernel $M(\rho, r)$ is the original kernel with the Cauchy singularity subtracted,

$$M(\rho, r) = \kappa(\rho, r) - \frac{1}{\rho - r}, \tag{2.6}$$

and will therefore be more suitable for numerical approximation. The left hand side of equation (2.5) can be inverted analytically in a number of ways, depending on the behaviour of $\gamma(\rho)$ at the endpoints. As mentioned earlier, Jones (2003) circumvented this ambiguity by directly applying Kelvin's circulation theorem through equation (1.6) as part of the solution. In this work we are primarily interested in solving the no penetration boundary condition for attached flow, and we therefore set the edge circulation to zero, making equation (1.6) automatically satisfied. In fact, we would expect the circulation on the disc to take the form $\Gamma(r) \sim (1 - r^2)^{1/2}$ (see e.g. Lindsay & Krasny (2001)), and since vortex sheet strength can be crudely thought of as the derivative of circulation, we expect it to take the form $\gamma(r) \sim r(1 - r^2)^{-1/2}$. We therefore choose the inversion formula for equations of the form (2.5) that automtically builds in singularities of that nature at $r = 1$ (note that $r = -1$ is outside of our domain); that is

$$\frac{1}{\pi}\int_a^b \frac{d\rho}{\rho - r}\gamma(\rho) = f(r) \quad \Rightarrow \quad \gamma(r) = \frac{-1}{\pi}\sqrt{\frac{r - a}{b - r}}\int_a^b \frac{d\sigma}{\sigma - r}\sqrt{\frac{b - \sigma}{\sigma - a}}f(\sigma). \tag{2.7}$$

We could have chosen an inversion formula which built in singularities at both ends, or neither end, but both those options would actually be a step *away* from the physical solution we expect, and would force the numerical method to build in singularities to account for those we have ignored, thus making it less accurate. Applying this inversion to equation (2.5) and rearranging gives us

$$\gamma(r) - \frac{1}{\pi}\frac{\sqrt{r}}{\sqrt{1-r}}\int_0^1 d\rho\, N(\rho,r)\gamma(\rho) = 2\frac{\sqrt{r}}{\sqrt{1-r}}\left(\nu + \nu_1(r;\zeta)\right), \tag{2.8}$$

with

$$\nu_1(r;\zeta) = \frac{1}{\pi}\int_0^1 \frac{d\sigma}{\sigma - r}\frac{\sqrt{1-\sigma}}{\sqrt{\sigma}}\left(\boldsymbol{\nabla}\psi(\sigma,\zeta)\cdot\boldsymbol{k}\right)$$

$$N(\rho,r) = \frac{1}{\pi}\int_0^1 \frac{d\sigma}{\sigma - r}\frac{\sqrt{1-\sigma}}{\sqrt{\sigma}}M(\rho,\sigma). \tag{2.9}$$

In this calculation we have used the integral identity in equation (A.1). $N(\rho,r)$ contains no unknowns, and we intend to evaluate it numerically. However, the reader will recall that there are logarithmic singularities in $M(\rho,\sigma)$ for all $\rho = \sigma$ and more strongly at $\rho = \sigma = 0$. These could make a numerical approximation of $M(\rho,\sigma)$ inaccurate and make the numerical evaluation of $N(\rho,r)$ more difficult, so we wish to take them out analytically.

2.1.2   Desingularising the integrand in $N(\rho,r)$

Expanding the term containing the elliptic integral of the first kind in equation (2.4) close to $\rho = r$ allows us to deduce the coefficient of the log singularity that we suspect this term contains;

$$\frac{1}{\rho + r}K\left(\frac{4\rho r}{(\rho + r)^2}\right) \sim \frac{1}{2r}\left(\log\left(\frac{1}{|\rho - r|}\right) + \log(r) + 3\log(2)\right) + O\left((\rho - r)\log|\rho - r|\right). \tag{2.10}$$

We wish to remove this singularity in a fashion similar to that used for the Cauchy singularity, and integrate it analytically so that we don't have to approximate it in our numerical evaluation of $N(\rho,r)$. Therefore, we write

$$N(\rho, r) = \frac{1}{\pi}\frac{1}{2\rho}\left(\fint_0^1 \frac{d\sigma}{\sigma - r}\frac{\sqrt{1-\sigma}}{\sqrt{\sigma}}L(\rho,\sigma) - \int_0^1 \frac{d\sigma}{\sigma - r}\frac{\sqrt{1-\sigma}}{\sqrt{\sigma}}\log\left|\frac{\rho - \sigma}{\rho + \sigma}\right|\right), \qquad (2.11)$$

where the new kernel $L(\rho, \sigma)$ is non-singular[1] for all ρ, $\sigma \in [0, 1]$;

$$L(\rho, \sigma) = 2\rho M(\rho, \sigma) + \log\left|\frac{\rho - \sigma}{\rho + \sigma}\right|.$$

This formulation of $N(\rho, r)$ has two advantages. First, the non-singular nature of $L(\rho, \sigma)$ makes it a lot easier to approximate numerically, and therefore makes our numerical approximation of $N(\rho, r)$ a lot more accurate. Then, there is the significant advantage that the singular part of $M(\rho, \sigma)$, that is, the logarithmic part, can be integrated out analytically (see appendix C). Furthermore, the choice of inversion formula that came about as a result of our deductions about the form of $\gamma(r)$ suggests that we should subsequently work under the ansatz

$$\gamma(r) = \frac{\sqrt{r}}{\sqrt{1 - r}}g(r). \qquad (2.12)$$

Combining all of this, with equation (C.10), equation (2.8) becomes

$$g(r) - \frac{1}{\pi}\int_0^1 \frac{d\rho\,\mathcal{N}(\rho, r)g(\rho)}{\sqrt{\rho}\sqrt{1-\rho}} - \frac{1}{\pi}\int_0^1 \frac{d\rho\,\mathcal{A}(\rho, r)g(\rho)}{\sqrt{\rho}\sqrt{1-\rho}} + \frac{1}{2}\frac{\sqrt{1-r}}{\sqrt{r}}\int_0^r \frac{d\rho\,g(\rho)}{\sqrt{\rho}\sqrt{1-\rho}} = 2\nu + 2\nu_1(r;\zeta),$$

$$(2.13)$$

where

$$\mathcal{N}(\rho, r) = \frac{1}{2\pi}\fint_0^1 \frac{d\sigma}{\sigma - r}\frac{\sqrt{1-\sigma}}{\sqrt{\sigma}}L(\rho, \sigma),$$

$$\mathcal{A}(\rho, r) = \frac{\sqrt{1 - r}}{\sqrt{r}}\arctan\left(\frac{\sqrt{r}\sqrt{1 + \rho}}{\sqrt{1 - r}\sqrt{\rho}}\right) - \text{arcsinh}(\sqrt{\rho}).$$

We have made a number of rearrangements here for convenience. First, we have split up equation (2.11), and taken the coefficient of $1/2$ inside the definitions of $\mathcal{N}$ and $\mathcal{A}$ whilst

---

[1]Note that whilst $L(\rho, \sigma)$ is *non-singular* for all ρ, $\sigma \in [0, 1]$, it is undefined at $\rho = \sigma = 0$. This phenomenon has ultimately arisen from the fact that the flow induced at radius r by a closed, circular vortex filament of radius ρ can be written as a function solely of the ratio ρ/r and is thus undefined at $\rho = r = 0$. The implications of this are discussed in more detail in chapter 3.

taking the coefficient of $1/\rho$ out into the integrals of equation (2.13). We have also split off the Heaviside function in equation (C.10) to be dealt with separately in equation (2.13) as the third integral term on the LHS. This is because we do not want to have to make a numerical approximation of a function that contains a finite jump, and we will integrate out this jump analytically in the next section.

The analytic work we have pursued in this section will make a numerical scheme to solve this equation vastly more efficient and accurate than if we had naïvely attacked equation (2.3). Let us now go on to consider how to exploit the properties of Chebyshev polynomials and eigenfunctions to develop such a numerical scheme.

2.2   Numerical scheme

In this section we begin by laying out the very basics of eigenfunctions theory of integral equations and how we intend to use that theory to solve equation (2.13). We then go on to apply that theory to the problem at hand and develop an efficient numerical scheme for finding $g(r)$ in equation (2.13) for general right hand side.

Let Λ denote the integral operator defined by

$$\Lambda(g)(r) := g(r) - \frac{1}{\pi}\int_0^1 \frac{d\rho\,\mathcal{N}(\rho,r)g(\rho)}{\sqrt{\rho}\sqrt{1-\rho}} - \frac{1}{\pi}\int_0^1 \frac{d\rho\,\mathcal{A}(\rho,r)g(\rho)}{\sqrt{\rho}\sqrt{1-\rho}} + \frac{1}{2}\frac{\sqrt{1-r}}{\sqrt{r}}\int_0^r \frac{d\rho\,g(\rho)}{\sqrt{\rho}\sqrt{1-\rho}}.$$

$$(2.14)$$

We would like to find the n eigenfunctions $\phi_n(r)$ and corresponding eigenvalues λ_n of Λ that satisfy

$$\Lambda(\phi_n)(r) = \lambda_n \phi_n(r), \tag{2.15}$$

and subsequently solve for the coefficients g_n such that

$$g(r) = \sum_{n=0}^{\infty} g_n \phi_n(r), \tag{2.16}$$

$$\Lambda(g)(r) = 2\nu + 2\nu_1(r;\zeta). \tag{2.17}$$

2.2.1 Finding the eigenfunctions and eigenvalues of Λ

Let us first consider the problem of finding the eigenfunctions and eigenvalues of Λ. We will define the eigenfunctions in terms of the shifted Chebyshev polynomials thus

$$\phi_n(r) = \sum_{n=0}^{\infty} \phi_{mn} T_m^*(r), \tag{2.18}$$

and seek to find the matrix ϕ_{mn}. We will deal with the three integrals in equation (2.14) separately and in quite different ways.

We start by considering the easiest term; that containing $\mathcal{A}(\rho, r)$ in equation (2.14). By defining this function as a series of shifted Chebyshev polynomials

$$\mathcal{A}(\rho, r) = \sum_{i=0}^{\infty} \sum_{j=0}^{\infty} \mathcal{A}_{ij} T_i^*(\rho) T_j^*(r),$$

we can use the identity in equation (F.4) to express

$$\frac{1}{\pi} \int_0^1 \frac{d\rho \, \mathcal{A}(\rho, r) \phi_n(\rho)}{\sqrt{\rho}\sqrt{1-\rho}} = \frac{1}{2} \sum_{i=0}^{\infty} \sum_{j=0}^{\infty} (1 + \delta_{0i}) \mathcal{A}_{ij} \phi_{in} T_j^*(r), \tag{2.19}$$

where the constant coefficients $\mathcal{A}_{ij}$ can be calculated through equation (F.7) if the sum is truncated at $i = j = N - 1$.

Now, consider the Heaviside term (the integral from 0 to r) of equation (2.14). We purposefully excluded this term from the definition $\mathcal{A}(\rho, r)$ because a Chebyshev series approximation of a function with a finite jump (such as a Heaviside function) converges very slowly. Instead, we can integrate out this jump analytically. Substituting equation (2.18) this term becomes

$$\frac{1}{2} \frac{\sqrt{1-r}}{\sqrt{r}} \int_0^r \frac{d\rho \, \phi_n(\rho)}{\sqrt{r}\sqrt{1-r}} = \frac{1}{2} \frac{\sqrt{1-r}}{\sqrt{r}} \sum_{i=0}^{\infty} \phi_{in} \int_0^r \frac{d\rho \, T_i^*(\rho)}{\sqrt{r}\sqrt{1-r}}.$$

We have replaced the m index with i for to make the indices consistent with the other terms. We 'un-shift' the Chebyshev polynomials by the substitution $s = 2\rho - 1$, and subsequently exploit the cosine definition of the Chebyshev polynomials (see appendix F) by the substitution $s = \cos\theta$ to give us

$$\frac{1}{2} \frac{\sqrt{1-r}}{\sqrt{r}} \sum_{i=0}^{\infty} \phi_{in} \int_0^r \frac{d\rho \, T_i^*(\rho)}{\sqrt{r}\sqrt{1-r}} = \frac{1}{2} \sum_{i=0}^{\infty} \phi_{in} H_i(r),$$

where $H_i(r)$ comes from actually evaluating the integral, and is defined piecewise as

$$H_i(r) = \frac{\sqrt{1-r}}{\sqrt{r}} \begin{cases} \pi - \arccos(2r-1) & , \quad i = 0, \\[2ex] \dfrac{-\sin\left(i\arccos(2r-1)\right)}{i} & , \quad i > 0. \end{cases}$$

Note that this function *is* defined for all $r \geq 0$. Now, in order to write this term in a similar form to equation (2.19), we define $H_i(r)$ as

$$H_i(r) = \sum_{j=0}^{\infty} H_{ij} T_j^*(r). \tag{2.20}$$

At this point, we would normally use equation (F.6) to find the coefficients H_{ij}, but the form of $H_i(r)$ makes it possible to find them analytically for $i > 0$. We start by multiplying both sides of equation (2.20) by $T_k^*(r)$ for some $k \in \mathbb{Z}^+$, but we then make use of the *continuous* orthogonality property (equation (F.4)) instead of the *discrete* one (equation (F.3)) by integrating both sides against the appropriate kernel;

$$\int_0^1 \frac{T_k^*(r) H_i(r)}{\sqrt{r}\sqrt{1-r}} dr = \sum_{j=0}^{\infty} H_{ij} \int_0^1 \frac{T_k^*(r) T_j^*(r)}{\sqrt{r}\sqrt{1-r}} dr. \tag{2.21}$$

Plugging in the definition of $H_i(r)$, and making similar substitutions as above ($\bar{r} = 2r - 1$ followed by $\bar{r} = \cos\theta$), the integral on the RHS of equation (2.21) can be done analytically (equation (A.2) in appendix A). This leads us to our definition of the coefficients

$$H_{ij} = (2 - \delta_{0j}) \begin{cases} \dfrac{1}{N} \displaystyle\sum_{k=0}^{N-1} H_i(r_k) T_j^*(r_k) & , \quad i = 0, \\[3ex] \dfrac{\delta_{ij} - 2}{2i} \begin{cases} 0 & , \quad j > i, \\ (-1)^{i+j+1} & , \quad j \leq i. \end{cases} & , \quad i > 0 \end{cases}$$

where r_k are the shifted Chebyshev zeros, as defined in equation (F.5). Despite looking rather complicated, this formulation is much faster and more accurate than computing *all* the coefficients H_{ij} by discrete cosine transforms. It is exactly this sort of vigorous analytic treatment of the integral terms which, in the long-run, could allow us to counter the massively increased computation times involved in fully three-dimensional calculations. Ultimately, we can write the Heaviside integral in equation (2.13) in a similar form to equation (2.19) by

$$\frac{1}{2}\frac{\sqrt{1-r}}{\sqrt{r}}\int_0^r \frac{d\rho\,\phi_n(\rho)}{\sqrt{r}\sqrt{1-r}} = \frac{1}{2}\sum_{i=0}^{\infty}\sum_{j=0}^{\infty}H_{ij}\phi_{in}T_j^*(r). \tag{2.22}$$

Now to consider the first integral term in equation (2.14). This is rather more difficult because we have no analytic expression for $\mathcal{N}(\rho,r)$. However, we do have an analytic definition of $L(\rho,\sigma)$, so we start by expressing a new function $\bar{L}(\rho,\sigma)=(1-\sigma)L(\rho,\sigma)$ as

$$\bar{L}(\rho,\sigma) = \sum_{i=0}^{\infty}\sum_{j=0}^{\infty}\bar{L}_{ij}T_i^*(\rho)T_j^*(\sigma),$$

where, again, we know the $\bar{L}_{ij}$ through equation (F.7). We use this new function so that we can apply the integral identity in equation (F.8) to

$$\mathcal{N}(\rho,r) = \frac{1}{2\pi}\sum_{i=0}^{\infty}\sum_{j=0}^{\infty}\bar{L}_{ij}T_i^*(\rho)\int_0^1 \frac{d\sigma}{\sigma-r}\frac{T_j^*(\sigma)}{\sqrt{\sigma}\sqrt{1-\sigma}}, \tag{2.23}$$

by transforming this integral onto the period -1 to 1 through the substitutions $\bar{\sigma}=2\sigma-1$ and $\bar{r}=2r-1$, thus giving us

$$\mathcal{N}(\rho,r) = \sum_{i=0}^{\infty}\sum_{j=1}^{\infty}\bar{L}_{ij}T_i^*(\rho)U_{j-1}^*(r),$$

where $U_j^*(r)$ is the jth shifted Chebyshev polynomial of the *second* kind. Notice that the coefficient of $1/2$ in equation (2.23) has been cancelled by a 2 that came from transforming the integral. However, we wish to express $\mathcal{N}(\rho,r)$ purely in terms of the *first* kind polynomials. To do this, we use the recurrence relation between the first and second kind polynomials in equation (F.10), and derive the backwards recurrence relation

$$\mathcal{N}(\rho,r) = \sum_{i=0}^{N-1}\sum_{j=0}^{N-1}\mathcal{N}_{ij}T_i^*(\rho)T_j^*(r),$$

$$\mathcal{N}_{ij} = \begin{cases} 0 & ,\quad j = N-1, \\ 2\bar{L}_{i,N-1} & ,\quad j = N-2, \\ (2-\delta_{0j})\left(\bar{L}_{i,j+1}+\dfrac{\mathcal{N}_{i,j+2}}{2}\right) & ,\quad 0 \le j \le N-3. \end{cases}$$

We have inevitably been forced to truncate the series at N terms for the backwards re-

currence relation to make any sense. However, given that we can choose N as large as we want, we will continue to refer to the upper limit of the sum as ∞ for continuity with the other terms in the equation. We can now put this definition into the first integral in equation (2.14), and following the same steps as for the integral containing the $\mathcal{A}(\rho, r)$ term, derive

$$\frac{1}{\pi} \int_0^1 \frac{d\rho \, \mathcal{N}(\rho, r)\phi_n(\rho)}{\sqrt{\rho}\sqrt{1-\rho}} = \frac{1}{2} \sum_{i=0}^{\infty} \sum_{j=0}^{\infty} (1 + \delta_{0i}) \mathcal{N}_{ij} \phi_{in} T_j^*(r). \tag{2.24}$$

Collating equations (2.19), (2.22) and (2.24) we have

$$\Lambda(\phi_n)(r) = \sum_{i=0}^{\infty} \sum_{j=0}^{\infty} \kappa_{ij} \phi_{in} T_j^*(r) = \lambda_n \sum_{i=0}^{\infty} \sum_{j=0}^{\infty} \phi_{in} \delta_{ij} T_j^*(r), \tag{2.25}$$

where the matrix κ_{ij} is fully known and comes from the calculations we have just done. We express it as

$$\kappa_{ij} = \delta_{ij} - \frac{1}{2}(1 + \delta_{0i})(\mathcal{N}_{ij} + \mathcal{A}_{ij}) + \frac{1}{2}H_{ij}. \tag{2.26}$$

Now since the shifted Chebyshev polynomials are orthogonal, equation (2.25) gives us a simple eigensystem to solve;

$$\sum_{i=0}^{\infty} \kappa_{ij} \phi_{in} = \lambda_n \phi_{jn}. \tag{2.27}$$

This implies that the columns of ϕ_{in} are the eigenvectors of the matrix $\alpha_{ij} = \kappa_{ij}^T$ with corresponding eigenvalues λ_n. There are a number of relatively fast, off the shelf packages for computing the eigensystem of a matrix so, given the fact that we only need to find them once, there is no need for us to write our own.

2.2.2   Computing the coefficients g_n

Once we have ϕ_{in}, we need to derive expressions similar to that in equation (2.16) for ν and $\nu_1(r; \zeta)$ in terms of $\phi_n(r)$. For constant ν, we simply need

$$\nu = \sum_{i=0}^{\infty} \sum_{n=0}^{\infty} \nu_n \phi_{in} T_i^*(r). \tag{2.28}$$

In order for the RHS of this equation to be constant we need the matrix-vector product $\phi_{in}\nu_n = \nu\delta_{0i}$, or $\nu_n = \nu\phi_{n0}^{-1}$; that is, the coefficients ν_n are the first column of the inverse of ϕ_{in}. Again, since there are a number of relatively fast, off the shelf packages for computing the inverse of a matrix, and since we only need do it once for all time, there will be no need for us to write our own.

Depending on the form of $\nu_1(r;\zeta)$, there may be a number of ways to compute the coefficients $\bar{\nu}_n$ that satisfy

$$\nu_1(r;\zeta) = \sum_{i=0}^{\infty}\sum_{n=0}^{\infty}\bar{\nu}_n\phi_{in}T_i^*(r). \tag{2.29}$$

For the purpose of this work, we are primarily concerned with the rapid solution of equation (2.13) for *general* right-hand side. Different authors may use different methods of modelling the vorticity in the wake of the disc; we are not particularly interested in that part of the calculation. As long as there is an accurate method of evaluating $\nu_1(r;\zeta)$ for given $(r;\zeta)$, we can use

$$\bar{\nu}_n = \sum_{i=0}^{N-1}\phi_{in}^{-1}\left(\frac{2-\delta_{0i}}{N}\sum_{k=0}^{N-1}\nu_1(r_k;\zeta)T_i^*(r_k)\right), \tag{2.30}$$

where the term in the brackets give the coefficients of the Chebyshev series approximation of $\nu_1(r;\zeta)$ as in equation (F.6). This method *is* crude, but will suffice for the purpose of the current study. Subsequently, equation (2.13) becomes

$$\Lambda(g)(r) = \sum_{i=0}^{\infty}\sum_{n=0}^{\infty}g_n\lambda_n\phi_{in}T_i^*(r) = \sum_{i=0}^{\infty}\sum_{n=0}^{\infty}\left(\nu_n+\bar{\nu}_n\right)\phi_{in}T_i^*(r). \tag{2.31}$$

Since ϕ_{in} has a unique inverse and the Chebyshev polynomials are orthogonal, we must have

$$g_n = \frac{\nu_n + \bar{\nu}_n}{\lambda_n}. \tag{2.32}$$

This is an extremely efficient method for finding the constants g_n. All 'expensive' work such as inverting matrices and computing eigenvectors/-values has been done *a priori* and all that is left is to compute the coefficients $\nu_n + \bar{\nu}_n$ at each timestep and divide by the λ_n element-wise. Computing these coefficients requires a scalar-vector product (to find ν_n) and a discrete cosine transform (DCT) followed by a matrix-vector product (to find $\bar{\nu}_n$), both of which are rapid calculations.

2.3   Numerical results

In this section we will consider solutions that arise from the numerical method set out in the preceding section. We will plot the solution and consider its accuracy, before going on to validate the numerical method.

We use a slightly amended version of an off-the-shelf discrete cosine transform (DCT) code, written in C and implemented in Xcode 3.1, from Press, et al. (2007) to compile the matrix κ_{ij}, and compute the eigenvalues and eigenvectors of $\alpha_{ij} = \kappa_{ij}^T$ (in equation (2.27) truncated at $i = N - 1$) using Wolfram Mathematica 7.0, which in turn uses the Implicitly Restarted Arnoldi Method (IRAM). Our method is specifically designed so that we need only perform these computations one time *a priori*, ensuring that the speed at which they occur is not crucial to the overall efficiency of the numerical method. For simplicity, we will only consider flows with *no* wake. The mathematical upshot of this is that all $\bar{\nu}_n = 0$, and it provides us with an easy way of testing the fundamental efficiency of our numerical method without introducing errors that might come about as a result of numerical integration required to compute the flow induced by the wake. Below is a plot of the flow solution computed through equation (1.4), where B is the surface of the disc defined by $r \in [0, 1]$ and $\theta \in [0, 2\pi)$, and where $\boldsymbol{\gamma}(\boldsymbol{\lambda}) = \gamma(\rho)\hat{\boldsymbol{\phi}}(\phi)$ comes from equations (2.12) and (2.16). This plot is a cross section of the actual flow.

From the density plot in figure 2.1 we can see that the fluid velocity appears to very high at the disc edges. In fact, the velocity becomes infinite around the edge. This is a result of not having applied the Kutta condition, and in a physical flow the bound vortex sheet on the surface of the disc would be obliged to separate at just the right rate to counteract this behaviour.

Table 2.1 shows the result of testing the convergence of the numerical method by the error estimate

$$E_N = \sqrt{\int_0^1 \left(\sum_{n=0}^{N-1} \sum_{m=0}^{N-1} g_n \phi_{mn} T_m(\rho) \right)^2 d\rho},$$

for selected values of N.

Whilst the numerical method appears to be convergent, it is interesting to look at the plots of $g(r)$ (green) and $\gamma(r)$ (red) in figure 2.1 as computed by the method outlined in the previous section. It is almost obvious to the naked eye that whilst $g(r)$ is non-singular, it *does* contain a singularity in its first derivative since $g(r) \sim \sqrt{r}$ near $r = 0$. In fact,
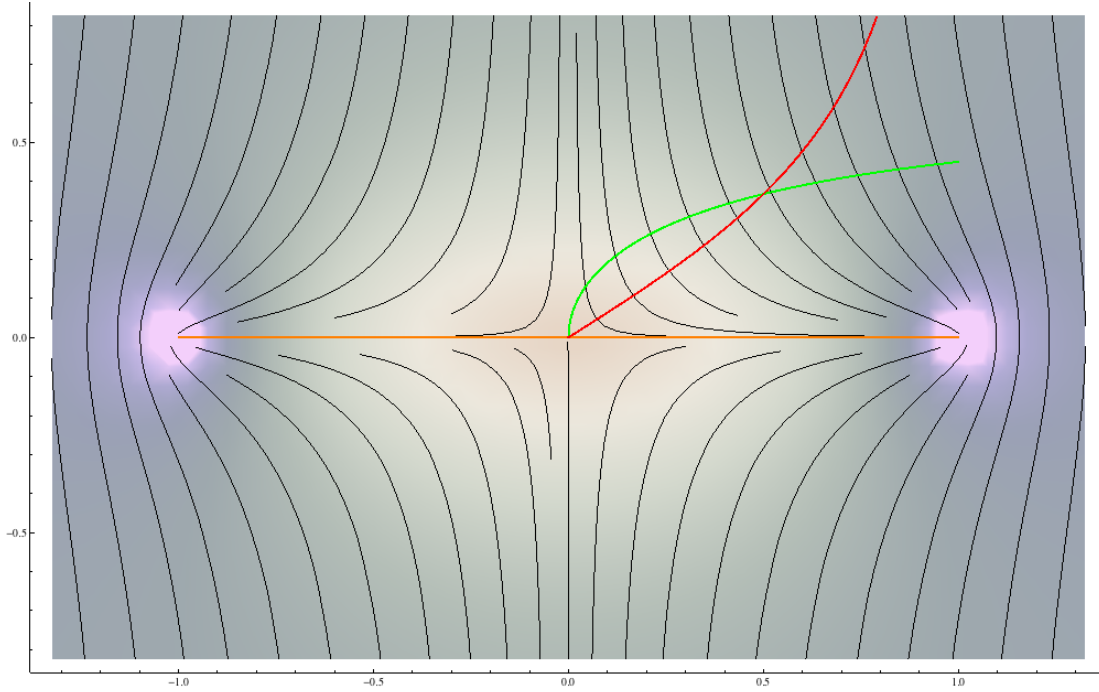
Figure 2.1: Streamlines of the flow relative to the disc induced by the bound vortex sheet attached to the disc (orange) through equation (1.4). The background density plot is of the magnitude of the flow velocity, and it appears to go infinite at the disc edges. Also superimposed are plots of $g(r)$ in green and $\gamma(r)$ in red for $N = 2048$. Further details about these functions can be found in the text.

figure 2.2 compares the *Chebyshev* coefficients (rather than the eigenfunction coefficients) of $g(r)$ with those of $\sqrt{r}$, and it shows a striking resemblance between the two. Chebyshev series approximations of non-analytic functions (such as square roots) generally have poor convergence, and a large number of coefficients are required to achieve good accuracy.

However, this non-analyticity at $r = 0$ is no longer present in $\gamma(r)$ because of the relationship between the two functions in equation (2.12), and the singularity at $r = 1$ has been accounted for analytically, and will therefore not impede the accuracy of the numerical method. In a way, we foresaw this problem in our discussion of the behaviour of the bound vortex sheet strength in section 2.1.1, where we conjectured that $\gamma(r) \sim r(1 - r^2)^{-1/2}$, and yet we chose the inversion formula in equation (2.7) and to work under the ansatz $\gamma(r) = g(r)\sqrt{r}/\sqrt{1 - r}$. This begs the question: why did we not work under a more suitable ansatz?

The answer comes in two parts. We were restricted in our choice of inversion formula (equation (2.7)), and the one we did use was in fact the most suitable. However, we could

N	$|E_{2048} - E_N|$
4	1.78×10^{-3}
16	2.12×10^{-5}
64	2.64×10^{-7}
256	2.72×10^{-9}
1024	8.60×10^{-11}

Table 2.1: Tabulated values of the error estimate for different values of N to test if the numerical method is convergent.
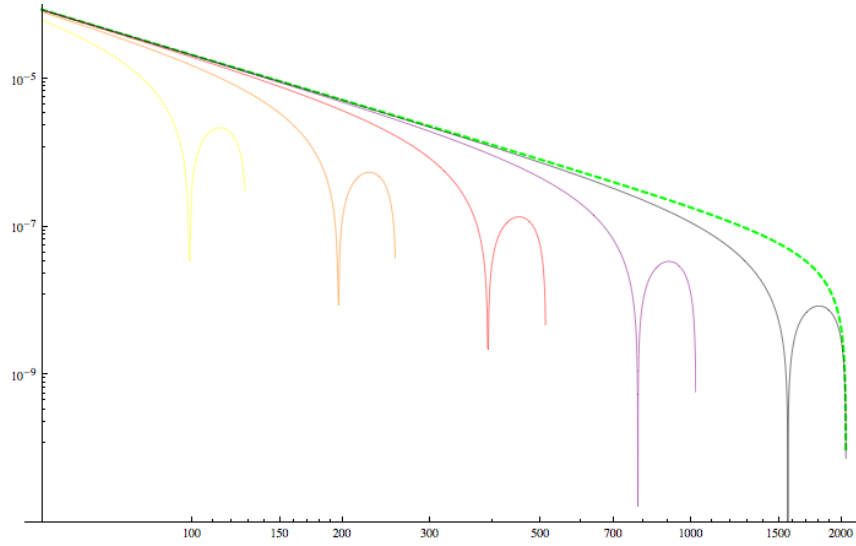
Figure 2.2: Log-log plots of the absolute value of the Chebyshev coefficients of $g(r)$ for $N = 128, 256, 512, 1024, 2048$ from yellow to black compared to those of $\sqrt{r}$ for $N = 2048$ only in dashed green. The large dips towards the end of each set of coefficients is a consequence of aliasing brought about by the truncation of the coefficients.

still have worked under the ansatz $\gamma(r) = g_1(r)r/\sqrt{1-r}$. This would have made equation (2.13) become

$$g_1(r) - \frac{1}{\pi}\frac{1}{\sqrt{r}}\int_0^1 \frac{d\rho\,\mathcal{N}(\rho,r)g_1(\rho)}{\sqrt{1-\rho}} - \frac{1}{\pi}\frac{1}{\sqrt{r}}\int_0^1 \frac{d\rho\,\mathcal{A}(\rho,r)g_1(\rho)}{\sqrt{1-\rho}}$$
$$+ \frac{1}{2}\frac{\sqrt{1-r}}{r}\int_0^r \frac{d\rho\,g_1(\rho)}{\sqrt{1-\rho}} = \frac{2\nu + 2\nu_1(r;\zeta)}{\sqrt{r}}. \quad (2.33)$$

Already, the denominator in the integrals make this equation look as though it lends itself less well to a numerical solution based upon Chebyshev polynomials, and the additional inverse square root coefficients make Chebyshev series approximations more complicated.

We did toy with methods of incorporating these coefficients into the series approximations of the functions $\mathcal{N}$ and $\mathcal{A}$; whilst these methods worked, they introduced errors that eliminated the benefits gained from the analyticity of $g_1(r)$.

To conclude this discussion, it seems as though the numerical procedure we have developed has the potential to be extremely efficient, but the equations it is trying to solve are not constructed in a way that fully exploits the underlying geometry of the solution. In the next section, we go on to look at how a different parameterisation of the no penetration boundary condition equation (1.12) allows us to construct an integral equation for the bound vortex sheet strength that lends itself well to the anticipated solution.

Chapter 3

Symmetrisation of the axisymmetric disc equation

In this chapter, we will revisit the axi-symmetric disc problem with the additional insight gained from our initial approach to it. Let us begin by making some general comments about the nature of our first solution for $\gamma(r)$. First, $\gamma(r)$ has an inverse square root singularity at $r = 1$, and is linear at $r = 0$. We anticipated this behaviour in section 2.1.1 but didn't fully implement it as an ansatz. A discussion of the reasons behind this are given at the end of the previous chapter.

Second, if we had somehow defined our problem for $r \in [-1, 1]$, we would expect $\gamma(r)$ to be odd in r. A massive advantage of this is that it would imply the anticipated inverse square root singularity at $r = -1$. When inverting a Fredholm integral equation of the first kind with a Cauchy kernel, such as that in equation (2.5), there is an element of choice in the inversion formula used. We can either place square root singularities at both the limits of integration, just at the top end, or at neither end. In equation (2.7) we chose the second of these options (the correct choice for the problem at hand), but if we were working on the domain $r \in [-1, 1]$ the natural choice would be to build in square root singularities at both ends because this corresponds with the physical solution we expect to find. Furthermore, this would naturally lead to the anticipated linear behaviour at the midpoint of the solution domain.

We will now go on to look at a way we can parameterise the no penetration boundary condition equation (1.12) on the domain $r \in [-1, 1]$ and the implications this has on the solution for $\gamma(r)$. This method will inevitably lead to some more complicated 'pen and paper' work being done, but it is precisely this level of analysis for which we are trying to set

a precedent, and which we believe holds the key to countering the increased computation times involved in fully three-dimensional calculations.

3.1   Symmetrising the integral equation

We begin by splitting the domain of integration B (the disc) in equation (1.12) into two equal parts[1], which we shall call $B_1 = \{\rho \in [0, 1], \phi \in [-\pi/2, \pi/2)\}$ and $B_2 = \{\rho \in [0, 1], \phi \in [\pi/2, 3\pi/2)\}$, where a point on the disc is defined as $\boldsymbol{\lambda} = \rho \cos \phi \boldsymbol{i} + \rho \sin \phi \boldsymbol{j} + \zeta \boldsymbol{k}$. Notice that we have changed the domain of ϕ from $[0, 2\pi)$ in the first problem formulation to $[-\pi/2, 3\pi/2)$ in this one. This is purely to make the integrals over ϕ easier and makes no difference to the solution.

We then define a point on the surface of the disc $\boldsymbol{\zeta} = r \cos \theta \boldsymbol{i} + r \sin \theta \boldsymbol{j} + \zeta \boldsymbol{k}$, but over the domain $r \in [-1, 1]$ and $\theta \in [-\pi/2, \pi/2)$. Since this problem is still axi-symmetric, it will ultimately have no θ-dependance, so we use $\theta = 0$ WLOG. Thus we have

$$
\frac{1}{4\pi} \fint_B dB \frac{(\hat{\boldsymbol{n}}(\boldsymbol{\zeta}) \times (\boldsymbol{\lambda} - \boldsymbol{\zeta})) \cdot \boldsymbol{\gamma}(\boldsymbol{\lambda})}{|\boldsymbol{\lambda} - \boldsymbol{\zeta}|^3}
$$
$$
= \frac{1}{4\pi} \int_0^1 d\rho \frac{\gamma(\rho)}{|r|} \frac{\beta}{(1 + \beta^2)^{\frac{3}{2}}} \int_{-\frac{\pi}{2}}^{\frac{\pi}{2}} d\phi \frac{\beta - \cos \phi}{(1 - \alpha \cos \phi)^{\frac{3}{2}}}
$$
$$
+ \frac{1}{4\pi} \int_0^1 d\rho \frac{\gamma(\rho)}{|r|} \frac{\beta}{(1 + \beta^2)^{\frac{3}{2}}} \int_{\frac{\pi}{2}}^{\frac{3\pi}{2}} d\phi \frac{\beta - \cos \phi}{(1 - \alpha \cos \phi)^{\frac{3}{2}}}, \tag{3.1}
$$

where $\beta = \rho/r$ and $\alpha = 2\beta/(1 + \beta^2)$. It is worth remarking that despite the fact that we have written both these integrals as Cauchy principal values, only one of them will actually need to be evaluated thus, depending on whether r is positive or negative.

The integrals over ϕ in equation (3.1) can be evaluated (appendix D), and the no penetration boundary condition becomes

$$
\frac{1}{2\pi} \int_0^1 d\rho \, \kappa_+(\rho, r) \gamma(\rho) + \frac{1}{2\pi} \int_0^1 d\rho \, \kappa_-(\rho, r) \gamma(\rho) = \nu - \boldsymbol{\nabla} \psi(r, \zeta) \cdot \boldsymbol{k}, \tag{3.2}
$$

---

[1]The pedantic reader will note that, in splitting the domain of integration, we are splitting the bound vortex sheet, and the azimuthal vortex filaments that make up each of the new bound vortex sheets are therefore no longer closed or ending on solid surfaces (they now end on the flat edge of the disc), thus breaking the law of conservation of mass. In a proper formulation of the problem, we would model each filament as closing along the flat edge of each semi-disc, and integrate along those portions of the disc in the no penetration boundary condition. However, the flow induced by one 'flat edge' will be exactly cancelled by that induced by the other, and we therefore automatically ignore their collective contribution.

where $\kappa_{\pm}(\rho, r) = G_{\pm}(\beta)/|r|$, with $\beta = \rho/r$ as before and where

$$G_{\pm}(\beta) = \frac{\mp 2\beta}{\sqrt{1+\beta^2}(1+\beta)(1-\beta)} + \mathrm{sgn}(1 \mp \beta) \left(\frac{F\left(\frac{\pi}{4}, \frac{\mp 4\beta}{(1 \mp \beta^2)}\right)}{1 \mp \beta} - \frac{E\left(\frac{\pi}{4}, \frac{\mp 4\beta}{(1 \mp \beta^2)}\right)}{1 \pm \beta} \right), \quad (3.3)$$

is defined in terms of the *incomplete* elliptic integrals $F(\phi, k)$ and $E(\phi, k)$ of the first and second kinds respectively. It is interesting to note that combining the two integrals in equation (3.2) and simplifying the resulting kernel $\kappa_+(\rho, r) + \kappa_-(\rho, r)$ returns equation (2.3) with the kernel $\kappa(\rho, r)$ defined in equation (2.4).

Under the assumption that $\gamma(\rho)$ is odd, we transform the domain of the second integral in equation (3.2) onto $\rho \in [-1, 0]$ and our no-penetration boundary condition now becomes

$$\frac{1}{\pi} \fint_{-1}^{1} d\rho \, \kappa(\rho, r) \gamma(\rho) = 2\nu - 2\boldsymbol{\nabla}\psi(r; \zeta) \cdot \boldsymbol{k}, \quad (3.4)$$

where the kernel is defined piecewise as

$$\kappa(\rho, r) = \begin{cases} \kappa_+(\rho, r) & , \quad \rho > 0 \\ 0 & , \quad \rho = 0 \\ -\kappa_-(-\rho, r) & , \quad \rho < 0 \end{cases}. \quad (3.5)$$

This function is continuous, but *not* smooth; it has a kink along $\rho = 0$ and is singular along $\rho = r$. We will now proceed in a manner similar to that of the previous chapter and work to remove these singularities analytically for the sake of a rapid numerical method.

3.2   Desingularising the kernel and inverting the symmetrised integral equation

In order to understand the singular nature of $\kappa(\rho, r)$ we look to the asymptotic expansion of $G_{\pm}(\beta)$ in the region of $\beta = \pm 1$, that is $\rho = \pm r$, respectively. We have

$$G_{\pm}(\beta) \sim \frac{-1}{1 \mp \beta} - \frac{1}{2}\log|1 \mp \beta| + \frac{1}{2}\left(3\log(2) - \log(1 + \sqrt{2})\right) + O\left((1 \mp \beta)\log|1 \mp \beta|\right). \quad (3.6)$$

Consider first the part of $\kappa(\rho, r)$ for $\rho > 0$. This will be singular along $\rho = r$ (or $\beta = 1$), and since we are only working on the domain $\rho > 0$ this implies $r > 0$ too. So for the purpose of this exercise we can define $\kappa_+(\rho, r) = G_+(\beta)/r$. Now for the part of $\kappa(\rho, r)$ for $\rho < 0$ we expect singular behaviour along $\beta = -1$, or $\rho = -r$. Now the function we are actually interested in is $-\kappa_-(-\rho, r)$, which will therefore be singular along $-\rho = -r$, or put simply, along $\rho = r$. Since this function only exists on the domain $\rho < 0$ this implies $r < 0$, so we can write $-\kappa_-(-\rho, r) = G_-(\beta)/r$, which is exactly as for $\rho > 0$. The asymptotic expansion of $\kappa(\rho, r)$ in the region $\rho - r << 1$ is therefore

$$\kappa(\rho, r) \sim \frac{1}{\rho - r} + \frac{1}{2r} \log\left|\frac{r}{\rho - r}\right| + \frac{1}{2r}\left(3\log(2) - \log(1 + \sqrt{2})\right) + O\left((\rho - r)\log|\rho - r|\right), \quad (3.7)$$

which is almost exactly the same as that of $\kappa(\rho, r)$ in the non-symmetrised calculation. We can now remove the leading order Cauchy type singularity in this kernel by writing

$$\frac{1}{\pi}\!\!\!\fint_{-1}^{1} \frac{d\rho}{\rho - r}\gamma(\rho) = 2\nu - 2\nabla\psi(r, \zeta)\cdot\boldsymbol{k} - \frac{1}{\pi}\int_{-1}^{1} d\rho M(\rho, r)\gamma(\rho), \quad (3.8)$$

where $M(\rho, r) = \kappa(\rho, r) - 1/(\rho - r)$. It is at this stage that the work on symmetrising this equation really comes into its own, because we now expect the solution to be unbounded at both endpoints, so we can apply the inversion formula

$$\frac{1}{\pi}\!\!\!\fint_{a}^{b} \frac{d\rho}{\rho - r}\gamma(\rho) = f(r) \quad \Rightarrow \quad \gamma(r) = -\frac{1}{\pi}\frac{1}{\sqrt{r - a}\sqrt{b - r}}\left(C + \fint_{a}^{b} d\frac{d\rho}{\rho - r}\sqrt{r - a}\sqrt{b - r}f(\rho)\right),$$
$$(3.9)$$

where the constant C is

$$C = \int_{-1}^{1} d\rho\,\gamma(\rho). \quad (3.10)$$

This is a form of equation (1.6), where the line $L(t; \boldsymbol{e}_+, \boldsymbol{e}_-)$ runs in a straight line from $r = -1$ to 1, and $\theta = 0$. The value of C is therefore related to the circulation at the edge of the disc, which, in the full separated problem, we would choose as part of the solution to satisfy the Kutta condition on the flow. However, since we are primarily concerned with solving the attached flow problem we do not need to satisfy this condition, so we set $C = 0$, as in section 2.1.1. Ultimately, equation (3.4) becomes

$$\gamma(r) - \frac{1}{\pi} \frac{1}{\sqrt{1+r}\sqrt{1-r}} \int_{-1}^{1} d\rho \, N(\rho, r)\gamma(\rho) = \frac{1}{\sqrt{1+r}\sqrt{1-r}} \left(2\nu r + \nu_1(r; \zeta)\right), \qquad (3.11)$$

where we have made use of the integral identity in equation (A.3), and where

$$\nu_1(r; \zeta) = \frac{1}{\pi} \fint_{-1}^{1} \frac{d\sigma}{\sigma - r} \sqrt{1+\sigma}\sqrt{1-\sigma} \left(\boldsymbol{\nabla}\psi(\sigma, \zeta) \cdot \boldsymbol{k}\right),$$

$$N(\rho, r) = \frac{1}{\pi} \fint_{-1}^{1} \frac{d\sigma}{\sigma - r} \sqrt{1+\sigma}\sqrt{1-\sigma} M(\rho, \sigma). \qquad (3.12)$$

The parallels with the previous problem continue as we seek to de-singularise $M(\rho, \sigma)$ by subtracting and integrating the appropriate logarithmic term. Using the asymptotic expansion of $\kappa(\rho, r)$ in equation (3.7) we can deduce that the function

$$L(\rho, \sigma) = 2\rho M(\rho, \sigma) + \log \left| \frac{\rho - \sigma}{\sqrt{\rho^2 + \sigma^2}} \right| - (3\log(2) - \log(2 + \sqrt{2})) \qquad (3.13)$$

is non-singular for all $\rho, \sigma \in [-1, 1]$. Notice that we have also removed the constant term so that $L(\rho, \sigma) = 0$ along $\rho = \sigma$. This is purely a matter of personal preference and is not wholly necessary.

There is a subtlety in our choice of $L(\rho, \sigma)$. Notice that in our choice of $L(\rho, \sigma)$ in the non-symmetrised case we subtracted the term $\log|\rho + \sigma|$ to eliminate the singularity at $\rho = \sigma = 0$. However, it also introduced another singularity along $\rho = -\sigma$. Now in the previous chapter $L(\rho, \sigma)$ only existed on the domain $\rho, \sigma \in [0, 1]$, so this singularity played no part in the calculation. We cannot use the same tactic in this calculation because of our extended domain. Instead, we remove the term $\log|\sqrt{\rho^2 + \sigma^2}|$. This still has the desired effect of removing the singularity at $\rho = \sigma = 0$ but reintroduces the new singularity in the complex plane at $\rho = i\sigma$. Whilst this makes the contour of integration a little more complicated in appendix E, it does not affect the accuracy of the numerical approximation of $L(\rho, \sigma)$. We now have

$$N(\rho, r) = \frac{1}{\pi} \frac{1}{2\rho} \left(\fint_{-1}^{1} \frac{d\sigma}{\sigma - r} \sqrt{1 + \sigma} \sqrt{1 - \sigma} L(\rho, \sigma) \right.$$
$$\left. - \fint_{-1}^{1} \frac{d\sigma}{\sigma - r} \sqrt{1 + \sigma} \sqrt{1 - \sigma} \left(\log \left| \frac{\rho - \sigma}{\sqrt{\rho^2 + \sigma^2}} \right| + (3\log(2) - \log(2 + \sqrt{2})) \right) \right). \tag{3.14}$$

The constant term in the second integral on the RHS of equation (3.14) can easily be integrated through equation (A.3), and we can evaluate the integral containing the log term analytically (appendix E). Then, working under the ansatz

$$\gamma(r) = \frac{2r}{\sqrt{1 + r}\sqrt{1 - r}} g(r), \tag{3.15}$$

where we anticipate $g(r)$ to be a very simple, analytic function, we have

$$g(r) - \frac{1}{2r} \frac{1}{\pi} \int_{-1}^{1} d\rho \frac{\mathcal{N}(\rho, r) g(\rho)}{\sqrt{1 + \rho}\sqrt{1 - \rho}} - \frac{1}{2r} \frac{1}{\pi} \int_{-1}^{1} d\rho \frac{\mathcal{A}(\rho, r) g(\rho)}{\sqrt{1 + \rho}\sqrt{1 - \rho}} = 2\nu + \frac{2\nu_1(r; \zeta)}{r}, \tag{3.16}$$

where the numerical integrand function is defined as

$$\mathcal{N}(\rho, r) = \frac{1}{\pi} \fint_{-1}^{1} \frac{d\sigma}{\sigma - r} \sqrt{1 + \sigma} \sqrt{1 - \sigma} L(\rho, \sigma), \tag{3.17}$$

and where we split up the analytic integrand function for the sake of the numerical scheme we will develop in section 3.3. We do this by writing

$$\mathcal{A}(\rho, r) = \sum_{i=1}^{5} A_i(\rho, r), \tag{3.18}$$

$$A_1(\rho, r) = \sqrt{1 + r}\sqrt{1 - r} \arctan \left(\frac{r\sqrt{1 - r^2} \left(\sqrt{1 + \rho^2} - |\rho| \right)}{r^2 \sqrt{1 + \rho^2} + (1 - r^2)|\rho|} \right),$$

$$A_2(\rho, r) = -\rho, \qquad A_3(\rho, r) = -r \operatorname{arcsinh}|\rho|,$$
$$A_4(\rho, r) = \sqrt{1 + r}\sqrt{1 - r} \left(\pi H(\rho - r) - \arccos(r) \right),$$
$$A_5(\rho, r) = -r \left(3\log(2) - \log \left(2 + \sqrt{2} \right) \right).$$

Now, as we go on to develop a numerical method for solving equation (3.16), we will start to see the fruits of our work.

3.3 Solving the attached flow problem

In this section we will show that it is possible to find a quasi-analytic solution to the attached flow problem in equation (3.16); that is for $\nu_1(r;\zeta) = 0$, or put another way, under the assumption that there is no wake. Under these circumstances, it is possible to show that there exists a solution to equation (3.16) of the form $g(r) = \text{constant}$. We thus consider the equation

$$g\left(1 - \frac{1}{2r}\left(\frac{1}{\pi}\int_{-1}^{1}d\rho\frac{\mathcal{N}(\rho,r)}{\sqrt{1+\rho}\sqrt{1-\rho}} + \frac{1}{\pi}\int_{-1}^{1}d\rho\frac{\mathcal{A}(\rho,r)}{\sqrt{1+\rho}\sqrt{1-\rho}}\right)\right) = \nu. \tag{3.19}$$

In order for this equation to be satisfied it must be the case that the sum of the two integrals on the LHS is of the form $\alpha\,r$, for some constant α. It is obvious that $A_3(\rho,r)$ and $A_5(\rho,r)$ are of this form when integrated against the $1/\sqrt{1+\rho}\sqrt{1-\rho}$ kernel, and they give us

$$\frac{1}{\pi}\int_{-1}^{1}d\rho\frac{A_3(\rho,r)}{\sqrt{1+\rho}\sqrt{1-\rho}} = -\frac{2Cr}{\pi}, \tag{3.20}$$

$$\frac{1}{\pi}\int_{-1}^{1}d\rho\frac{A_5(\rho,r)}{\sqrt{1+\rho}\sqrt{1-\rho}} = -r\left(3\log(2) - \log\left(2+\sqrt{2}\right)\right), \tag{3.21}$$

where C is the Catalan constant (≈ 0.916). We also have that when both $A_2(\rho,r)$ and $A_4(\rho,r)$ are integrated against this kernel the result is zero. We must have, therefore,

$$\frac{1}{\pi}\int_{-1}^{1}d\rho\frac{\mathcal{N}(\rho,r)}{\sqrt{1+\rho}\sqrt{1-\rho}} + \frac{1}{\pi}\int_{-1}^{1}d\rho\frac{A_1(\rho,r)}{\sqrt{1+\rho}\sqrt{1-\rho}} = \alpha\,r. \tag{3.22}$$

This can be shown, numerically, by approximating $\mathcal{N}(\rho,r)$ and $A_1(\rho,r)$ as Chebyshev series. This is relatively easy for the latter (we have already done it for functions of this form in the previous chapter), and when integrating it we have

$$\frac{1}{\pi}\sum_{i=0}^{N-1}\sum_{j=0}^{N-1}A_{ij}T_j(r)\int_{-1}^{1}d\rho\frac{T_i(\rho)}{\sqrt{1+\rho}\sqrt{1-\rho}} = \sum_{j=0}^{N-1}A_{0j}T_j(r), \tag{3.23}$$

where the A_{ij} are the coefficients of the Chebyshev series approximation of $A_1(\rho, r)$. The equivalent calculation for $\mathcal{N}(\rho, r)$ is not quite as simple. If we can write

$$L(\rho, r) = \sum_{i=0}^{N-1} \sum_{j=1}^{N} \bar{L}_{ij} T_i(\rho) U_{j-1}(r), \tag{3.24}$$

where $U_j(r)$ is the jth Chebyshev polynomial of the second kind, then we can use the integral identity in equation (F.9) to express

$$\mathcal{N}(\rho, r) = -\sum_{j=0}^{N-1} \sum_{k=1}^{N} \bar{L}_{jk} T_j(\rho) T_k(r). \tag{3.25}$$

This combines with equation (3.23) in equation (3.22) to give us

$$\sum_{j=0}^{N-1} A_{0j} T_j(r) - \sum_{j=1}^{N} \bar{L}_{0j} T_j(r) = \alpha\, r. \tag{3.26}$$

If this is true, then we must have $A_{01} - \bar{L}_{01} = \alpha$ and $A_{00} = 0$, $A_{0j} - \bar{L}_{0j} = 0$ for $j = 2, 3, ...$ To test this hypothesis we compute a few of these coefficients numerically by expressing A_{0j} and $\bar{L}_{0j}$ through the continuous orthogonality conditions on the Chebyshev polynomials of the first *and* second kind, giving us

$$A_{0j} = \frac{2 - \delta_{0j}}{\pi^2} \int_{-1}^{1} d\rho \int_{-1}^{1} dr \frac{A_1(\rho, r) T_j(r)}{\sqrt{1 + \rho}\sqrt{1 - \rho}\sqrt{1 + r}\sqrt{1 - r}}, \tag{3.27}$$

$$\bar{L}_{0j} = \frac{2}{\pi^2} \int_{-1}^{1} d\rho \int_{-1}^{1} dr \frac{\sqrt{1 + r}\sqrt{1 - r}}{\sqrt{1 + \rho}\sqrt{1 - \rho}} L(\rho, r) U_{j-1}(r). \tag{3.28}$$

Computing these integrals numerically, along with equations (3.20) and (3.21), allows us to compute the value of the constant α, and therefore the constant g for given ν. We find that g tends towards $2\nu/\pi$, implying that

$$\gamma(r) = \frac{2\nu r}{\pi\sqrt{1 + r}\sqrt{1 - r}}. \tag{3.29}$$

Whilst a formal proof of this is lacking, this solution passes all numerical tests and satisfies equations (3.4) and (2.3) in the case of no wake.

3.4 Numerical scheme for full symmetrised integral equation

Whilst the analytic solution derived in the previous section effectively renders the attached flow problem solved, in order that we can solve the full separated flow problem we will need a numerical scheme similar to that in section 2.2. In this section we will develop a numerical method for computing the eigenfunctions, $\phi_n(r)$, of the integral operator

$$\Psi(g)(r) := g(r) - \frac{1}{2r}\frac{1}{\pi}\int_{-1}^{1} d\rho \frac{\mathcal{N}(\rho, r)g(\rho)}{\sqrt{1+\rho}\sqrt{1-\rho}} - \frac{1}{2r}\frac{1}{\pi}\int_{-1}^{1} d\rho \frac{\mathcal{A}(\rho, r)g(\rho)}{\sqrt{1+\rho}\sqrt{1-\rho}}, \qquad (3.30)$$

such that $\Psi(\phi_n)(r) = \lambda_n \phi_n(r)$, and seek a solution to equation (3.16) of the form

$$g(r) = \sum_{n=0}^{N-1} g_n \phi_n(r), \qquad (3.31)$$

$$\Psi(g)(r) = 2\nu + \frac{2\nu_1(r;\zeta)}{r}, \qquad (3.32)$$

where g_n is the unknown vector to be solved for.

3.4.1 Finding the eigenfunctions and eigenvalues of Ψ

We proceed through this section in much the same way as in the non-symmetrised problem, only with a few more complications. First, we seek to express the eigenfunctions of Ψ as a series of Chebyshev polynomials

$$\phi_n(r) = \sum_{m=0}^{N-1} \phi_{mn} T_m^*(r), \qquad (3.33)$$

by finding the matrix ϕ_{mn}. Now since we expect $\gamma(r)$ to be odd, we must have that $g(r)$ is even. Since $g(r)$ is a linear combination of eigenfunctions, all the eigenfunctions must also be even. By the same logic, since each eigenfunction is a linear combination of Chebyshev polynomials, the coefficient of every odd numbered Chebyshev polynomial must be zero, and therefore every odd numbered row of ϕ_{mn} must be zero. This means we can express the eigenfunctions as

$$\phi_n(r) = \sum_{m=0}^{\frac{N}{2}-1} \phi_{2m,n} T_{2m}(r), \tag{3.34}$$

for even N. Equation (3.31) implies that the *Chebyshev* coefficients of $g(r)$ come from the matrix-vector product $\phi_{mn}g_n$, but since every odd indexed row of ϕ_{mn} is zero, we only need to find the even coefficients of g_n. This has already halved the amount of work needed to achieve the same accuracy in the previous problem, a benefit which by itself would have made this additional work worthwhile.

We can now plug in this definition into the integral operator as before and try to form a matrix equation for which we will calculate the eigenvectors and eigenvalues. However, we now have the coefficient of $1/2r$ in front of the integral terms in equation (3.16) to make life a little more complicated. For brevity, we define the integral operator

$$\Phi_n(f)(r) := \frac{1}{2r}\frac{1}{\pi}\int_{-1}^{1} d\rho \frac{f(\rho,r)\phi_n(\rho)}{\sqrt{1+\rho}\sqrt{1-\rho}}. \tag{3.35}$$

We use the same separation of terms in $\mathcal{A}(\rho,r)$ as in the previous section. Let us start by considering some of the simple terms. We work throughout under the ansatz that all $\phi_n(r)$ are even functions, and we have therefore

$$\Phi_n(A_2)(r) = 0, \tag{3.36}$$

because the integrand will be odd, so the integral will evaluate to zero for all values of r. Now consider the term $A_1(\rho,r)/2r$. We bring the $1/2r$ coefficient into this term to avoid having to account for it later. This term is now even in both ρ and r, so we can express it solely in terms of the even indexed Chebyshev polynomials thus

$$\frac{1}{2r}A_1(\rho,r) = \sum_{j=0}^{\frac{N}{2}-1}\sum_{k=0}^{\frac{N}{2}-1} A_{2j,2k}T_{2j}(\rho)T_{2k}(r). \tag{3.37}$$

Plugging this definition into the operator Φ_n (and multiplying by $2r$ to cancel that taken out earlier) along with the Chebyshev series approximation of $\phi_n(\rho)$ we can write

$$2r\Phi_n(A_1)(r) = \frac{1}{2}\sum_{i=0}^{\frac{N}{2}-1}\sum_{k=0}^{\frac{N}{2}-1} \phi_{2i,n} A_{2i,2k}T_{2k}(r)\left(1+\delta_{0i}\right). \tag{3.38}$$

If we can write all the terms in equation (3.16) in this form, we will be able to derive a

system of matrix-vector equations like in equation (2.27). Since both $A_3(\rho, r)$ and $A_5(\rho, r)$ have coefficients of r, we can cancel these analytically with the coefficient of $1/2r$ in Φ_n, and since they are therefore even in ρ and r they are relatively easy to deal with, and we have

$$\Phi_n(A_3)(r) = -\frac{1}{2} \sum_{i=0}^{\frac{N}{2}-1} \sum_{k=0}^{\frac{N}{2}-1} \phi_{2i,n} a_{2i} \left(1 + \delta_{0i}\right) \delta_{0k} T_{2k}(r),$$

$$\text{where} \quad \frac{1}{2r} A_3(\rho, r) = \sum_{i=0}^{\frac{N}{2}-1} a_{2i} T_{2i}(\rho),$$

$$\Phi_n(A_5)(r) = \sum_{i=0}^{\frac{N}{2}-1} \sum_{k=0}^{\frac{N}{2}-1} \phi_{2i,n} \frac{1}{2} \left(-3\log(2) + \log\left(2 + \sqrt{2}\right)\right) \delta_{0i} \delta_{0k} T_{2k}(r). \tag{3.39}$$

This leaves us with only the term $A_4(\rho, r)$ which we must deal with in a novel fashion. Plugging in the Chebyshev series approximation of $\phi_n(\rho)$ we have

$$\Phi_n(A_4)(r) = \frac{\sqrt{1+r}\sqrt{1-r}}{2r} \left(-\arccos(r)\phi_{0n} + \sum_{i=0}^{\frac{N}{2}-1} \phi_{2i,n} \int_r^1 d\rho \frac{T_{2i}(\rho)}{\sqrt{1+\rho}\sqrt{1-\rho}}\right). \tag{3.40}$$

After making the substitution $\rho = \cos\theta$ in the integral on the RHS of this equation, the first term in the sum (that is, for $i = 0$) perfectly cancels the $\arccos(r)\phi_{0n}$, leaving us with

$$\Phi_n(A_4)(r) = \sum_{i=1}^{\frac{N}{2}-1} \phi_{2i,n} H_{2i}(r),$$

$$\text{where} \quad H_i(r) = \frac{\sqrt{1+r}\sqrt{1-r}}{2r} \frac{\sin\left(i \arccos(r)\right)}{i}. \tag{3.41}$$

We would like to express $H_i(r)$ as a Chebyshev series approximation in the form

$$H_i(r) = \sum_{j=1}^{N-1} H_{ij} T_j(r), \tag{3.42}$$

but rather than using a discrete cosine transform to do so, we can use a similar method to that in section 2.2.1 by exploiting the *continuous* orthogonality property of the Chebyshev

polynomials. The exact integral which needs to be evaluated can be shown to be exactly the same as that in equation (A.2) with the exception of 'half-indices' by the substitution $\theta = \phi/2$, and we arrive at

$$\Phi_n(A_4)(r) = \sum_{i=0}^{\frac{N}{2}-1} \sum_{k=0}^{\frac{N}{2}-1} \phi_{2i,n} H_{2i,2k} T_{2k}(r), \tag{3.43}$$

$$\text{where} \quad H_{ik} = \frac{(2-\delta_{0k})\,(2-\delta_{ik})}{4i} \begin{cases} 0 & , \quad i=0\,||\,k>i\,||\,k\,\text{odd}\,||\,i\,\text{odd} \\ (-1)^{\frac{i+k}{2}+1} & , \quad k \leq i \end{cases}$$

$$\tag{3.44}$$

Let us no go on to consider $\Phi_n(\mathcal{N})(r)$. We would like to compute the coefficients $\bar{L}_{ij}$ in equation (3.24) by a discrete cosine transform rather than by numerical integration. To do this, we begin by approximating

$$L(\rho, \sigma) = \sum_{j=0}^{N-1} \sum_{k=0}^{N-1} L_{jk} T_j(\rho) T_k(\sigma), \tag{3.45}$$

where the coefficients L_{jk} are computed in the normal fashion; that is, by a discrete cosine transform. It is worth mentioning here that $L_{jk} = 0$ for all $j+k$ odd; this is probably a consequence of the fact that $L(\rho, \sigma)$ can be solely written as a function of ρ/σ, and whilst we have been unable to formally prove this conjecture, it is a useful property nonetheless. Now, we use the relationship between the first and second kind polynomials to convert the sum over k into one over the Chebyshev polynomials of the second kind through the recurrence relation

$$\sum_{j=0}^{N-1} \sum_{k=0}^{N-1} L_{jk} T_j(\rho) T_k(\sigma) = \sum_{j=0}^{N-1} \sum_{k=1}^{N} \bar{L}_{jk} T_j(\rho) U_{k-1}(\sigma),$$

$$\bar{L}_{jk} = \frac{1}{2} \left((1+\delta_{1k}) L_{j,k-1} - L_{j,k+1} \right), \tag{3.46}$$

where the truncation at N implies $L_{jN} = L_{j,N+1} = 0$. This shift in the k index just means that the first column of $\bar{L}_{jk}$ is indexed with a 1 instead of a 0, and means that $\bar{L}_{jk} = 0$ whenever $j+k$ is even. We can therefore derive an expression for $\mathcal{N}(\rho, r)$ as in equation (3.25), which goes through the integral operator Φ_n in the same way as in the previous

section, so that

$$\Phi_n(\mathcal{N})(r) = -\frac{1}{4r} \sum_{i=0}^{N-1} \sum_{k=1}^{N} \phi_{in} \bar{L}_{ik} T_k(r) \left(1 + \delta_{0i}\right). \tag{3.47}$$

Since every *odd* indexed row of ϕ_{in} is zero (that is, for all odd values of i), we can automatically dismiss the odd valued rows of $\bar{L}_{ik}$; there is no need to sum over them since we know they will all be multiplied by zero. Then, recalling the fact that $\bar{L}_{ik} = 0$ whenever $i + k$ is even, we must have that for each even value of i over which we sum, every term in $\bar{L}_{ik}$ for k even will be zero, so we need only sum over the odd values of k, allowing us to write

$$\Phi_n(\mathcal{N})(r) = -\frac{1}{4r} \sum_{i=0}^{\frac{N}{2}-1} \sum_{k=0}^{\frac{N}{2}-1} \phi_{2i,n} \bar{L}_{2i,2k+1} T_{2k+1}(r) \left(1 + \delta_{0i}\right). \tag{3.48}$$

If we want to eventually have an equation of the same form as that in equation (2.27) we need to incorporate the $1/r$ coefficient by an appropriate shift in the coefficients of the Chebyshev series. By equation (F.1) we can show that

$$\frac{1}{r} \sum_{i=0}^{\frac{N}{2}-1} \alpha_{2i+1} T_{2i+1}(r) = \sum_{i=0}^{\frac{N}{2}-1} \beta_{2i} T_{2i}(r)$$

$$\Rightarrow \beta_{N-2} = 2\alpha_{N-1},$$

$$\beta_{2i} = 2\alpha_{2i+1} - \beta_{2i+2}, \quad i = N/2 - 2, \, N/2 - 3, \, ..., \, 3, \, 2$$

$$\beta_0 = \alpha_1 - \frac{1}{2}\beta_2, \tag{3.49}$$

allowing us to write this numerical term in the form we would like;

$$\Phi_n(\mathcal{N})(r) = -\frac{1}{4} \sum_{i=0}^{\frac{N}{2}-1} \sum_{k=0}^{\frac{N}{2}-1} \phi_{2i,n} L^*_{2i,2k} T_{2k}(r) \left(1 + \delta_{0i}\right). \tag{3.50}$$

Combining the work of this section we have

$$\Psi(\phi_n)(r) = \sum_{i=0}^{\frac{N}{2}-1} \sum_{j=0}^{\frac{N}{2}-1} \kappa_{2i,2j} \phi_{2i,n} T_{2j}(r) = \lambda_n \sum_{i=0}^{\frac{N}{2}-1} \sum_{j=0}^{\frac{N}{2}-1} \phi_{2i,n} \delta_{ij} T_{2j}(r), \tag{3.51}$$

where the matrix κ_{ij} is

$$\kappa_{ij} = \delta_{ij} - \left(\left(-\frac{1}{4}L_{ij}^* - \frac{1}{2}a_i\delta_{0j} + \frac{1}{2}A_{ij}\right)(1 + \delta_{0i}) + H_{ij} + \frac{-3\log(2) + \log\left(2 + \sqrt{2}\right)}{2}\delta_{0i}\delta_{0j}\right).$$
(3.52)

As in the non-symmetrised problem, the orthogonality of the Chebyshev polynomials implies that

$$\sum_{i=0}^{\frac{N}{2}-1} \kappa_{2i,2i}\phi_{2i,n} = \lambda_n\phi_{2j,n}.$$
(3.53)

As before, the columns of the matrix $\phi_{2i,n}$ are, therefore, the eigenvectors of the matrix $\alpha_{2i,2j} = \kappa_{2i,2j}^T$ where n is any even number between 0 and $N - 1$. Once we have computed these, we can compute our solution vector g_{2i} in much the same way as in section 2.2.2, and we will therefore not go through the calculation again.

3.5   Numerical results

Given the fact that we already know the analytic solution for the attached flow problem, this should provide us with a very good test to see if the numerical scheme we have just developed is sound. By taking $\nu_1(r;\zeta) = 0$ the numerical scheme should return $\phi_{2i,n}g_n = 2\nu\delta_{0i}/\pi$. This, however, is not the case.

For reasons that are not entirely clear, the Chebyshev approximation of $g(r)$ that arises as the numerical solution to the attached flow problem is constant for all values of r, but takes a different value at $r = 0$, which is very difficult for the Chebyshev series to approximate and destroys the additional accuracy gained by the symmetrisation of the problem in the first place.

It is strongly suspected that the cause of this problem is the original Chebyshev approximation of $L(\rho, \sigma)$. This function can be expressed solely as a function of ρ/σ and as a result it is undefined (multi-valued) at $\rho = \sigma = 0$, and constant along the lines $\rho = 0$ and $\sigma = 0$ (and indeed along any line $\rho = m\sigma$ for constant m). This means that, for example, for small values of σ, the function changes rapidly between $\rho \in (-\sigma, \sigma)$. However, at $\sigma = 0$ it returns to being constant.

The problem arises because when computing the coefficients of the Chebyshev series approximation of $L(\rho, \sigma)$ we sample the function at the zeros of the Nth Chebyshev poly-

nomial; that is, at a set of points $x_k \in (-1, 1)$ as defined in equation (F.2). This set of nodes *does not* include the mid-point, so the function is never actually sampled along the lines $\rho = 0$ or $\sigma = 0$. For that reason, the Chebyshev series approximation does not know that the function remains constant along $\rho = 0$ and $\sigma = 0$ and tries to work in a different value at $\rho = \sigma = 0$. An example of this is given graphically in figure 3.1. Whilst the actual

(a) $\rho = -0.1$ (b) $\rho = 0$ (c) $\rho = 0.1$

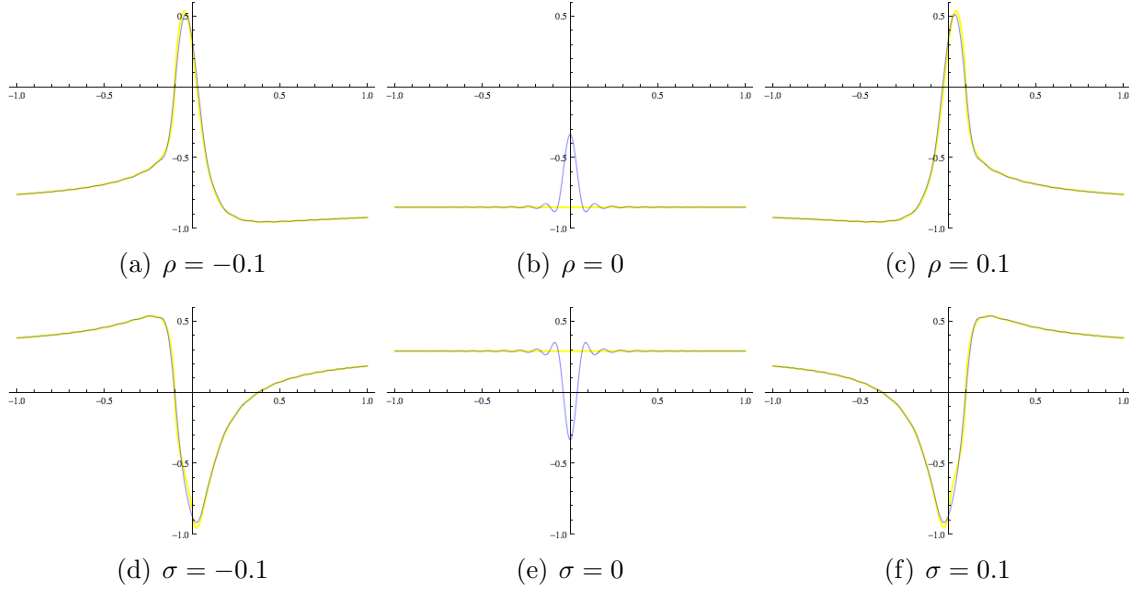(d) $\sigma = -0.1$ (e) $\sigma = 0$ (f) $\sigma = 0.1$

Figure 3.1: Plots comparing the Chebyshev approximation of $L(\rho, \sigma)$ defined in equation (3.13) for $N = 64$ (blue) to the analytic definition (yellow), for σ from -1 to 1 (top) and for ρ from -1 to 1 (bottom) for three different values of the other independent variable. The plots show how the Chebyshev series approximation struggles to work in the multi-valuedness of the function at $\rho = \sigma = 0$ because of the fact that the Chebyshev zeros at which the function is sampled do not include the line $\rho = 0$ or $\sigma = 0$.

effect of this on the accuracy of the final solution for $\gamma(r)$ is comparatively small, it is large enough to eliminate any additional accuracy gained by the extra work of symmetrisation. It is anticipated, therefore, that anybody wishing to continue this work by adding a wake into the flow will need to address these issues by a new way of approximating $L(\rho, \sigma)$ or $\mathcal{N}(\rho, r)$, preferably one which *exploits* its ρ/σ dependence rather than fighting against it.

Chapter 4

Conclusions

In this section we will briefly review what the thesis was aimed at doing, indicate the main results and how they expound ideas in the area, note the limitations of the work and how these might be overcome, and summarise the overall contribution to understanding and studying the original problem.

We began this thesis with an in-depth discussion of insect flight and how vortex sheet theory could be used to model it realistically and efficiently. The reader would be forgiven, however, for thinking that the subsequent work was very far removed from that goal. Having justified the use of vortex sheet theory, the introduction then went on to discuss why it might prove difficult to implement in three-dimensions; not least of those difficulties being the massively increased computational resources required. We then went on to explain the belief of this author and the real aim of this thesis; that the only way to counteract the increased computational resources whilst maintaining accuracy is to pursue a rigorous analysis of the governing equations, specifically their singular nature, and to set a precedent for the level of analysis required. It is against this aim that we will judge the success of the thesis.

This thesis provides the reader with two main sections; the first is a complete calculation that provides a relatively accurate numerical method for solving the no-penetration boundary condition in the separated flow problem[1], but is hampered by inaccuracies caused by the method of parameterisation, and the second employs an intelligent method of pa-

---

[1]As mentioned towards the end of section 1.2.4, we treat the problem of modelling the evolution of the separated vortex sheet as having already been solved. Therefore, whilst our model presents a *method* for solving the separated flow problem, it does not actually attempt to employ that method in order to plot a solution. However, as was mentioned in section 2.2.2, all that would be required to solve the no-penetration boundary condition in the presence of a wake is a method for computing the flow induced by the wake on the surface of the membrane.

rameterisation that provides an exact solution to the attached flow problem, but remains incomplete in terms of its potential to solve the separated flow problem because of failings in the numerical method.

In chapter 2 we parameterised the no-penetration boundary condition in the form of equation (1.12) by the most obvious means; cylindrical polar coordinates. This allowed us to test the efficacy of the methods used by Shukla & Eldredge (2007) to invert the Fredholm integral equation of the first kind, and to experiment with analytically integrating the logarithmic singularities, thus obviating the need to represent these singularities numerically. There followed a numerical method founded upon eigenfunction theory, the accuracy of which was tested in section 2.3. It was found that approximating the solution $\gamma(r)$ that satisfied the no-penetration boundary condition through 2^N nodes produced an error of $O(10^{-(N+1)})$. Whilst this might seem to be a high level of accuracy, it requires approximation through more than 32,000 nodes to achieve accuracy to machine precision.

This first method was novel, and it explored methods of solving the governing equations of fluid flow that, to the author's knowledge, have not been explored in such detail before. However, the precedent it set for accuracy was simply not high enough to transfer to a fully three dimensional theory, so a different method of parameterisation that fully exploited the underlying geometry of the anticipated solution was sought.

We began chapter 3 by explaining the reasons behind the new method of parameterisation. The key to this method was in considering the single axisymmetric disc as two half-discs. This allowed us to seek a solution over the interval $r \in [-1, 1]$ which would be odd in r, and would therefore lend itself well to the inversion formulae for Fredholm integral equations of the first kind. A very similar method to that used in the previous chapter was then applied to invert and desingularise the governing equation. The result of this work was an exact solution to the attached flow problem and a numerical method which looked as though it would guarantee, at the very least, the same level of accuracy with half the number of nodes as the previous method. However, tests of the accuracy of that numerical method against the exact solution proved rather inaccurate. A short discussion of the suspected reasons for this is given in chapter 3.5.

There are two main extensions to this work; modelling a *separated*, rather than *attached*, flow problem, and extending to a fully three-dimensional model. We will now consider what would be needed to realise these extensions.

Both the numerical methods developed in this work should lend themselves well to a formulation of the separated flow problem. The main requirement of such an extension is

a method of calculating the flow induced *by* the wake *on* the surface of the bound vortex sheet, referred to in the body of the thesis as $\nu_1(r; \zeta)$. Such methods already exist for fully three-dimensional wake structures such as vortex sheets, so an extension such as this is quite realisable. Another requirement would be a method of satisfying the unsteady Kutta condition on the flow solution at the disc edge. This was discussed in chapter 1, and it was proposed that the most natural method of doing so was that developed by Jones (2003), which used Kelvin's circulation theorem to derive a constraint on the bound vortex sheet strength (in terms of the circulation at the edge of the bound vortex sheet) that could be solved at the same time as the no-penetration boundary condition, thus guaranteeing the satisfaction of the unsteady Kutta condition. A future author wishing to employ this method would have to extend it to three-dimensions.

An extension to a fully three-dimensional problem would require a bit more work. First, one wouldn't have the advantage of being able to integrate over ϕ as we have, so the resulting integral equations would be in two variables, making any analytic work more complicated. Second, it would be wise to parameterise the problem in terms of a Lagrangian coordinate system based on the circulation strength, such as those developed by Birkhoff (1962) and Rott (1956). This would give rise to a more complicated geometry and further complicate the analytical work that is necessary to counteract the additional computation resources required.

These proposed extensions seem to entail a great deal of work, and it is regrettable that the extent of the research in this thesis has been stunted by the limitations imposed by time constraints. We would have liked to develop a complete and working numerical scheme for a flow with separated wake structures by the symmetrisation of the governing equations presented in chapter 3, and we would have liked to look closer at how to solve the integral equations that arise in the fully three-dimensional problem to get an idea of the level of analysis required in that problem.

It could be argued that the simplifications made in the model presented in this thesis make the governing equations so much simpler than those that would arise in the fully three-dimensional problem that any precedent set in this thesis would not apply to a more realistic model. However, it is the belief of this author that in setting an example for the rigorousness of the analytical treatment of the governing equations, we *have* set a precedent for the level of analysis required in future extensions of this work.

Appendix A

Useful integral identities

Here are a number of integral identities used in the text

$$\frac{1}{\pi}\!\!\int_0^1 \frac{d\sigma}{\sigma - r}\frac{\sqrt{1-\sigma}}{\sqrt{\sigma}} = -1. \tag{A.1}$$

$$\frac{1}{\pi}\int_0^\pi \frac{\cos(j\theta)\sin(i\theta)(1-\cos\theta)}{\sin\theta}d\theta = \frac{2-\delta_{ij}}{2}\left\{\begin{array}{ll} 0 & , \quad j > i, \\ (-1)^{i+j+1} & , \quad j \leq i. \end{array}\right. \tag{A.2}$$

$$\frac{1}{\pi}\!\!\int_{-1}^1 \frac{d\sigma}{\sigma - r}\sqrt{1+\sigma}\sqrt{1-\sigma} = -r. \tag{A.3}$$

Appendix B

Evaluating the integrals over ϕ in the axisymmetric disc problem

We wish to evaluate

$$I_1(\alpha) = \int_0^\pi \frac{du}{(1 - \alpha \cos u)^{\frac{3}{2}}}, \tag{B.1}$$

$$I_2(\alpha) = \int_0^\pi \frac{du \cos u}{(1 - \alpha \cos u)^{\frac{3}{2}}}. \tag{B.2}$$

in terms of the elliptic integrals of the first and second kind ($K(m)$ and $E(m)$ respectively)

$$K(m) = \int_0^{\frac{\pi}{2}} \frac{du}{\sqrt{1 - m \sin^2 u}},$$

$$E(m) = \int_0^{\frac{\pi}{2}} du \sqrt{1 - m \sin^2 u}.$$

First, consider

$$\int_0^\pi \frac{du}{\sqrt{1 - \alpha \cos u}} = \frac{2}{\sqrt{1 + \alpha}} K\left(\frac{2\alpha}{1 + \alpha}\right), \tag{B.3}$$

which can be shown by making the substitutions $u = 2\theta$ followed by $\phi = \theta + \pi/2$, then by exploiting the symmetry of the resulting integrand about $\pi/2$. Differentiating both sides with respect to α and making use of the identity

$$\frac{1}{(1 - \alpha \cos u)^{\frac{3}{2}}} = \frac{1}{\sqrt{1 - \alpha \cos u}} + \frac{\alpha \cos u}{(1 - \alpha \cos u)^{\frac{3}{2}}}, \tag{B.4}$$

gives us

$$I_1(\alpha) = \frac{2}{\sqrt{1 + \alpha}} K\left(\frac{2\alpha}{1 + \alpha}\right) + 4\alpha \frac{d}{d\alpha}\left(\frac{1}{\sqrt{1 + \alpha}} K\left(\frac{2\alpha}{1 + \alpha}\right)\right), \tag{B.5}$$

$$I_2(\alpha) = 4\frac{d}{d\alpha}\left(\frac{1}{\sqrt{1 + \alpha}} K\left(\frac{2\alpha}{1 + \alpha}\right)\right). \tag{B.6}$$

We then apply the differential property of the elliptic integral of the first kind

$$\frac{d}{dm}K(m) = \frac{1}{2m(1 - m)}\Big(E(m) - (1 - m)K(m)\Big),$$

and the relevant simplifications give us equation

$$I_1(\alpha) = \frac{2}{(1 - \alpha)\sqrt{1 + \alpha}} E\left(\frac{2\alpha}{1 + \alpha}\right), \tag{B.7}$$

$$I_2(\alpha) = \frac{2}{(1 - \alpha)\sqrt{1 + \alpha}}\left(E\left(\frac{2\alpha}{1 + \alpha}\right) - (1 - \alpha)K\left(\frac{2\alpha}{1 + \alpha}\right)\right), \tag{B.8}$$

Appendix C

Evaluating the logarithmic integrals in $N(\rho, r)$

We begin by considering

$$\mathcal{L}_1(\rho, r) = \frac{1}{\pi} \int_0^1 \frac{d\sigma}{\sigma - r} \frac{\sqrt{1 - \sigma}}{\sqrt{\sigma}} \log |\rho - \sigma|. \tag{C.1}$$

where both $\rho, r \in [0, 1]$. To evaluate this integral, we consider the integral of the function

$$f(z) = \frac{\log(z - \rho)}{z - r} \left(\frac{\sqrt{z - 1}}{\sqrt{z}} - 1 \right),$$

around the contour C in figure C.1 in the limit $R \to \infty$ and $\epsilon \to 0$. We choose this contour because it excludes all the branch cuts and singularities of $f(z)$, so by Cauchy's integral theorem the total value of the integral will be zero. Just above and below the real line, the function can be evaluated piecewise as

$$\lim_{\nu \to 0^\pm} f(\lambda + i\nu) = \begin{cases} \dfrac{\log(\rho - \lambda) \pm i\pi}{\lambda - r} \left(\dfrac{\sqrt{1 - \lambda}}{\sqrt{-\lambda}} - 1 \right) & , \quad -\infty < \lambda < 0, \\[3mm] \dfrac{\log(\rho - \lambda) \pm i\pi}{\lambda - r} \left(\dfrac{\pm i\sqrt{1 - \lambda}}{\sqrt{\lambda}} - 1 \right) & , \quad 0 < \lambda < \rho, \\[3mm] \dfrac{\log(\lambda - \rho)}{\lambda - r} \left(\dfrac{\pm i\sqrt{1 - \lambda}}{\sqrt{\lambda}} - 1 \right) & , \quad \rho < \lambda < 1, \end{cases} \tag{C.2}$$

where the superscript $\pm$ is used to distinguish between the function value when approaching from above or below the x-axis. The jump across the x-axis is
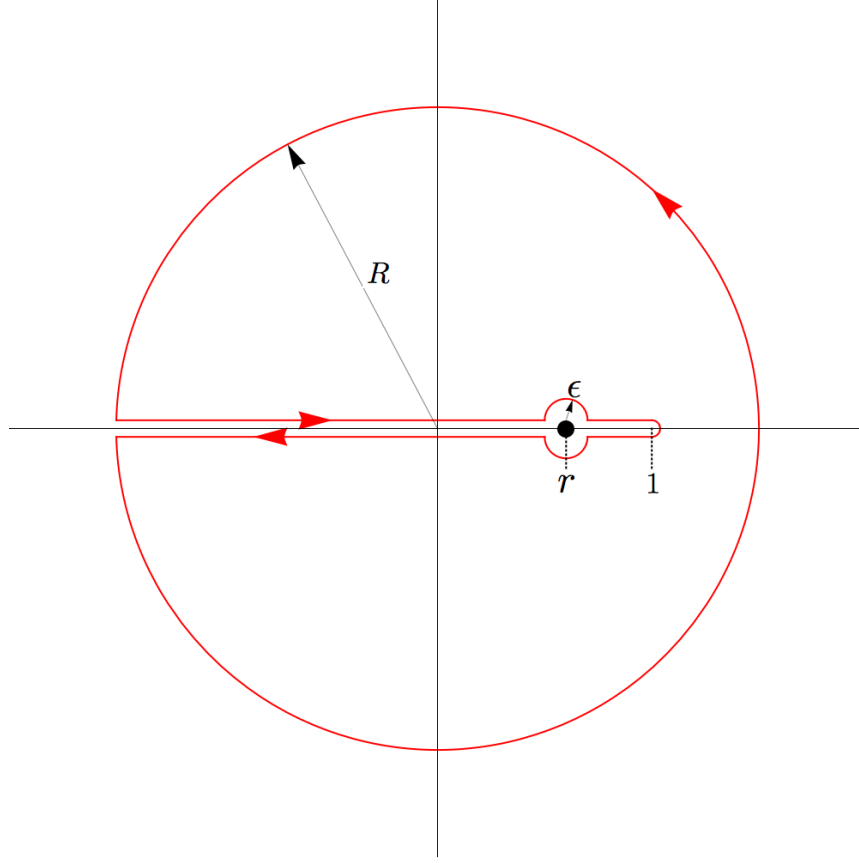
Figure C.1: The contour about which we integrate $f(z)$. We take the limit $R \to \infty$ and $\epsilon \to 0$. The parts of the contour that appear to run along the x-axis are to be thought of as infinitely close to but slightly above and below the x-axis. The part we are really interested in is from 0 to 1.

$$\left[f^{\pm}(\lambda)\right]_{-}^{+} = \begin{cases} \dfrac{2\pi i}{\lambda - r}\left(\dfrac{\sqrt{1-\lambda}}{\sqrt{-\lambda}} - 1\right) & , \quad -\infty < \lambda < 0, \\[3ex] 2\pi i\left(\dfrac{1}{\pi}\dfrac{\log(\rho - \lambda)}{\lambda - r}\dfrac{\sqrt{1-\lambda}}{\sqrt{\lambda}} - \dfrac{1}{\lambda - r}\right) & , \quad 0 < \lambda < \rho, \\[3ex] 2i\dfrac{\log(\lambda - \rho)}{\lambda - r}\dfrac{\sqrt{1-\lambda}}{\sqrt{\lambda}} & , \quad \rho < \lambda < 1, \end{cases} \qquad (C.3)$$

Integrating over the outer circle

We begin by showing that $\lim_{R\to\infty} f(z)dz = 0$ for $z = Re^{i\phi}$, $dz = Rie^{i\phi}d\phi$. Writing $\delta = 1/Re^{i\phi}$, we have

$$\lim_{R \to \infty} dz f(z) = \lim_{R \to \infty} R i e^{i\phi} d\phi f(R i e^{i\phi}) = i d\phi \lim_{\delta \to 0} \frac{\log(1 - \rho\delta) - \log(\delta)}{1 - r\delta} \left(\sqrt{1 - \delta} - 1 \right) \quad \text{(C.4)}$$

Expanding close to $\delta = 0$, we have $\sqrt{1 - \delta} \sim 1 - \delta/2 + O(\delta^2)$ and we can show that this part of the integral disappears.

Integrating from 0 to 1

Next, we consider the part of the integral between 0 and 1, taking into account both parts of the contour, above and below the axis. The function we are integrating is different for $\rho < r$ and $\rho > r$ so we deal with each case separately, starting with the former.

Case 1: $\rho < r$

The part of the integral from 0 to ρ does not contain the Cauchy singularity at $\lambda = r$, so it evaluates trivially to

$$\int_0^\rho f^+(\lambda) d\lambda + \int_\rho^0 f^-(\lambda) d\lambda = \int_0^\rho \left[f^\pm(\lambda) \right]_-^+ d\lambda =$$

$$2\pi i \left(\frac{1}{\pi} \int_0^\rho \frac{d\lambda}{\lambda - r} \frac{\sqrt{1 - \lambda}}{\sqrt{\lambda}} \log(\rho - \lambda) - \int_0^\rho \frac{d\lambda}{\lambda - r} \right). \quad \text{(C.5)}$$

Notice that the first integral on the RHS of equation (C.5) is of the form (C.1). Now, consider the part of the integral from ρ to 1. To evaluate this we must take a Cauchy principal value by going around the point r, so in the region of that point we write $\lambda = r + \epsilon e^{i\phi}$, and take the limit $\epsilon \to 0$. This gives us

$$\int_\rho^1 \left[f^\pm(\lambda) \right]_-^+ d\lambda = \fint_\rho^1 \left[f^\pm(\lambda) \right]_-^+ d\lambda$$

$$+ \lim_{\epsilon \to 0} \left(\int_\pi^0 \epsilon i e^{i\phi} f^+(r + \epsilon e^{i\phi}) d\phi + \int_0^{-\pi} \epsilon i e^{i\phi} f^-(r + \epsilon e^{i\phi}) d\phi \right).$$

The limit $\epsilon \to 0$ evaluates trivially to $\log(r - \rho)$ and eliminates all terms in ϕ. Upon including the integral from $-\infty$ to 0 we have the integral around the entire contour, which

we know must evaluate to zero, so we have

$$\mathcal{L}_1(\rho, r) = \frac{-1}{2\pi i} \int_{-\infty}^{0} \left[f^{\pm}(\lambda) \right]_{-}^{+} d\lambda - \int_0^{\rho} \frac{d\lambda}{\lambda - r} + \log(r - \rho), \qquad \rho < r.$$

Case 2: $\rho > r$

The calculation with $\rho > r$ goes through very much the same as that for $\rho < r$, only with a slight difference in the limit term, so that

$$\mathcal{L}_1(\rho, r) = \frac{-1}{2\pi i} \int_{-\infty}^{0} \left[f^{\pm}(\lambda) \right]_{-}^{+} d\lambda - \int_0^{\rho} \frac{d\lambda}{\lambda - r} + \log(\rho - r) - \frac{\pi\sqrt{1-r}}{\sqrt{r}}, \qquad \rho > r.$$

Integrating from $-\infty$ to 0

We use the integral identities

$$\int_0^{\rho} \frac{d\lambda}{\lambda - r} = \int_0^{\rho} \frac{d\lambda}{\lambda - r} = \log|\rho - r| - \log(r), \tag{C.6}$$

$$\int_{-\infty}^{0} \frac{d\lambda}{\lambda - r} \left(\frac{\sqrt{1-\lambda}}{\sqrt{-\lambda}} - 1 \right) = \log(4) + \log(r) + \frac{2\sqrt{1-r}}{\sqrt{r}} \arctan\left(\frac{\sqrt{1-r}}{\sqrt{r}} \right). \tag{C.7}$$

The first of these is relatively trivial. The second can be shown by first making the substitution $\lambda \to -\lambda$, then splitting the integrand into

$$\frac{d\lambda}{\lambda + r} \left(\frac{\sqrt{1+\lambda}}{\sqrt{\lambda}} - 1 \right) = \frac{1 - r}{(\lambda + r)\sqrt{1+\lambda}\sqrt{\lambda}} + \frac{1}{\sqrt{1+\lambda}\sqrt{\lambda}} - \frac{1}{\lambda + r}, \tag{C.8}$$

and making use of the log definitions of the hyperbolic trigonometric functions to ensure that the correct terms cancel as $\lambda \to \infty$. Ultimately, the result we require is

$$\mathcal{L}_1(\rho, r) = \frac{2\sqrt{1-r}}{\sqrt{r}} \arctan\left(\frac{\sqrt{1-r}}{\sqrt{r}} \right) + \log(4) - \pi H(\rho - r)\frac{\sqrt{1-r}}{\sqrt{r}},$$

where $H(\rho - r)$ is the Heaviside function.

Now, consider

$$\mathcal{L}_2(\rho, r) = \frac{1}{\pi} \int_0^1 \frac{d\sigma}{\sigma - r} \frac{\sqrt{1-\sigma}}{\sqrt{\sigma}} \log(\rho + \sigma).$$

Here, we integrate the function

$$f(z) = \frac{\log(z + \rho)}{z - r}\left(\frac{\sqrt{z-1}}{\sqrt{z}} - 1\right),$$

around the exact same contour. The function takes the following values just above and below the x-axis;

$$\lim_{\nu \to 0^{\pm}} f(\lambda + i\nu) = \begin{cases} \dfrac{\log(\rho - \lambda) \pm i\pi}{\lambda - r}\left(\dfrac{\sqrt{1-\lambda}}{\sqrt{-\lambda}} - 1\right) &, \quad \lambda < -\rho, \\[2mm] \dfrac{\log(\lambda + \rho)}{\lambda - r}\left(\dfrac{\sqrt{1-\lambda}}{\sqrt{-\lambda}} - 1\right) &, \quad -\rho < \lambda < 0, \\[2mm] \dfrac{\log(\lambda + \rho)}{\lambda - r}\left(\dfrac{\pm i\sqrt{1-\lambda}}{\sqrt{\lambda}} - 1\right) &, \quad 0 < \lambda < 1, \end{cases}$$

Following the exact same methods as before, we arrive at

$$\mathcal{L}_2(\rho, r) = \int_{\rho}^{\infty} \frac{d\lambda}{\lambda + r}\left(\frac{\sqrt{1-\lambda}}{\sqrt{\lambda}} - 1\right) - \log(r + \rho). \tag{C.9}$$

The part of the integral from $-\rho$ to 0 disappears because there is no branch cut here. Evaluating the integral on the RHS of equation (C.9) as before, we derive

$$\mathcal{L}_2(\rho, r) = \log(4) - 2\mathrm{arcsinh}(\sqrt{\rho}) + \frac{2\sqrt{1-r}}{\sqrt{r}}\left(\arctan\left(\frac{\sqrt{r}\sqrt{1+\rho}}{\sqrt{1-r}\sqrt{\rho}}\right) - \arctan\left(\frac{\sqrt{r}}{\sqrt{1-r}}\right)\right).$$

By use of the identity $\arctan(x) + \arctan(1/x) = \pi/2$ (for $x > 0$) to simplify the equation, we have the final integral

$$\int_0^1 \frac{d\sigma}{\sigma - r}\frac{\sqrt{1-\sigma}}{\sqrt{\sigma}}\log\left|\frac{\rho - \sigma}{\rho + \sigma}\right| = 2\mathrm{arcsinh}(\sqrt{\rho}) - \frac{2\sqrt{1-r}}{\sqrt{r}}\arctan\left(\frac{\sqrt{r}\sqrt{1+\rho}}{\sqrt{1-r}\sqrt{\rho}}\right)$$
$$+ \pi H(r - \rho)\frac{\sqrt{1-r}}{\sqrt{r}}. \tag{C.10}$$

Appendix D

Evaluating the integrals over ϕ in the symmetrised axi-symmetric disc problem

We wish to evaluate

$$I_1^\pm(\alpha) = \int_{\pm\frac{\pi}{2}}^{\pi\pm\frac{\pi}{2}} \frac{d\phi}{(1 - \alpha\cos\phi)^{\frac{3}{2}}}, \tag{D.1}$$

$$I_2^\pm(\alpha) = \int_{\pm\frac{\pi}{2}}^{\pi\pm\frac{\pi}{2}} \frac{d\phi\,\cos\phi}{(1 - \alpha\cos\phi)^{\frac{3}{2}}}, \tag{D.2}$$

in terms of the incomplete elliptic integrals of the first and second kind

$$F(\phi, k) = \int_0^\phi \frac{du}{\sqrt{1 - k\sin^2 u}}$$

$$E(\phi, k) = \int_0^\phi du\sqrt{1 - k\sin^2 u}$$

We begin by considering the integral

$$\int_{-\frac{\pi}{2}}^{\frac{\pi}{2}} \frac{d\phi}{\sqrt{1 - \alpha\cos\phi}} = \frac{4}{\sqrt{1 - \alpha}} F\left(\frac{\pi}{4}, \frac{-2\alpha}{1 - \alpha}\right), \tag{D.3}$$

69

which can be shown by first exploiting the evenness of the integrand about $\phi = 0$ to just evaluate the integral over the period 0 to $\pi/2$, then subsequently making the substitution $\phi = 2u$. We can use a similar method on the integrals from $\pi/2$ to $3\pi/2$, and differentiating both sides of this equation with respect to α, and making use of the identity in equation (B.4), it follows that

$$I_1^{\pm}(\alpha) = \frac{4}{\sqrt{1 \pm \alpha}} F\left(\frac{\pi}{4}, \frac{\pm 2\alpha}{1 \pm \alpha}\right) + 8\alpha \frac{d}{d\alpha}\left(\frac{4}{\sqrt{1 \pm \alpha}} F\left(\frac{\pi}{1}, \frac{\pm 2\alpha}{1 \pm \alpha}\right)\right), \tag{D.4}$$

$$I_2^{\pm}(\alpha) = 8 \frac{d}{d\alpha}\left(\frac{4}{\sqrt{1 \pm \alpha}} F\left(\frac{\pi}{1}, \frac{\pm 2\alpha}{1 \pm \alpha}\right)\right). \tag{D.5}$$

We can then use the differential properties of elliptic integrals, that

$$\frac{d}{dk} F\left(\frac{\pi}{4}, k\right) = -\frac{\sqrt{2}}{4} \frac{1}{\sqrt{2-k}} \frac{1}{(1-k)} + \frac{E\left(\frac{\pi}{4}, k\right)}{2k(1-k)} - \frac{F\left(\frac{\pi}{4}, k\right)}{2k}, \tag{D.6}$$

along with the necessary simplifications to give us the results we require;

$$I_1^{\pm}(\alpha) = 4\left(\frac{\mp \alpha}{1 - \alpha^2} + \frac{\sqrt{1 \pm \alpha}}{1 - \alpha^2} E\left(\frac{\pi}{4}, \frac{\pm 2\alpha}{1 \pm \alpha}\right)\right), \tag{D.7}$$

$$I_2^{\pm}(\alpha) = 4\left(\frac{\mp 1}{1 - \alpha^2} + \frac{\sqrt{1 \pm \alpha}}{\alpha(1 - \alpha^2)} E\left(\frac{\pi}{4}, \frac{\pm 2\alpha}{1 \pm \alpha}\right) - \frac{1}{\alpha\sqrt{1 \pm \alpha}} F\left(\frac{\pi}{4}, \frac{\pm 2\alpha}{1 \pm \alpha}\right)\right), \tag{D.8}$$

Appendix E

Symmetrised log integrals

Integrating first log term

We begin by considering

$$\mathfrak{L}_1(\rho, r) = \frac{1}{\pi} \int_{-1}^{1} d\sigma \frac{\sqrt{1+\sigma}\sqrt{1-\sigma}}{\sigma - r} \log |\sigma - \rho|, \qquad (E.1)$$

where both $\rho, r \in [-1, 1]$. It should be noted that this integral appeared in a similar form in Appendix A of Jones (2003) and the following calculation was done in part with help from the author of that paper. To evaluate this integral, we consider the integral of the function

$$f(z) = \frac{\log(z - \rho)}{z - r} \left(\sqrt{z+1}\sqrt{z-1} - z \right), \qquad (E.2)$$

around the same contour as in figure C.1; indeed, this integral will have many similarities with that one. By Cauchy's integral theorem the integral around the entire contour will evaluate to zero, and just above and below the real line it can be evaluated piecewise as

$$\lim_{\nu \to 0^\pm} f(\lambda + i\nu) = \begin{cases} \dfrac{\log|\lambda - \rho| \pm i\pi}{\lambda - r} \left(-\sqrt{-\lambda - 1}\sqrt{1 - \lambda} - \lambda \right) &, \quad -\infty < \lambda < -1 \\[2ex] \dfrac{\log|\lambda - \rho| \pm i\pi}{\lambda - r} \left(\pm i\sqrt{1 + \lambda}\sqrt{1 - \lambda} - \lambda \right) &, \quad -1 < \lambda < \rho \\[2ex] \dfrac{\log|\lambda - \rho|}{\lambda - r} \left(\pm\sqrt{1 + \lambda}\sqrt{1 - \lambda} - \lambda \right) &, \quad \rho < \lambda < 1, \end{cases} \qquad (E.3)$$

where we have defined the superscripts on $f(z)$ to distinguish whether we are considering the limit from above or below the real line. The difference between these functions is

$$
\left[f^{\pm}(\lambda)\right]^{+}_{-} = \begin{cases} -\dfrac{2\pi i}{\lambda - r}\left(\sqrt{-1-\lambda}\sqrt{1-\lambda} + \lambda\right) & , \quad -\infty < \lambda < -1 \\[2em] 2i\dfrac{\log|\lambda - \rho|}{\lambda - r}\sqrt{1+\lambda}\sqrt{1-\lambda} - 2\pi i\dfrac{\lambda}{\lambda - r} & , \quad -1 < \lambda < \rho \\[2em] 2i\dfrac{\log|\lambda - \rho|}{\lambda - r}\sqrt{1+\lambda}\sqrt{1-\lambda} & , \quad -\rho < \lambda < 1. \end{cases}
\tag{E.4}
$$

Integrating over the outer circle

As before, we begin by showing that the integral over the outer circle goes to zero in the limit $R \to \infty$. By making the substitution $z = Re^{i\phi}$ and replacing the limit $R \to \infty$ with $\delta \to 0$ where $\delta = 1/Re^{i\phi}$ we have

$$
\lim_{R \to \infty} iRe^{i\phi}d\phi\, f(Re^{i\phi}) = \lim_{\delta \to 0}\left(\frac{i}{\delta}\frac{\log(1-\rho\delta) - \log(\delta)}{(1-r\delta)/\delta}\left(\sqrt{\frac{1+\delta}{\delta}}\sqrt{\frac{1-\delta}{\delta}} - \frac{1}{\delta}\right)\right), \tag{E.5}
$$

and by $\sqrt{1-\delta^2} \sim 1 - \delta^2/2 +)(\delta^4)$ we can show that this part of the integral disappears in the limit.

Integrating from -1 to 1

As in the previous log integrals, the function we have chosen to integrate changes across $\lambda = \rho$, so we consider the two cases $\rho < r$ and $\rho > r$ separately, starting with the former.

Case 1: $\rho < r$

The part of the integral from -1 to ρ and back again does not contain the Cauchy singularity at $\lambda = r$, so it evaluates trivially to

$$\int_{-1}^{\rho} f^+(\lambda)d\lambda + \int_{\rho}^{-1} f^-(\lambda)d\lambda$$

$$= 2\pi i \left(\frac{1}{\pi} \int_{-1}^{\rho} d\lambda \frac{\log|\lambda - \rho|}{\lambda - r} \sqrt{1+\lambda}\sqrt{1+\lambda} - \int_{-1}^{\rho} d\lambda \frac{\lambda}{\lambda - r} \right), \quad \text{(E.6)}$$

where it is worth noting that the first integral on the RHS of this equation takes the form of that in equation (E.1). Now when considering the part of the integral from ρ to 1 we must go *around* the Cauchy singularity at $\lambda = r$ by writing $\lambda = r + \epsilon e^{i\phi}$ and considering the limit $\epsilon \to 0$. This gives us

$$\int_{\rho}^{1} \left[f^\pm(\lambda) \right]_{-}^{+} d\lambda = \fint_{\rho}^{1} \left[f^\pm(\lambda) \right]_{-}^{+} d\lambda$$

$$+ \lim_{\epsilon \to 0} \left(\int_{\pi}^{0} i\epsilon e^{i\phi} f^+(r + \epsilon e^{i\phi})d\phi + \int_{0}^{-\pi} i\epsilon e^{i\phi} f^-(r + \epsilon e^{i\phi})d\phi \right), \quad \text{(E.7)}$$

and the limit evaluates trivially. With the integral from $-\infty$ to -1 we have the integral over the entire contour, and since we know this will evaluate to zero, we have

$$\mathfrak{L}_1(\rho, r) = \int_{-\infty}^{-1} d\lambda \frac{\sqrt{-1-\lambda}\sqrt{1-\lambda} + \lambda}{\lambda - r} + \int_{-1}^{\rho} d\lambda \frac{\lambda}{\lambda - r} - r \log|r - \rho|, \qquad \rho < r. \quad \text{(E.8)}$$

Case 2: $\rho > r$

In the case $\rho > r$ the calculation goes through almost exactly the same, only there is an additional term in the Cauchy principal value limit, which gives us

$$\mathfrak{L}_1(\rho, r) = \int_{-\infty}^{-1} d\lambda \frac{\sqrt{-1-\lambda}\sqrt{1-\lambda} + \lambda}{\lambda - r}$$

$$+ \fint_{-1}^{\rho} d\lambda \frac{\lambda}{\lambda - r} - r \log|r - \rho| - \pi\sqrt{1+r}\sqrt{1-r}, \qquad \rho > r. \quad \text{(E.9)}$$

Integral from $-\infty$ to -1 and result

We use the integral identities

$$\int_{-1}^{\rho} d\lambda \frac{\lambda}{\lambda - r} = \fint_{-1}^{\rho} d\lambda \frac{\lambda}{\lambda - r} = 1 + \rho - r \log|1 + r| + r \log|r - \rho|, \tag{E.10}$$

$$\int_{-\infty}^{-1} d\lambda \frac{\sqrt{-1 - \lambda}\sqrt{1 - \lambda} + \lambda}{\lambda - r} = -1 + r \log|1 + r| + r \log(2) + \sqrt{1 + r}\sqrt{1 - r} \arccos(r). \tag{E.11}$$

As in the previous contour integral, whilst the first of these integrals is relatively easy, the second is a little more complicated. Whilst no formal proof is given, it will suffice to say that it can be done by first making the substitution $\lambda \to -\lambda$ then splitting the integrand into

$$\frac{\sqrt{\lambda + 1}\sqrt{\lambda - 1} - \lambda}{\lambda + r} = \frac{r}{\lambda + r} - 1 + \frac{\lambda - r}{\sqrt{\lambda + 1}\sqrt{\lambda - 1}} - \frac{(1 + r)(1 - r)}{\sqrt{\lambda + 1}\sqrt{\lambda - 1}(\lambda + r)}, \tag{E.12}$$

and using the log definitions of the hyperbolic trigonometric functions to ensure the correct terms cancel as $\lambda \to \infty$. Ultimately, the result we require is

$$\mathfrak{L}_1(\rho, r) = \rho + r \log(2) + \sqrt{1 + r}\sqrt{1 - r} \arccos(r) - \pi\sqrt{1 + r}\sqrt{1 - r}H(\rho - r), \tag{E.13}$$

where $H(\rho - r)$ is the Heaviside function.

Integrating second log term

Let us now consider the (slightly) more complicated integral

$$\mathfrak{L}_2(\rho, r) = \frac{1}{2\pi}\int_{-1}^{1} d\sigma \frac{\sqrt{1 + \sigma}\sqrt{1 - \sigma}}{\sigma - r} \log\left(\sigma^2 + \rho^2\right), \tag{E.14}$$

with $\rho, r \in [-1, 1]$. Since this integral is even in ρ, we will assume $\rho > 0$ and the result will be the same as for $\rho < 0$. We will compute this integral by considering the function

$$f(z) = \frac{\log\left(z^2 + \rho^2\right)}{z - r}\left(\sqrt{z + 1}\sqrt{z - 1} - z\right), \tag{E.15}$$

which we split into $f(z) = f_1(z) + f_2(z)$ with

$$f_1(z) = \frac{\log(\rho + iz)}{z - r} \left(\sqrt{z+1}\sqrt{z-1} - z \right), \tag{E.16}$$

$$f_2(z) = \frac{\log(\rho - iz)}{z - r} \left(\sqrt{z+1}\sqrt{z-1} - z \right), \tag{E.17}$$

and integrate $f_1(z)$ and $f_2(z)$ around the contours C_1 and C_2 in figures E.1(a) and E.1(b) respectively. Both these contours are specifically designed to exclude the branch cuts and
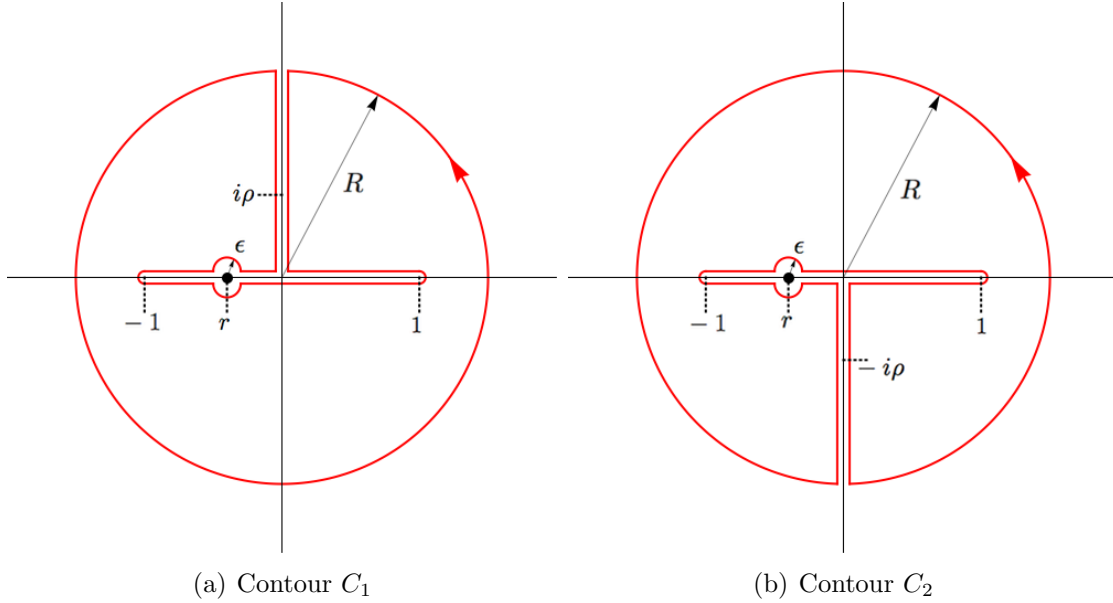

(a) Contour C_1 (b) Contour C_2

Figure E.1: The two contours C_1 and C_2 around which we integrate the functions $f_1(z)$ and $f_2(z)$ respectively. We take the limit $R \to \infty$ and $\epsilon \to 0$. The parts that appear to run along axis are to be thought of as adjacent to the axis in the limit of approaching the axis from their respective sides.

singularities in the functions they apply to for $\rho > 0$. Let us consider the positions of these branch cuts; first in $f_1(z)$, along the real axis we use the argand definition of the complex number $\rho + iz$ to split the log term into its real and imaginary parts, and we have

$$\lim_{\nu \to 0^{\pm}} f_1(\lambda + i\nu) = \frac{\frac{1}{2}\log\left(\rho^2 + \lambda^2\right) + i\arg(\rho + i\lambda)}{\lambda - r} \left(\pm i\sqrt{1+\lambda}\sqrt{1-\lambda} - \lambda \right), \tag{E.18}$$

$$\left[f_1^{\pm}(\lambda) \right]_-^+ = 2i \frac{\frac{1}{2}\log\left(\rho^2 + \lambda^2\right) + i\arg(\rho + i\lambda)}{\lambda - r} \sqrt{1+\lambda}\sqrt{1-\lambda}, \tag{E.19}$$

where the $\pm$ refer to approaching the real axis from above or below, as before. Now along the positive imaginary axis, we consider the cases $0 < \nu < \rho$ and $\rho < \nu < \infty$ (for $z = \lambda + i\nu$) separately. When $0 < \nu < \rho$ we have

$$\lim_{\lambda \to 0^\pm} f_1(\lambda + i\nu) = \frac{\log(\rho - \nu)}{\nu + ir} \left(\sqrt{1 + \nu^2} - \nu \right). \tag{E.20}$$

This implies that there is *no* branch cut in $f_1(z)$ along the imaginary axis between $0 < \nu < \rho$, so the integral along that portion of the contour in one direction will be exactly cancelled by that in the opposite direction. However, for $\rho < \nu < \infty$ we have

$$\lim_{\lambda \to 0^\pm} f_1(\lambda + i\nu) = \frac{\log(\nu - \rho) \pm i\pi}{\nu + ir} \left(\sqrt{1 + \nu^2} - \nu \right), \tag{E.21}$$

$$\left[f_1^\pm(i\nu) \right]_-^+ = \frac{2\pi i}{\nu + ir} \left(\sqrt{1 + \nu^2} - \nu \right). \tag{E.22}$$

Integrating over outer circle

We start the integration of $f_1(z)$, as before, by showing that the function decays rapidly enough to disappear when integrated over the outer circle in the limit $R \to \infty$. Once again, we do this by making the substitution $z = Re^{i\phi}$ and replacing the limit $R \to \infty$ with $\delta \to 0$ for $\delta = 1/Re^{i\phi}$, and we have

$$\lim_{R \to \infty} iRe^{i\phi} d\phi f_1\left(Re^{i\phi} \right) = \lim_{\delta \to 0} \left(id\phi \frac{\log(\rho\delta + i) - \log(\delta)}{1 - r\delta} \frac{1}{\delta} \left(\operatorname{sgn}(\delta) \sqrt{1 - \delta^2} - 1 \right) \right), \tag{E.23}$$

and by $\sqrt{1 - \delta^2} \sim 1 - \delta^2/2 + O\left(\delta^4 \right)$ it is trivial to show that this is zero in the limit.

Integrating from -1 to 1

In the integral from -1 to 1 we must go around the Cauchy singularity at $\lambda = r$, as before, by writing $\lambda = r + \epsilon e^{i\phi}$ in the region of that point. It is also worth noting that whilst the contour in this region technically has three parts, from 0 to 1 above the real axis, from 1 to -1 below the real axis and back from -1 to 0 above the real axis, there is *no* branch cut in the function as it crosses the imaginary axis in the limit $\nu \to 0^+$, so we can treat the two parts of the contour above the axis as a single line, and by extension the integral

along those lines becomes a single integral. Thus we have

$$
\int_{-1}^{1} \left[f_1^{\pm}(\lambda) \right]_{-}^{+} d\lambda = \oint_{-1}^{1} \left[f^{\pm}(\lambda) \right]_{-}^{+} d\lambda
$$
$$
+ \lim_{\epsilon \to 0} \left(\int_{\pi}^{0} i\epsilon e^{i\phi} f_1^{+}(r + \epsilon e^{i\phi}) d\phi + \int_{0}^{-\pi} i\epsilon e^{i\phi} f_1^{-}(r + \epsilon e^{i\phi}) d\phi \right), \quad \text{(E.24)}
$$

and upon evaluating the limit we have

$$
\int_{-1}^{1} \left[f_1^{\pm}(\lambda) \right]_{-}^{+} d\lambda = 2i \oint_{-1}^{1} d\lambda \frac{\frac{1}{2}\log\left(\rho^2 + \lambda^2\right)}{\lambda - r} \sqrt{1+\lambda}\sqrt{1-\lambda}
$$
$$
- 2 \int_{-1}^{1} d\lambda \frac{\frac{1}{2}\arg\left(\rho + i\lambda\right)}{\lambda - r} \sqrt{1+\lambda}\sqrt{1-\lambda}
$$
$$
+ 2\pi i r \left(\frac{1}{2}\log\left(\rho^2 + r^2\right) + i\arg\left(\rho + ir\right) \right). \quad \text{(E.25)}
$$

Upon including the integrals from $\nu = \rho$ to ∞ and back (remembering that the integrals from $\nu = 0$ to ρ and back cancels) we have the integral around the entire contour, which we know must equal zero, so we have

$$
\frac{1}{\pi} \oint_{-1}^{1} d\lambda \frac{\frac{1}{2}\log\left(\rho^2 + \lambda^2\right)}{\lambda - r} \sqrt{1+\lambda}\sqrt{1-\lambda} = \frac{2}{2\pi i} \oint_{-1}^{1} d\lambda \frac{\arg\left(\rho + i\lambda\right)}{\lambda - r} \sqrt{1+\lambda}\sqrt{1-\lambda}
$$
$$
- r \left(\frac{1}{2}\log\left(\rho^2 + r^2\right) + i\arg\left(\rho + ir\right) \right) + i \int_{\rho}^{\infty} d\nu \frac{\sqrt{1+\nu^2} - \nu}{\nu + ir}.
$$
$$
\text{(E.26)}
$$

We can follow an almost identical method for integrating $f_2(z)$ around C_2. Along the real axis, $f_2(z)$ takes the values

$$
\lim_{\nu \to 0^{\pm}} f_2(\lambda + i\nu) = \frac{\frac{1}{2}\log\left(\rho^2 + \lambda^2\right) - i\arg(\rho + i\lambda)}{\lambda - r} \left(\pm i\sqrt{1+\lambda}\sqrt{1-\lambda} - \lambda \right), \quad \text{(E.27)}
$$
$$
\left[f_2^{\pm}(\lambda) \right]_{-}^{+} = 2i \frac{\frac{1}{2}\log\left(\rho^2 + \lambda^2\right) - i\arg(\rho + i\lambda)}{\lambda - r} \sqrt{1+\lambda}\sqrt{1-\lambda}. \quad \text{(E.28)}
$$

As before, there is no branch cut between $0 > \nu > -\rho$, and between $-\rho > \nu > -\infty$ we have

$$\lim_{\lambda \to 0^{\pm}} f_2(\lambda + i\nu) = \frac{\log(-\nu - \rho) \mp i\pi}{\nu + ir} \left(-\sqrt{1 + \nu^2} - \nu \right), \tag{E.29}$$

$$\left[f_2^{\pm}(i\nu) \right]_{-}^{+} = \frac{2\pi i}{\nu + ir} \left(\sqrt{1 + \nu^2} + \nu \right). \tag{E.30}$$

Following the same steps as in the calculation for $f_1(z)$ we arrive at

$$\frac{1}{\pi} \int_{-1}^{1} d\lambda \frac{\frac{1}{2} \log(\rho^2 + \lambda^2)}{\lambda - r} \sqrt{1 + \lambda} \sqrt{1 - \lambda} = -\frac{2}{2\pi i} \int_{-1}^{1} d\lambda \frac{\arg(\rho + i\lambda)}{\lambda - r} \sqrt{1 + \lambda} \sqrt{1 - \lambda}$$
$$- r \left(\frac{1}{2} \log(\rho^2 + r^2) - i \arg(\rho + ir) \right) - i \int_{\rho}^{\infty} d\nu \frac{\sqrt{1 + \nu^2} - \nu}{\nu - ir}, \tag{E.31}$$

where we have made the substitution $\nu \to -\nu$ in the integral between ρ and ∞. Now, adding together equations (E.26) and (E.31) and making the relevant cancelations, we have

$$\mathcal{L}_2(\rho, r) = r \int_{\rho}^{\infty} d\nu \frac{\sqrt{1 + \nu^2} - \nu}{\nu^2 + r^2} - \frac{r}{2} \log(\rho^2 + r^2). \tag{E.32}$$

The integral on the RHS of this equation can be evaluated by splitting the integrand into

$$\frac{\sqrt{1 + \nu^2} - \nu}{\nu^2 + r^2} = \frac{1}{\sqrt{1 + \nu^2}} + \frac{1 - r^2}{\sqrt{1 + \nu^2}\,(\nu^2 + r^2)} - \frac{\nu}{\nu^2 + r^2}, \tag{E.33}$$

and making use of the log definition of arcsinh to ensure the correct terms cancel as $\nu \to \infty$ and the integral identity

$$\int \frac{1 - r^2}{\sqrt{1 + \nu^2}\,(\nu^2 + r^2)} = \frac{\sqrt{1 - r^2}}{r} \arctan\left(\frac{\nu\sqrt{1 - r^2}}{r\sqrt{1 + \nu^2}} \right). \tag{E.34}$$

Finally, we neaten up the equation by $\arctan(x) + \arctan(y) = \arctan((x + y)/(1 - xy))$ and we have our result

$$\mathfrak{L}_2(\rho, r) = \sqrt{1+r}\sqrt{1-r}\arctan\left(\frac{r\sqrt{1-r^2}\left(\sqrt{1+\rho^2}-|\rho|\right)}{r^2\sqrt{1+\rho^2}+(1-r^2)\,|\rho|}\right) + r\log(2) - r\,\mathrm{arcsinh}|\rho|.$$

$$(\text{E.35})$$

This result is true for all $\rho \in [-1, 1]$ and features absolute values of terms in ρ because the integral must be even in ρ. Bringing this together with equation (E.13) we have the integral we require

$$\mathfrak{L}_1(\rho, r) - \mathfrak{L}_2(\rho, r) = \frac{1}{\pi}\int_{-1}^{1}\frac{d\sigma}{\sigma - r}\sqrt{1+\sigma}\sqrt{1-\sigma}\log\left|\frac{\rho - \sigma}{\sqrt{\rho^2+\sigma^2}}\right|$$

$$= \rho + r\,\mathrm{arcsinh}|\rho| - \sqrt{1+r}\sqrt{1-r}\left(\pi H(\rho - r) - \arccos(r)\right)$$

$$- \sqrt{1+r}\sqrt{1-r}\arctan\left(\frac{r\sqrt{1-r^2}\left(\sqrt{1+\rho^2}-|\rho|\right)}{r^2\sqrt{1+\rho^2}+(1-r^2)\,|\rho|}\right). \quad (\text{E.36})$$

Appendix F

Chebyshev polynomials - background

The Chebyshev polynomials of the first kind $T_n(x)$ are a sequence of orthogonal polynomials. They arise as the solution to

$$(1 - x^2)y'' - xy' + n^2 y = 0,$$

and can be generated by the recurrence relation

$$T_0(x) = 1, \qquad T_1(x) = x, \qquad T_{n+1}(x) = 2xT_n(x) - T_{n-1}(x). \tag{F.1}$$

They can be expressed as $T_n(x) = \cos(n \arccos(x))$ and they satisfy the orthogonality condition

$$\int_{-1}^{1} \frac{T_m(x)T_n(x)}{\sqrt{1-x}\sqrt{1+x}} dx = \frac{1}{2}\pi\delta_{mn}(1 + \delta_{0n}) \equiv \begin{cases} 0 & , \quad n \neq m \\ \pi & , \quad n = m = 0 \\ \pi/2 & , \quad n = m \neq 0 \end{cases},$$

where δ_{nm} is the Kronecker delta. It is evident from the cosine definition that the zeros of $T_n(x)$ are at

$$x_k = \cos\left(\frac{\pi(k + 1/2)}{n}\right) \quad , \quad k = 0, 1, \dots, n - 1. \tag{F.2}$$

Hence, if x_k are the N zeros of $T_N(x)$, we also have a discrete orthogonality condition (Mason & Handscomb 2002)

$$\sum_{k=0}^{N-1} T_i(x_k)T_j(x_k) = \frac{1}{2}N\delta_{ij}(1 + \delta_{0j}) \equiv \begin{cases} 0 & , \quad i \neq j \\ N & , \quad i = j = 0 \\ N/2 & , \quad i = j \neq 0 \end{cases} . \tag{F.3}$$

We also have the *shifted* Chebyshev polynomials

$$T_n^*(x) = T_n(2x - 1),$$

which have a similar orthogonality condition

$$\int_0^1 \frac{T_m^*(x)T_n^*(x)}{\sqrt{x}\sqrt{1-x}}dx = \frac{1}{2}\pi\delta_{mn}(1 + \delta_{0n}) \equiv \begin{cases} 0 & , \quad n \neq m \\ \pi & , \quad n = m = 0 \\ \pi/2 & , \quad n = m \neq 0 \end{cases} . \tag{F.4}$$

Similarly, the zeros of the shifted Chebyshev polynomials are

$$x_k = \frac{1}{2}\left(\cos\left(\frac{\pi(k + 1/2)}{n}\right) + 1\right) \quad , \quad k = 0, 1, \dots, n - 1, \tag{F.5}$$

and the discrete orthogonality condition holds as in equation (F.3). Now, if one were to approximate a function as a series of N Chebyshev polynomials

$$f(x) = \sum_{i=0}^{N-1} a_i T_i(x),$$

then multiplying both sides by $T_j(x)$ and evaluating at the k'th zero of $T_N(x)$ gives

$$T_j(x_k)f(x_k) = \sum_{i=0}^{N-1} a_i T_i(x_k)T_j(x_k).$$

Then, summing over all the zero nodes (that is, over all k), gives us

$$\sum_{k=0}^{N-1} T_j(x_k)f(x_k) = \frac{1}{2}a_j N(1 + \delta_{0j}).$$

by equation (F.3). Therefore, we can compute the coefficients a_i by

$$a_i = \frac{2 - \delta_{0i}}{N} \sum_{k=0}^{N-1} T_i(x_k)f(x_k).$$

This method has one particularly attractive asset. By $T_n(x) = \cos(n \arccos(x))$ we have

$$a_i = \frac{2 - \delta_{0i}}{N} \sum_{k=0}^{N-1} \cos\left(\frac{i\pi(k + 1/2)}{N}\right) f(x_k). \tag{F.6}$$

This sum can be rapidly computed by a discrete cosine transform (for this reason, we usually take $N = 2^m$ for some $m \in \mathbb{N}$). We can do the exact same procedure for a function of two variables

$$g(x, y) = \sum_{i=0}^{N-1} \sum_{j=0}^{N-1} g_{ij} T_i(x) T_j(y),$$

with

$$g_{ij} = \frac{(2 - \delta_{0i})(2 - \delta_{0j})}{N^2} \sum_{k=0}^{N-1} \sum_{m=0}^{N-1} T_i(x_k) T_j(y_m) g(x_k, y_m),$$

where x_k and y_m are the zeros of $T_N(x)$ or $T_N(y)$ as before. Again, this can be rapidly computed as $2N$ discrete cosine transforms

$$g_{ij} = \frac{(2 - \delta_{0i})(2 - \delta_{0j})}{N^2} \sum_{m=0}^{N-1} \bar{g}_i(y_m) \cos\left(\frac{j\pi(m + 1/2)}{N}\right),$$

$$\text{where} \quad \bar{g}_i(y_m) = \sum_{k=0}^{N-1} g(x_k, y_m) \cos\left(\frac{i\pi(k + 1/2)}{N}\right). \tag{F.7}$$

We will also require the integral identities

$$\fint_{-1}^{1} \frac{d\lambda}{\lambda - r} \frac{T_j(\lambda)}{\sqrt{1 - \lambda}\sqrt{1 + \lambda}} = U_{j-1}(r), \tag{F.8}$$

$$\fint_{-1}^{1} \frac{d\lambda}{\lambda - r} \sqrt{1 + \lambda}\sqrt{1 - \lambda} U_{k-1}(\lambda) = -\pi T_k(r), \tag{F.9}$$

where $U_j(r)$ is the Chebyshev polynomial of the second kind, and satisfies the recurrence relation

$$T_0(r) = U_0(r), \quad T_1(r) = \frac{1}{2}U_1(r),$$
$$T_j(r) = \frac{1}{2}\left(U_j(r) - U_{j-2}(r)\right), \tag{F.10}$$

and the continuous orthogonality condition

$$\frac{2}{\pi} \int_{-1}^{1} d\lambda \sqrt{1+\lambda}\sqrt{1-\lambda}U_i(\lambda)U_j(\lambda) = \delta_{ij}, \quad i \geq 0, \, j \geq 0. \tag{F.11}$$

Again, these properties have relevant translations into the shifted polynomial case.

Bibliography

S. Alben (2009). 'Simulating the dynamics of flexible bodies and vortex sheets'. *J. Comp. Phys.* **228**:2587–2603.

R. S. Anderssen, et al. (1980). *The application and numerical solution of integral equations.* Sijthoff & Noordhoff International.

S. A. Ansari, et al. (2006a). 'Non-linear unsteady aerodynamic model for insect-like flapping wings in the hover. Part 1: methodology and analysis'. *Proc. IMechE.* **220**:61–83.

S. A. Ansari, et al. (2006b). 'Non-linear unsteady aerodynamic model for insect-like flapping wings in the hover. Part 2: implementation and validation'. *Proc. IMechE.* **220**:169–186.

G. R. Baker, et al. (1982). 'Generalized vortex methods for free-surface flow problems'. *J. Fluid Mech.* **123**:477–501.

R. W. Barber & A. Fonty (2003). 'Comparison of vortex-element and finite-volume simulations of low Reynolds number flow over a confined backward facing step'. *Proc. of the 11th Ann. Conf. of the CFD soc. of Canada* **1**:780–787.

G. K. Batchelor (1967). *An Introduction to Fluid Dynamics.* Cambrdige University Press.

M. G. Benson, et al. (1989). 'A viscous splitting algorithm applied to low Reynolds number flows around a circular cyclinder'. *J. Fluids and Structures* **3**:439–479.

J. M. Birch & M. H. Dickinson (2001). 'Spanwise flow and the attachment of the leading-edge vortex on insect wings'. *Letters to Nature* **412**:729–733.

J. M. Birch, et al. (2004). 'Force production and flow structure of the leading edge vortex on flapping wings at high and low Reynolds number'. *J. Exp. Biol.* **207**:1063–1072.

G. Birkhoff (1962). 'Helmholtz and Taylor instability'. *Proceedings of Symposium in Applied Mathematics, vol. XIII, Am. Math. Soc.* .

M. Brady, et al. (1998). 'Regularized vortex sheet evolution in three dimensions'. *J. Comp. Phys.* **146**:520–545.

A. K. Brodsky (1991). 'Vortex formation in the tethered flight of the peacock butterfly *Inachis io* L. (Lepidoptera, Nymphalidae) and some aspects of insect flight in evolution'. *J. Exp. Biol.* **161**:77–95.

R. E. Caflisch & O. F. Orellana (1986). 'Long time existence for a slightly perturbed vortex sheet'. *Comm. on Pure and Appl. Math* **39**:807–838.

A. J. Chorin (1973). 'Numerical study of slightly viscous flow'. *J. Fluid Mech.* **57**:785–796.

A. J. Chorin & P. S. Bernard (1973). 'Disretization of a vortex sheet, with an example of Roll-Up'. *J. Comp. Phys.* **13**:423–429.

R. Clements & D. Maull (1975). 'The representation of sheets of vorticity by discrete vortices'. *Progress in Aerospace Sciences* **16**:129–146.

R. J. Cooter & P. S. Baker (1977). 'Weis-Fogh clap and fling mechanism in *Locusta*'. *Nature* **269**:53–54.

L. Cortelezzi, et al. (1997). 'Nonlinear feedback control of the wake past a plate: From a low-order model to a higher-order model'. *Phys. Fluids* **9**:2009–2022.

B. de Bernardinis, et al. (1981). 'Oscillatory flow around disks and through orifices'. *J. Fluid Mech.* **102**:279–299.

M. H. Dickinson (1994). 'The effects of wing rotation on unsteady aerodynamic performance at low Reynolds numbers'. *J. Exp. Biol.* **192**:179–206.

M. H. Dickinson (1996). 'Unsteady mechanisms of force generation in aquatic and aerial locomotion'. *A. Zool.* **36**:537–554.

M. H. Dickinson & K. G. Gotz (1993). 'Unsteady aerodynamic performance of model wings at low Reynolds number'. *J. Exp. Biol.* **174**:45–64.

M. H. Dickinson, et al. (1999). 'Wing Rotation and the aerodynamic basis of insect flight'. *Science* **284**:1954–1960.

C. P. Ellington, et al. (1996). 'Leading edge vortices in insect flight'. *Nature* **384**:626–630.

D. L. Grodnitsky & P. P. Morozov (1993). 'Vortex formation during tethered flight of functionality and morphologically two-winged insects, including evolutionary considerations on insect flight'. *J. Exp. Biol.* **182**:11–40.

S. Ho, et al. (2003). 'Unsteady aerodynamics and flow control for flapping wing flyers'. *Progress in Aerospace Sciences* **39**:635–681.

T. Y. Hou, et al. (2006). 'A 3D numerical method for studying vortex formation behind a moving flat plate'. *Commun. Comput. Phys.* **1**(2):207–228.

T. Ishihara & Y. Kaneda (1995). 'Singularity formation in three-dimensional motion of a vortex sheet'. *J. Fluid Mech.* **300**:339–366.

M. A. Jones (2003). 'The separated flow of an inviscid fluid around a moving flat plate'. *J. Fluid Mech.* **496**:405–441.

M. A. Jones & M. J. Shelley (2005). 'Falling Cards'. *J. Fluid Mech.* **540**:393–425.

Y. Kaneda (1990). 'A representation of the motion of a vortex sheet in a three-dimensional flow'. *Phys. Fluids A* **2**:458–461.

S. D. Kelly & H. Xiong (2010). 'Self-propulsion of a free hydrofoil with localised discrete vortex shedding: analytical modelling and simulation'. *Theor. Comput. Fluid Dyn.* **24**:45–50.

G. H. Keulegan & L. H. Carpenter (1958). 'Forces on cylinders and plates in an oscillating fluid'. *J. Res. Natl. Bureau Standards* **60**:423–440.

R. Krasny (1986a). 'A study of singularity formation in a vortex sheet by the point-vortex approximation'. *J. Fluid Mech.* **167**:65–93.

R. Krasny (1986b). 'Desingularization of periodic vortex sheet roll-up'. *J. Comp. Phys.* **65**:292–313.

R. Krasny (1987). 'Computation of vortex sheet roll-up in the Trefftz plane'. *J. Fluid Mech.* **184**:123–155.

R. Krasny (1991). 'Vortex sheet computations: Roll-up, Wakes, separation'. *Lectures in Appl. Math.* **28**:385–402.

K. Lindsay & R. Krasny (2001). 'A Particle method and adaptive treecode for vortex motion in three-dimensional flow'. *J. Comp. Phys.* **172**:879–907.

H. Liu, et al. (1998). 'A computational fluid dynamic study of hawkmoth hovering'. *J. Exp. Biol.* **201**:461–477.

H. Liu & K. Kawachi (1998). 'A numerical study of insect flight'. *J. Comp. Phys.* **146**:124–156.

Y. Lu & G. X. Shen (2008). 'Three-dimensional flow structures and evolution of the leading edge vortices on a flapping wing'. *J. Exp. Biol.* **211**:1221–1230.

A. Magnan (1934). *La Locomotion chez les Animaux*. Paris: Hermann et Cie.

J. C. Mason & D. C. Handscomb (2002). *Chebyshev Polynomials*. Chapman & Hall.

T. Maxwothy (1979). 'Experiments on the Weis-Fogh mechanism of lift generation by insects in hovering fight. Part 1. Dynamics of the 'fling''. *J. Fluid Mech.* **93**:47–63.

S. Michelin & S. G. L. Smith (2009). 'An unsteady point vortex method for coupled fluid-solid problems'. *Theor. Comput. Fluid. Dyn* **23**:127–153.

L. M. Milne-Thompson (1949). *Theoretical Hydrodynamics*. Macmillan.

R. Mittal (2004). 'Computational modelling in biohydrodynamics: Trends, challenges, and recent advances'. *IEEE Journal of Oceanic Engineering* **29**:595–604.

D. W. Moore (1971). 'The discrete vortex approximation of a vortex sheet'. *Calif. Inst. Technol. Rep.* **AFOSR**:1084–69.

D. W. Moore (1979). 'The spontaneous appearance of a singularity in the shape of an evolving vortex sheet'. *Proc. R. Soc. Lon. A* **365**:105.

N. I. Muskhelishvili (1946). *Singular Integral Equations*. Nordhoff - Groningen, Holland.

M. Nitsche & R. Krasny (1994). 'A numerical study of vortex ring formation at the edge of a circular tube'. *J. Fluid Mech.* **276**:139–161.

C. Poelma, et al. (2006). 'Time-resolved reconstruction of the full velocity field around a dynamically-scaled flapping wing'. *Experiments in Fluids* **41**:213–225.

L. Prandtl & O. G. Tietjens (1934). *Fundamentals of Hydro- and Aeromechanics.* Republished by Dover in 1957.

W. H. Press, et al. (2007). *Numerical Recipes - The art of scientific computing (Third edition).* Cambridge University Press.

R. Ramamurti & W. C. Sandberg (2002). 'A three-dimensional computational study of the aerodynamic mechanisms of insect flight'. *J. Exp. Biol.* **205**:1507–1518.

L. Rosenhead (1931). 'The formation of vortices from a surface of discontinuity'. *Proc. R. Soc. Lond. A* **134**:170–192.

N. Rott (1956). 'Diffraction of a weak shock with vortex generation'. *J. Fluid Mech.* **1**:111–128.

P. G. Saffman (1992). *Vortex Dynamics.* Cambridge University Press.

P. G. Saffman & G. R. Baker (1979). 'Vortex Interactions'. *Ann. Rev. Fluid Mech.* **11**:95–122.

S. P. Sane & M. H. Dickinson (2001). 'The control and flight force by a flapping wing: lift and drag production'. *J. Exp. Biol.* **204**:729–733.

M. J. Shelley (1992). 'A study of singularity formation in vortex-sheet motion by a spectrally accurate vortex method'. *J. Fluid Mech.* **244**:493–526.

R. K. Shukla & J. D. Eldredge (2007). 'An inviscid model for vortex shedding from a deforming body'. *Theor. Comput. Fluid Mech.* **21**:343–368.

C. Sulem, et al. (1981). 'Finite time analyticity for the two and three dimensional Kelvin-Helmholtz instability'. *Commun. Math. Phys.* **80**:485–516.

M. Sun & J. Tang (2002). 'Unsteady aerodynamic force generation by a model fruit fly wing in flapping motion'. *J. Exp. Biol.* **205**:55–70.

C. van den Berg & C. P. Ellington (1997). 'The vortex wake of a "Hovering" model Hawkmoth'. *Phil. Trans. R. Soc. Lond. B* **352**:317–328.

T. Weis-Fogh (1973). 'Quick estimates of flight fitness in hovering animals, including novel mechanisms for lift production'. *J. Exp. Biol.* **59**:169–230.

A. P. Willmott, et al. (1997). 'Flow visualisation and unsteady aerodynamics in the flight of the hawkmoth, Manduca sexta'. *Phil. Trans. R. Soc. Lond. B* **352**:303–316.

Y. Yu, et al. (2003). 'An analytic approach to theoretical modelling of highly unsteady viscous flow excited by wing flapping in small insects'. *Acta Mechanica Sinica* **19**(6):508–516.

R. Zbikowksi (2002). 'On aerodynamic modelling of an insect-like flapping wing in hover for micro air vehicles'. *Phil. Trans. R. Soc. Lond. A* **360**:273–290.